SPATIAL AND TEMPORAL VARIATIONS IN THE IONOSPHERIC RADIOWAVE ABSORPTION

A Thesis submitted for the Degree of

Master of Philosophy

(Physics)

in the

University of London

by

Robin Lodowick Douglas Rees, B.Sc. (Lond.)

January 1973

ProQuest Number: 10107241

All rights reserved

INFORMATION TO ALL USERS
The quality of this reproduction is dependent upon the quality of the copy submitted.

In the unlikely event that the author did not send a complete manuscript
and there are missing pages, these will be noted. Also, if material had to be removed
a note will indicate the deletion.

ProQuest 10107241

Published by ProQuest LLC(2016). Copyright of the Dissertation is held by the Author.

All rights reserved.
This work is protected against unauthorized copying under Title 17, United States Code
Microform Edition © ProQuest LLC.

ProQuest LLC
789 East Eisenhower Parkway
P.O. Box 1346
Ann Arbor, MI 48106-1346

ABSTRACT

The D and E Regions of the Ionosphere are reviewed historically; the methods of measurement of both the electron density and the gross properties of the neutral atmosphere are discussed. The various reactions of electron production and loss are listed, and their relative importance assessed. The mechanism of ionospheric radio wave absorption is described; the Sen and Wyller generalisation of the Appleton-Hartree equation yields an expression for the absorption coefficient, in which are implied certain temporal variations. The results of previous experimental work are considered.

An analysis of long term Al measurements at three stations, of approximate latitude 50° N, suggests that absorption does not follow a direct $\cos^{n}\chi$ law, the departure from such a law being a function of wave frequency, location, and sunspot number. Comparable effects are shown to exist at 7° N, 35° N, and 51° S.

A theoretical absorption model is constructed, for which a revised profile for the electron loss coefficient, and a seasonally varying nitric oxide profile are proposed. It is suggested that the effect may be related to the ledge in electron density, occurring at around 87 km, which in turn may be caused by the steep gradient in the atomic oxygen concentration.

The asymmetric seasonal variations in other relevant parameters are discussed.

ACKNOWLEDGMENTS

I wish to place on record my very grateful thanks to my supervisor, Dr. E.S. Owen Jones, for having suggested the project, and for his helpful advice at all stages.

The present work would not have been possible without access to a computer, and I thank Dr. P. Pal and all his staff at the Bedford College Computing Unit for their assistance and encouragement in this aspect of the work.

I am most grateful to the Council of Bedford College for awarding me a special grant.

CONTENTS.

		Page
Title of Thesis		1
Abstract		2
Acknowledgments		3
	CHAPTER ONE : INTRODUCTION	
1.1	General and Historical Introduction	9
1.2	Methods of Investigation	
1.2.1	The Ionosonde	10
1.2.2	The Topside Sounder	11
1.2.3	Partial Reflection	11
1.2.4	Wave Interaction	12
1.2.5	Incoherent Scatter	12
1.2.6	Rocket Measurements	13
1.3	Electron Production	
1.3.1	The Chapman Theory	16
1.3.2	Table of Ionisation Processes	18
1.4	Electron Loss Processes	
1.4.1	Recombination	19
1.4.2	Attachment	20
1.4.3	The Meaning of the Effective Electron Loss Coefficient	21
1.5	Classification of Layers	23
	CHAPTER TWO : THE NEUTRAL ATMOSPHERE	
2.1	Introduction	25
2.2	Measurement of Atmospheric Properties	
2.2.1	Density of Neutral Gas	25
2.2.2	Temperature	26
2.2.3	Pressure	27
2.2.4	Standard Atmosphere Models	27

Page

2.3 Composition

2.3.1 Equilibrium 31

2.3.2 Molecular Oxygen and Nitrogen and Atomic Oxygen 32

2.3.3 Ozone 33

2.3.4 Metastable Molecular Oxygen 33

2.3.5 Nitric Oxide 34

2.3.6 Water Vapour 36

2.3.7 Positive Ions 36

2.3.8 Negative Ions 38

CHAPTER THREE : ABSORPTION

3.1 Introduction

3.1.1 Attenuation 39

3.1.2 Units of Absorption 39

3.1.3 Collision Frequency 40

3.2 The Appleton-Hartree Equation

3.2.1 The Complex Refractive Index 41

3.2.2 Conditions for Reflection 42

3.2.3 The Critical (Penetration) Frequency 42

3.2.4 Quasi-Longitudinal and Quasi-Transverse Approximations 43

3.3 Evaluation of the Absorption Coefficient

3.3.1 Use of the Appleton-Hartree Equation 44

3.3.2 Categories of Absorption 44

3.3.3 Generalised Collision Statistics 45

3.3.4 Full Wave Theory 46

3.4 Implied Variations in the Absorption Coefficient 46

3.5 Experimental Methods

3.5.1 Vertical Incidence Pulse Absorption 48

3.5.2 Relative Ionospheric Opacity, Riometer 49

3.5.3 The Continuous Wave Oblique Incidence Method 49

Page

CHAPTER FOUR : PREVIOUS EXPERIMENTAL WORK

4.1 Superimposition of Temporal Variations 51

4.2 Solar Cycle Variation 51

4.3 Diurnal and Seasonal Variations in Absorption

4.3.1 Some Theoretical Considerations 53

4.3.2 Presentation of Results 54

4.3.3 Previous Results 54

4.3.4 Diurnal Deviations from $\cos^n\chi$ Law 56

4.3.5 Seasonal Deviations from $\cos^n\chi$ Law 57

4.4 Further Experimental Absorption Results

4.4.1 The Variation of Absorption with Frequency 57

4.4.2 Winter Anomaly and Sudden Stratospheric Warmings 58

CHAPTER FIVE : THE PRESENT EXPERIMENTAL WORK

5.1 Equipment 60

5.2 The Method 63

5.3 The Results and Discussion 63

CHAPTER SIX : THE ANALYSIS

6.1 List of the Stations 65

6.2 The Choice and Reduction of Data 71

6.3 Seasonal Variation in Absorption

6.3.1 Preliminary Observations 72

6.3.2 The Investigation of the Lag in Absorption 72

6.3.3 The Degree of the Polynomial 74

6.3.4 The Computing 79

6.3.5 The Results 79

CHAPTER SEVEN : THE EVALUATION OF A THEORETICAL ABSORPTION MODEL, AND ITS USE IN A DISCUSSION ON THE DELAY EFFECT IN ABSORPTION

7.1 The Production of the Model

7.1.1 The Aim 81

7.1.2 The Sources of the Values of Parameters used in the Calculation 81

Page

7.1.3 Seasonal Variation of Molecular Oxygen, Atomic Oxygen, and Molecular Nitrogen Concentrations 83

7.1.4 The Computing

7.1.4.1 Evaluation of the Optical Depth and Electron Production Rate 85

7.1.4.2 Evaluation of Mono-Energetic Collision Frequencies 87

7.1.4.3 Evaluation of Script Integrals 87

7.1.4.4 Evaluation of K , and $\int K\, dh$ 89

7.1.5 The Choice of Profile for the Effective Electron Loss Coefficient 91

7.1.6 The Choice of Profile of Nitric Oxide Concentration 102

7.2 Tests on the Model

7.2.1 Electron Density Profiles and Critical Frequency Variations 104

7.2.2 Agreement of Model with Experimental Values of Absorption and "Delay" at R = 100 118

7.3 Observations from the Model

7.3.1 The Relative Importance of the Different Ionisation Processes for the Various Solar Activities 119

7.3.2 The Model's Values of Absorption at Low and High Sunspot Numbers, and a Comparison with Experimental Values 119

7.4 The Variations in Delay

7.4.1 An Extension of the Model to Lower Frequencies 120

7.4.2 The Effects of Varying Solar Activity on Experimental and Theoretical Values of Delay 125

7.5 Interpretation of Experimental Results at Low Latitudes for R = 100 129

7.6 Interpretation of the Absorption Data for Individual Years 130

7.7 A Suggested Explanation of the Delay Phenomenon 134

Page

7.8 Other Parameters related to Absorption

7.8.1 Minor Constituents 137

7.8.2 The Variations of b and b' 144

7.8.3 Winds and Turbulence 147

7.9 The Implications of the Present Work 149

Appendix A : Suggestions for Further Work 151

Appendix B : Computer Program of the Theoretical Absorption Model 152

References 155

CHAPTER ONE

INTRODUCTION

1.1 General and Historical Introduction.

The presence of a conducting layer in the earth's atmosphere was first suggested in 1860 by Lord Kelvin from studies of geomagnetism. Previously, Gauss in 1839 had postulated that the small diurnal variations in the earth's magnetic field might be caused by atmospheric electric currents. Developing this idea, Balfour Stewart (1882) put forward the theory that at some altitude the atmosphere becomes sufficiently conducting for electric fields and currents to be induced when it is driven by winds across the earth's magnetic field.

Thomson's discovery of the electron in 1900, and the successful transmission by Marconi of radio signals across the Atlantic in 1901, led Kennelly (1902) and Heaviside (1902) independently to postulate the existence of an ionised layer which might reflect radio waves. This explained the observed bending of waves round the earth's curved surface more satisfactorily than diffraction effects. Heaviside further suggested solar radiation of wavelength shorter than visible light as a cause of the ionisation, thereby being the first to imply solar cycle and seasonal variations in this electrically conducting region. About this time cosmic rays were also discovered. These high speed electrons, protons, and other light nuclei coming from outer space, impinge on the earth equally by day and night, and are now known to be the principal source of ionisation below about 65 km.

Eccles (1912) and Larmor (1924) provided a basic theory, but it was not until direct evidence was supplied by Appleton and Barnett (1925) that the concept was finally accepted. This was achieved by comparing the intensities of the "ground" and reflected "sky" waves.

Further confirmation was provided by the detection of down-coming waves by Smith-Rose and Barfield (1926,1927), using directional aerials. Breit and Tuve (1925,1926) used the first pulse-sounding technique to demonstrate the reflection of different frequencies at different altitudes, while the work of Hulbert (1928) and Chapman (1931) forms the basis of the theory today.

The term "Ionosphere" was devised in 1926 by Watson-Watt. This sphere of ions and electrons extends from a height of about 50 km to the upper limits of the atmosphere, and is divided into regions according to the convention of Appleton. The present work will be concerned principally with the D and Lower E Regions (60-110 km), for it is in this zone that the absorption and reflection of vertically incident radio waves of frequency up to about 3 MHz occur.

1.2 Methods of Investigation.

1.2.1 The Ionosonde.

The first workers to use the ionosonde were Breit and Tuve (1925,1926). The method consists essentially of a pulsed radar sounding device in which the frequency can be varied from about 1 MHz to 25 MHz. It measures directly as a function of frequency the time taken for a vertically incident pulse to travel to the ionosphere and back again. If one assumes that the waves travel with their free space velocity, then it is possible by this means to measure the virtual height of reflection of a wave of a particular frequency. Moreover, the application of the Appleton-Hartree condition for reflection will yield the electron density at that virtual height.

The ionosonde has a major advantage in that the virtual height under normal conditions depends neither on the transmitter output nor receiver gain. It can operate without supervision, but is, however, unsuitable for the D Region because of the very high absorption at the

necessarily low frequencies required for D Region reflection, and also the presence of partial reflections. In addition, in those cases where the electron density does not increase monotonically, the ionosonde cannot distinguish the "valleys" so created. The real height, h, of reflection cannot be found directly, but must be calculated by numerical integration of the equation:-

$$h' = \int_0^h \mu' \, dh$$

where h' is the virtual height, and μ', the group refractive index, is a function both of frequency and electron density.

1.2.2 The Topside Sounder.

This technique was originated by Warren (1963), and involves placing an ionosonde in a satellite at the top of the ionosphere at 500-1000 km. This method, however, provides little information of direct relevance to the present work.

1.2.3 Partial Reflection.

This method, devised by Gardner and Pawsey (1953) uses weak reflections from small discontinuities of refractive index in the height range 50-90 km. Magneto-ionic theory shows that in a dispersive medium in the presence of an imposed magnetic field, there will be two different modes of propagation; the Ordinary (O), and the Extraordinary (X). 2-3 MHz pulses are transmitted vertically, and comparison of the amplitudes of the O and X pulses over a range of heights enables the electron density, N(e), to be calculated, provided that a profile of the mono-energetic electron collision frequency is found by other means.

1.2.4 Wave Interaction.

Wave interaction, or the Luxembourg Effect, was first demonstrated by Bailey and Martyn (1934). Two pulses are propagated vertically in quick succession. The first "disturbing" wave is absorbed by the ionosphere, and this energy re-appears in the form of a rise in the electron temperature. This will cause an increase in the electron collision frequency, and hence a change in the absorption coefficient. The following "wanted" wave thus suffers a change in its total absorption, compared with its value in the absence of the disturbing wave. The method is insufficient in isolation to determine the electron density. Barrington and Thrane (1962), using in addition partial reflection data, were able to obtain results reasonably consistent with those of other methods.

The interaction effect is usually less than 10^{-3} of the wanted signal amplitude. The method has been reviewed, and its theory discussed by Smith (1966a)

1.2.5 Incoherent Scatter.

Gordon (1958) investigated the necessary conditions for the classical Thomson process of scattering by free electrons as a function of height. The scattered signal strength is found to be directly proportional to electron density. The mean free path of the electron must be greater than the radio wavelength and the scale size of electron gas irregularities arising from their random thermal motion. Taylor (1969) has described the apparatus used for obtaining data, some of which is used for comparison purposes in the present work. The Royal Radar Research Establishment equipment operates at a peak power of 7 MW, pulsed 150 times per second with a pulse length of 33 μs. The value of electron density is found by normalising the plot against $N_m(e)_E$ data, obtained by the Radio and Space Research Centre, Slough.

The scattered signal is very weak, so the receiving apparatus must be extremely sensitive. The receiving aerial must receive as little of the incident signal as possible, nor receive reflections off ground-based objects. The R.R.E. can operate satisfactorily measuring scatter between 75 and 140 km, although the method is not normally used below the F1 Region. Unlike the ionosonde, valleys in the electron density profile can be detected by incoherent scatter.

1.2.6 Rocket Measurements.

Rocket data can be divided into four categories:-

a In the Differential Doppler Shift method, developed by Seddon (1953), there are two transmitters aboard a rocket, one of 4.3 MHz, and the other n (usually 6) times this frequency. The rocket flight is nominally vertical, and is monitored by a ground station vertically below. It may be shown that Δf, the instantaneous differential Doppler frequency, is proportional to the ambient electron density.

b In the lower ionosphere the Differential Absorption technique may be used. Seddon (1958) used a single frequency of 7.75 MHz transmitted from a rocket and measured at ground level the relative amplitudes of the ordinary and extraordinary waves. The theory is similar to that for partial reflections, and as in that case, independent data is needed before a solution may be found. Kane (1962) combined this data with that of differential Doppler shift to obtain profiles both for electron density and collision frequency.

c Faraday Rotation.

If a plane polarised wave passes through the ionosphere in the presence of a magnetic field, it may be thought of as having two circularly polarised components, one clockwise and one anti-clockwise. As the speeds of propagation of the two components are different, the

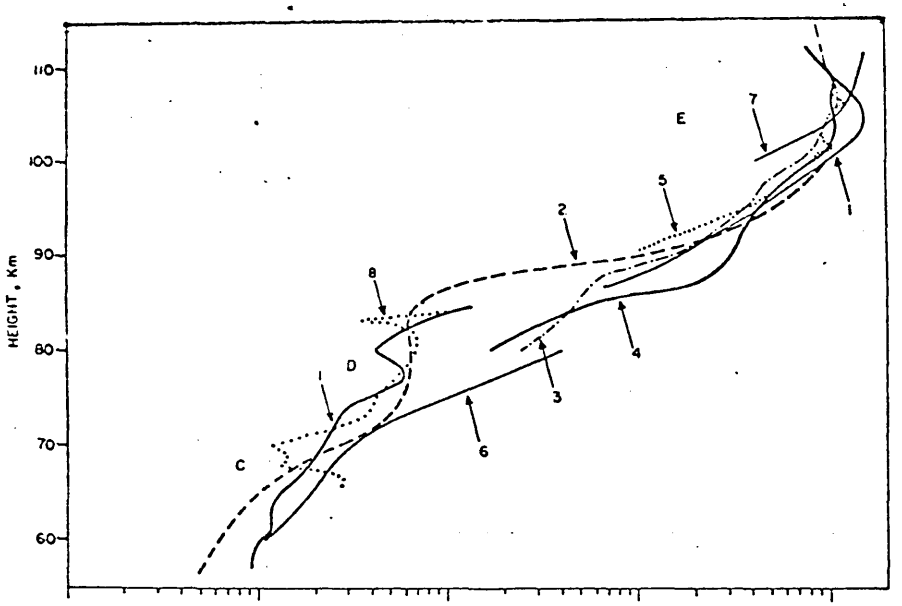

Fig. 1.1 Electron Density Profiles, N(e) (After Belrose, 1965)

1. Partial reflection, 10.30, May 61, Canada.
2. Theoretical, midday, mid-latitude.
3. Rocket Langmuir probe, 15.32, Sep.60, Japan.
4. Rocket propagation, 12.37, Sep.59, Canada.
5. Rocket propagation, 17.30, Jun.54, mid-latitude.
6. Pulse cross-modulation, 10.00-14.00, Mar.-Apr.60, Norway.
7. Ionosonde, 12.00, Mar.57, England.
8. Rocket Faraday rotation, 14.30, Mar.63, 38°N.

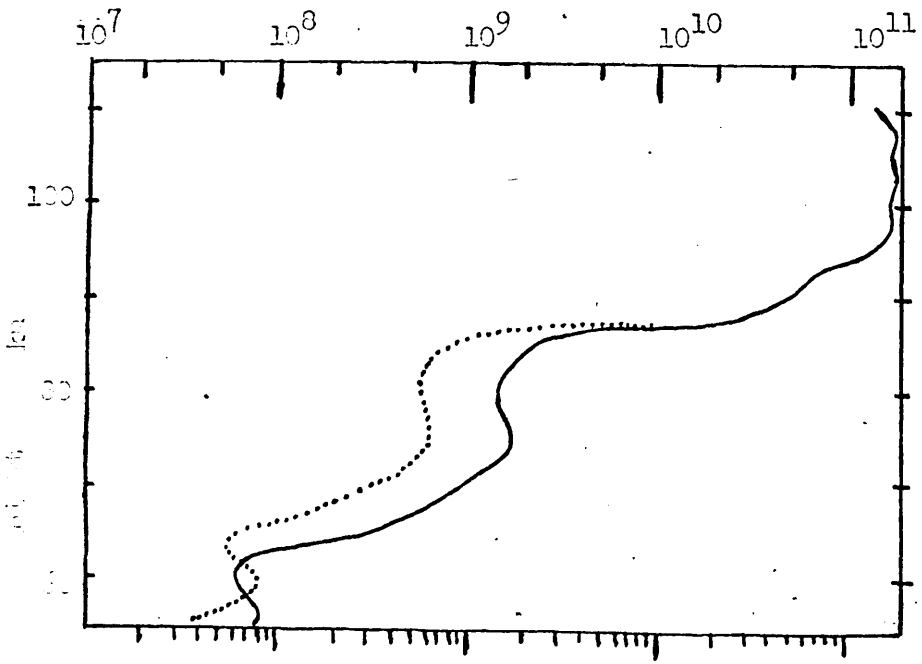

(m^{-3})

Fig. 1.2 N(e)

Dotted line:- VLF measurement (Thrane, 1972, using the data of Bain).

Continuous line:- Theoretical, computed in the present work, corresponding to July midday at 50°N for R = 100.

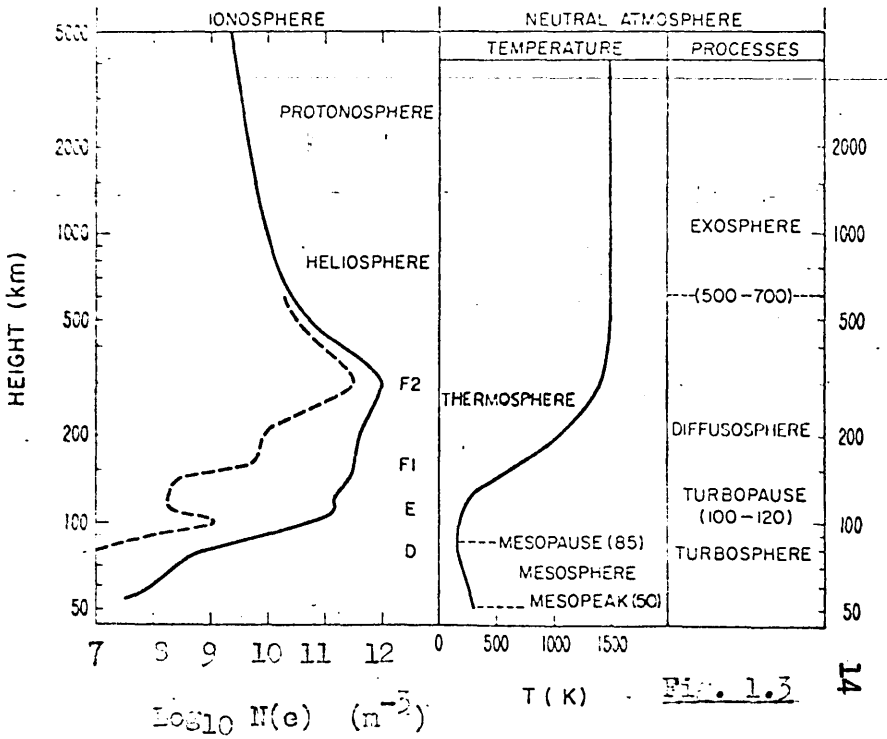

Fig. 1.3

(After VanZandt and Knecht, 1964)

relative phase changes, and hence there is a steady rotation of the plane of polarisation of the resultant wave. Such signals have been transmitted from rockets (and also satellites), and received at the ground by means of a linear antenna, from which electron density profiles have been deduced (Aikin et al., 1963).

d The Langmuir Probe is a metal wire projecting into a plasma, and partially enclosed by a metal grid. If the current is measured as a function of the probe voltage with respect to the grid, then the ambient electron density can be deduced. The method has been used by Smith (1962) and Yonezawa (1962). Some of the assumptions necessary for the deduction, however, lead to difficulties when D Region measurements are being interpreted, due to the similar magnitude of the mean free path of the electron and the probe dimensions. An estimate of temperature may be obtained from the current/voltage gradient.

Direct measurements by mass spectrometer aboard rockets measure the relative concentrations of different types of ions. In the present work, however, it is the electron density profiles that are of greater relevance, because of their effect on the propagation of radio waves.

Fig. 1.1 shows some typical electron density profiles found by various different methods. Fig. 1.2, drawn to the same scale, shows both a typical profile computed by the means described in Chapter Seven of the present work, and also a profile derived from VLF measurements.

1.3 Electron Production.

1.3.1 The Chapman Theory.

Developing the theory of Chapman (1931) to allow for the various types of ionising radiation, the ion pair production rate at a height h is given by:-

$$\sum_{\lambda} q_h = \sum_{\lambda} \left[\sum_{j} \sigma_j' n_j \right]_\lambda I_{\infty,\lambda} \exp\left(-\mathrm{Sec}\,\chi \sum_{j} \sigma_j \int_h^\infty n_j \, dh \right)_\lambda ,$$

where $\sum_{\lambda}$ indicates the summation over all ionising radiation wavelengths,

$\sum_{j}$ indicates summation over species j,

$I_{\infty,\lambda}$ = the incident flux of wavelength λ,

χ = the solar zenith angle,

σ_j , σ_j' , n_j = the absorption cross section, ionisation cross section, and number density of the jth species.

The term:-

$$\left(\mathrm{Sec}\,\chi \sum_{j} \sigma_j \int_h^\infty n_j \, dh \right)_\lambda$$

is known as the optical depth of the atmosphere at height h for wavelength λ.

The ionisation efficiency of the jth species for a particular wavelength is defined as:-

$$\epsilon = \frac{\sigma_j'}{\sigma_j} .$$

Chapman considered the effect with one absorbent and ionisable gas only, and an isothermal atmosphere. The production equation then reduces to:-

$$q_h = \sigma \epsilon n I_\infty \exp\left(-\mathrm{Sec}\,\chi \, \sigma \int_h^\infty n \, dh \right) ,$$

which, together with the equation:-

$$n = n_0 \exp\left(\frac{-h}{H}\right)$$

where the scale height, H, is given by:-

$H = \frac{kT}{mg}$ (k = Boltzmann's constant, m = molecular mass),

yield the result:-

$$q_h = \sigma \epsilon I_\infty n_0 \exp\left(\frac{-h}{H} - H \sigma n_0 \sec\chi \exp\left(\frac{-h}{H}\right)\right)$$

The maximum rate of ionisation occurs where $\frac{dq}{dh} = 0$.

$$h_0 = H \, Ln\,(H \sigma \epsilon n_0 \sec\chi)$$

or $= H \, Ln\,(H \sigma n_0 \sec\chi)$, assuming $\epsilon = 1$.

and the maximum ionisation rate is given by:-

$$q_m = \frac{I_\infty}{\exp(1)} \cos\chi$$

This occurs at unit optical depth.

Maximum ionisation occurs at different heights for the various different wavelengths of ionising radiation, and thus several distinct layers will occur.

For the present study it will be unnecessary to consider the effect of curvature of the earth.

1.3.2 Table of Ionisation Processes.

Type of radiation, and wavelength(s) Å	Ionisation Equation(s)	Constituents that absorb radiation without being ionised	Approximate mean annual height of maximum ionisation
Lyman Alpha 1216	$NO + h\nu \rightarrow NO^+ + e.$	O_2 , N_2	105 km (according to Meira's (1971) data)
Ultra Violet 1027-1118	$O_2(^1\Delta_g) + h\nu \rightarrow O_2^+ + e.$	O_2	85-105 km depending on wavelength
Lyman Beta 1026	$O_2 + h\nu \rightarrow O_2^+ + e.$	N_2	105 km
E.U.V. 120-1000	No significant effects below 120 km.		
X Rays 30-120	$O + h\nu \rightarrow O^+ + e.$ $O_2 + h\nu \rightarrow O_2^+ + e.$ $N_2 + h\nu \rightarrow N_2^+ + e.$	—	(95-105 km (depending (on (wavelength
Short Wavelength X Rays 2-10			(70-95 km (depending (on (wavelength
Galactic Cosmic Rays	All constituents ionised to some extent.		Below 30 km
Solar Cosmic Rays	Negligible in undisturbed solar conditions.		

1.4 Electron Loss Processes.

1.4.1 Recombination.

The simple assumption used by Chapman is that free electrons are lost in exactly the opposite process to that of their formation. The rate of loss will thus be proportional to the product of the electron and positive ion concentrations, and if there are few negative ions, then these two quantities will be equal because of the atmosphere's electrical neutrality. Hence it is possible to write:-

$$\frac{dN(e)}{dt} = \Sigma q - \alpha N^2(e)$$

where Σq is the total production rate previously calculated, and α is called the recombination coefficient. A simple Radiative Recombination process would be of the type:-

$$M^+ + e \rightarrow M + h\nu$$

where M^+ is any atomic or molecular ion present. Such a recombination coefficient would be independent of height.

An alternative mechanism is known as Three Body Recombination:-

$$M^+ + e + L \rightarrow M + L$$

where L is a neutral molecule. This process occurs more frequently than radiative recombination, since conservation of energy and momentum can be achieved with much greater ease. The recombination coefficient for this reaction would be proportional to the number density of neutral molecules, hence the process would be of importance in the lower ionosphere.

Bates and Massey (1947) concluded that these two processes, however, were insufficient to explain the observed electron loss rates, and postulated Dissociative Recombination, examples being:-

$$O_2^+ + e \rightarrow O + O$$

$$N_2^+ + e \rightarrow N + N$$

$$NO^+ + e \rightarrow N + O$$

In the case of atomic ions, which are significant above about 90 km, a molecular ion must first be formed as an intermediate product either by charge transfer or an ion-atom interchange, e.g.:-

$$O^+ + O_2 \rightarrow O + O_2^+$$

$$O^+ + N_2 \rightarrow N + NO^+$$

1.4.2 Attachment.

Nicolet and Swider (1963) have suggested that in the D Region, especially at lower altitudes with the higher concentration of neutral molecules, the process of attachment becomes important:-

(i) $e + M \rightarrow M^- + h\nu$ Radiative Attachment,

(ii) $e + M + L \rightarrow M^- + L$ Three Body Attachment,

where M may be O_2 or O, but not N_2 or N. At night time attachment can take place to a small extent in the E Region.

Nicolet and Swider suggest also that the negative ions so formed are lost in processes such as:-

(iii) $M^- + L^+ \rightarrow M + L$ Ion-ion Neutralisation,

(iv) $M^- + h\nu \rightarrow M + e$ Photo Detachment,

(v) $M^- + L \rightarrow M + L + e$ Collisional Detachment.

Reaction (iv) is the main cause of the day/night change in λ, the negative ion/electron concentration ratio in the lower D Region.

From the standpoint of radio propagation, positive and negative ions are not usually considered, owing to their much greater inertia than that of free electrons.

If radiative attachment were the only loss mechanism, then, neglecting the sources of secondary electrons in (iv) and (v), the continuity equation would take the form:-

$$\frac{dN(e)}{dt} = \Sigma q - \beta' N(e)$$

where β', the effective electron attachment coefficient, would be a function of neutral molecule number density.

1.4.3 The Meaning of the Effective Electron Loss Coefficient.

If a single species ionosphere is considered (i.e. one species for each loss process), and diffusion is neglected, it has been shown by Whitten and Poppoff (1971) that the complete continuity equation becomes:-

(i) $$\frac{dN(e)}{dt} = \Sigma q - \alpha_D N(e) N^+ - \beta N(e) m + \gamma N^- n + \rho N^-$$

where N^+ is the positive ion number density,

N^- the negative ion number density,

m the attaching species number density,

n the detaching species number density,

α_D the ion-electron recombination coefficient,

β $(\neq \beta')$ the electron attachment coefficient,

ρ the photo detachment rate,

and γ is the collisional detachment coefficient.

In addition:-

(ii) $$\frac{dN^-}{dt} = -\alpha_i N^- N^+ + \beta N(e) m - \gamma N^- n - \rho N^-$$

(iii) $$\frac{dN^+}{dt} = \Sigma q - \alpha_D N(e) N^+ - \alpha_i N^- N^+$$

where α_i is the ion-ion recombination coefficient. Using:-

(iv) $$\lambda = N^-/N(e)$$, and

(v) $$N^+ = N(e) + N^-$$,

the equations simplify to:-

(vi) $$\frac{dN(e)}{dt} = \frac{\Sigma q}{1+\lambda} - (\alpha_D + \lambda \alpha_i) N^2(e) - \frac{N(e)}{1+\lambda} \frac{d\lambda}{dt}$$, and

(vii) $$\frac{1}{1+\lambda} \frac{d\lambda}{dt} = \beta m - \lambda \left(\rho + \gamma n + N(e)(\alpha_i - \alpha_D) + \frac{\Sigma q}{N(e)(1+\lambda)} \right)$$

Except at sunrise and sunset, λ varies slowly with time, hence:-

(viii) $$\frac{d\lambda}{dt} \approx 0$$,

(ix) $$\frac{dN(e)}{dt} = \frac{\Sigma q}{1+\lambda} - (\alpha_D + \lambda \alpha_i) N^2(e)$$, and

(x) $$\lambda \approx \frac{\beta m}{\rho + \gamma n}$$, because the last two terms in equation (vii) are usually insignificant. In the sunlit hemisphere:-

$\rho \gg \gamma n$, hence:-

$$\lambda = \frac{\beta m}{\rho}$$

Whitten and Poppoff indicate that a useful concept in principle is the Effective Recombination Coefficient α_{eff} , but that there are three possible definitions of this quantity, each derived from equation (ix):-

(xi) $$\frac{dN(e)}{dt} = \Sigma q - \alpha_{eff} N^2(e)$$

This can be valid only if $\lambda \ll 1$, in which case $\alpha_{eff} = \alpha_D$, although values of α_{eff} outside this range are frequently calculated using this method.

In those few cases where λ is measured or calculated, either of the following two equations may be used:-

(xii) $\frac{dN(e)}{dt} = \frac{\Sigma q}{1+\lambda} - \alpha'_{eff} N^2(e)$; i.e. $\alpha'_{eff} = \alpha_D + \lambda\alpha_i$

(xiii) $(1+\lambda)\frac{dN(e)}{dt} = \Sigma q - \alpha_{eff} N^2(e)$; i.e. $\alpha_{eff} = (1+\lambda)(\alpha_D + \lambda\alpha_i)$

Many authors fail to state which definition has in fact been used to calculate α_{eff}, in which case even values obtained by a perfectly valid method have limited usefulness. In the present work, however, where mid-day values will principally be studied, when $dN(e)/dt \approx 0$, equation (xiii) reduces to:-

$$0 = \Sigma q - \alpha_{eff} N^2(e)$$

or $$\alpha_{eff} = \frac{\Sigma q}{N^2(e)}$$

With a knowledge of α_{eff}, previously calculated in this way, and a knowledge of the seasonal variation in the sum of the electron production rates, then, provided that α_{eff} does not vary seasonally, the seasonal variation in electron density may be calculated according to:-

$$N(e) = \sqrt{\frac{\Sigma q}{\alpha_{eff}}}$$

Henceforth in the present work α_{eff} will be referred to simply as α, and be given the rather more meaningful title of Effective Electron Loss Coefficient.

1.5 Classification of Layers.

Fig. 1.3 indicates the various layers in the ionosphere. In ionograms of the E Region, two cusps sometimes appear. Of these, one cusp shows a regular diurnal variation, and it is this one whose frequency is tabulated as the critical frequency of the E Region, and is denoted by $f_o E$. The total E Region ionisation is the result of several different processes each of which having its own height of maximum ionisation. An ionogram, however, cannot resolve all of these, and generally indicates one layer only.

In addition to the ordinary ionisation , there is another layer in the E Region, known as Sporadic E, Es, which exhibits most irregular behaviour. It occurs simultaneously over areas of several hundred kilometers. It can take the form of dense patches of ionisation, usually less than 1 km thick, in the range 100 km to 120 km, or alternatively it can be patchy and partially transparent to waves reflected from higher layers. Although it is random in its times of appearance, near the equator it occurs mainly in the daytime. In mid latitudes it is less frequent, and is more likely during the day than at night, whilst at high latitudes it is mainly a night-time phenomenon. Smith and Matsushita (1962) have reviewed the effect, and Whitehead (1967) has suggested that in mid latitudes it may be caused by vertical wind shears. In high latitudes the cause is thought to be corpuscular bombardment, and, in equatorial regions, plasma instabilities in the equatorial electrojet.

As it is of a transient nature, sporadic E is not of direct application to the present work. It is of use, however, for night-time calibration purposes in radio wave absorption measurements by the carrier wave oblique incidence A3 method, as it acts as a strong reflector. This very fact, however, may result in the transmission of signals, by the sky wave, to far greater distances than was intended (by the ground wave alone). This can cause serious interference between stations.

CHAPTER TWO

THE NEUTRAL ATMOSPHERE

2.1 Introduction.

Although in the D and lower E Regions there are sufficient free electrons to affect significantly the propagation of radio waves, it should be borne in mind that in these regions the highest ratio of concentrations of electrons to neutral molecules is approximately 1 in 10 Thus the atmosphere may still be considered to be predominantly unionised. This Chapter deals with the measurement of the gross properties of the atmosphere in these regions, including the concentrations of the neutral and ionised constituents.

2.2 Measurement of Atmospheric Properties.

2.2.1 Density of Neutral Gas.

Reliable measurements of neutral gas density at altitudes up to 130 km have been obtained, using a light inflatable sphere ejected from a rocket (Faucher, 1963 and 1967). The downward acceleration, a, is found by means of three orthogonal accelerometers inside the sphere. The mass density, ρ , is given by:-

$$\rho = \frac{2m}{v^2 C_D}(g - a)$$

where m is the sphere mass,

v the sphere velocity,

and C_D , a dimensionless drag coefficient, which is a function of v and of Reynold's Number. The main inaccuracy in the experiment is the evaluation of the velocity by integration of the acceleration.

2.2.2 Temperature.

Temperatures in the altitude range 60-110 km cannot be measured directly due to the low thermal capacity of the atmosphere. Use is therefore made of the fact that the velocity C of sound in a gas is a function of temperature, namely:-

$$C = \left(\frac{\gamma R T}{M}\right)^{\frac{1}{2}}$$

where γ is the specific heats ratio,

R the gas constant,

and M the average mass in grams of 1 gram molecule.

As a rocket ascends, measurements are taken at a number of points on the ground of the time of arrival of sound waves from grenades detonated every few kilometres. M is measured by a mass spectrometer in which the incoming neutral particles are ionised by an electron beam. With additional ground receiving stations, Stroud et al. (1960) have been also able to determine horizontal wind velocities.

An alternative method for determining temperatures in this height range is the application of the hydrostatic relationship and the equation of state to the density results obtained in the falling sphere experiment.

Below 65 km, temperatures can be measured directly using a rocket-mounted thermistor. For greater heights Fedele (1966) has used as a measure of temperature the Doppler broadening of the D Lines of sodium vapour trails released from rockets for wind observations.

2.2.3 Pressure.

Below about 85 km, the pressure is sufficient for a rocket-borne Pirani Gauge to be used. Current is passed through a wire of temperature-dependent resistance, and the steady state temperature of the wire will be a function of the pressure. The gauge is mounted in a heavy metal case, to reduce the temperature change during flight to a few degrees, connected to a hole on the rocket skin.

Above 85 km an ionisation gauge is used. The air inside the gauge is ionised by alpha particles or electrons. For a given potential difference between the electrodes, the measured current indicates the amount of ionisation, and hence the gas density may be estimated.

2.2.4 Standard Atmosphere Models.

Groves (1970) has produced seasonal and latitudinal models of atmospheric temperature, pressure, and mass density in the range 25 km-110 km. The models of the latitudinal variations in temperature were obtained using all known reliable measurements of the parameter, and the thermal wind equation. Of more direct relevance to the present work, however, are his methods for obtaining the pressure models. The temperatures have been measured by thermistors up to 50 km, and by the grenade and falling sphere experiments. The pressure at a height h is calculated from:-

$$p(h) = p(30)\ \exp\left(-\int_{30\,km}^{h} \frac{Mg}{RT}\,dh\right)$$

where $p(30)$ is the pressure at 30 km, for which Groves has calculated a seasonally varying model from the results of balloon flights, the symbols having the same meaning as in § 2.2.2. M is numerically equal to the mean molecular weight, which Groves varies as a function of height. It may well vary seasonally also above about 100 km with the variation in the $n(O)/n(O_2)$ ratio, but it may be taken as nominally constant.

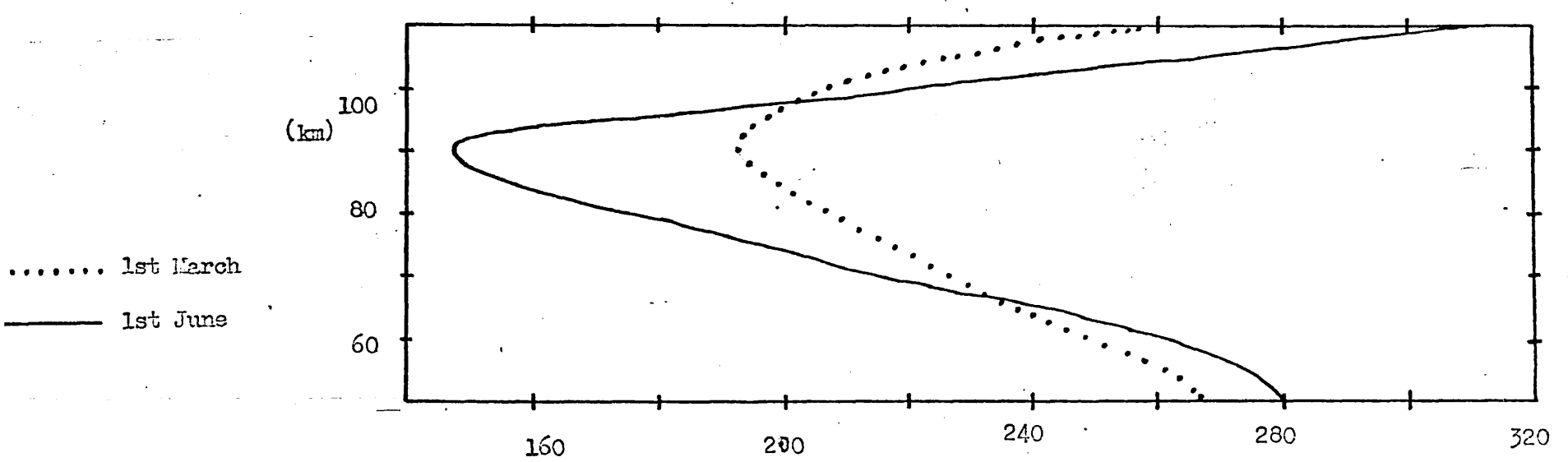
..... 1st March
——— 1st June
(km)
100
80
60
160
200
240
280
320
Temperature (K)

Fig. 2.1

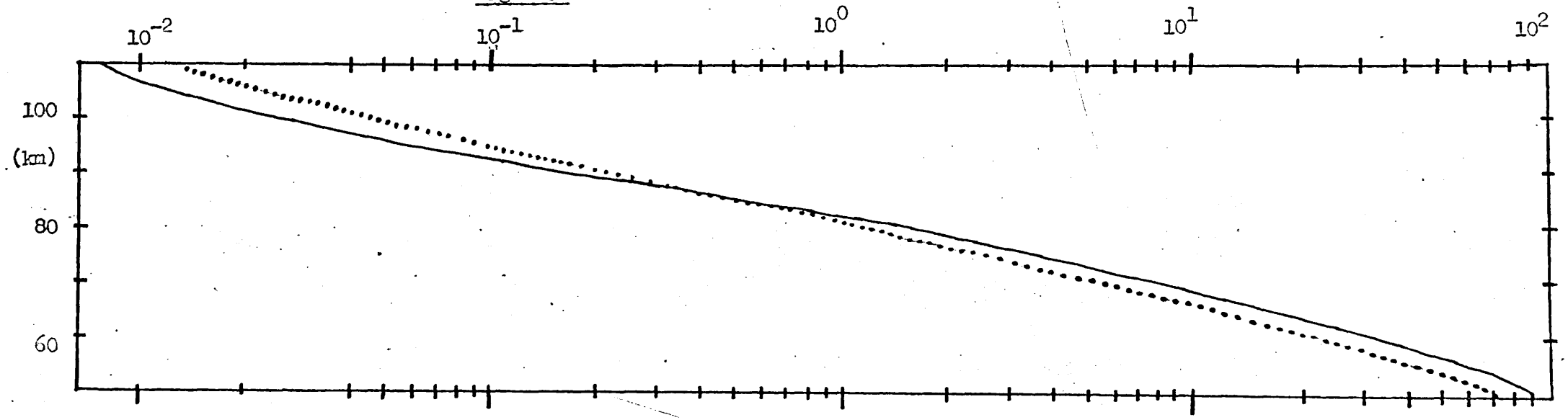
Pressure (Nm^{-2})
10^{-2}
10^{-1}
10^{0}
10^{1}
10^{2}
100
(km)
80
60

Fig. 2.2

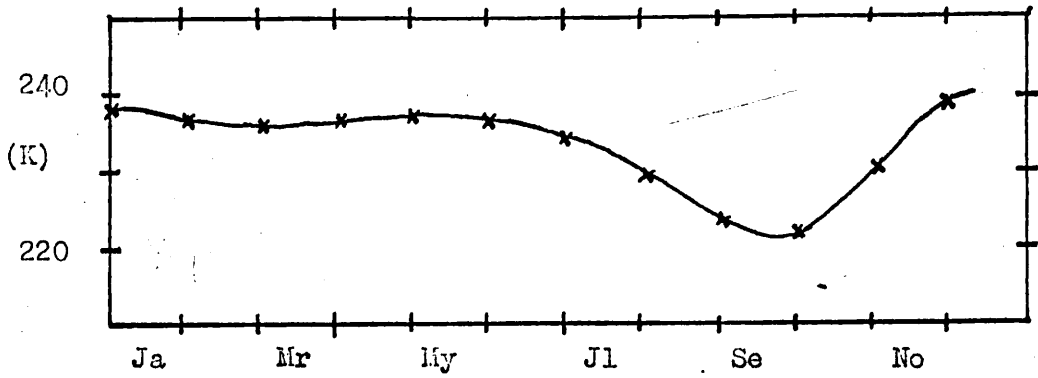

Fig. 2.3

65 km

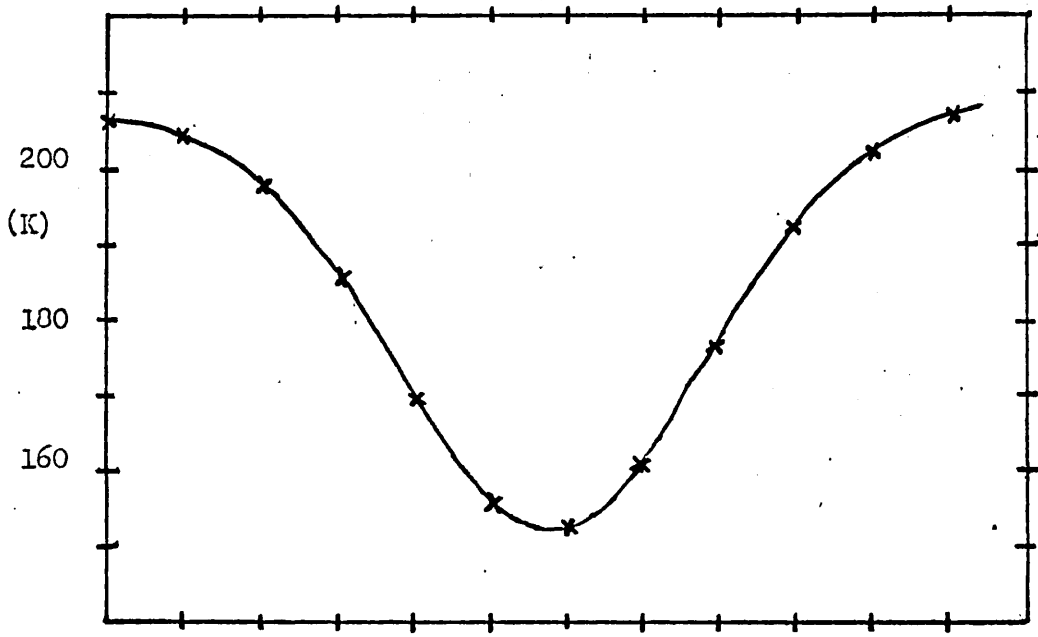

Fig. 2.4

85 km

SEASONAL VARIATION IN TEMPERATURE

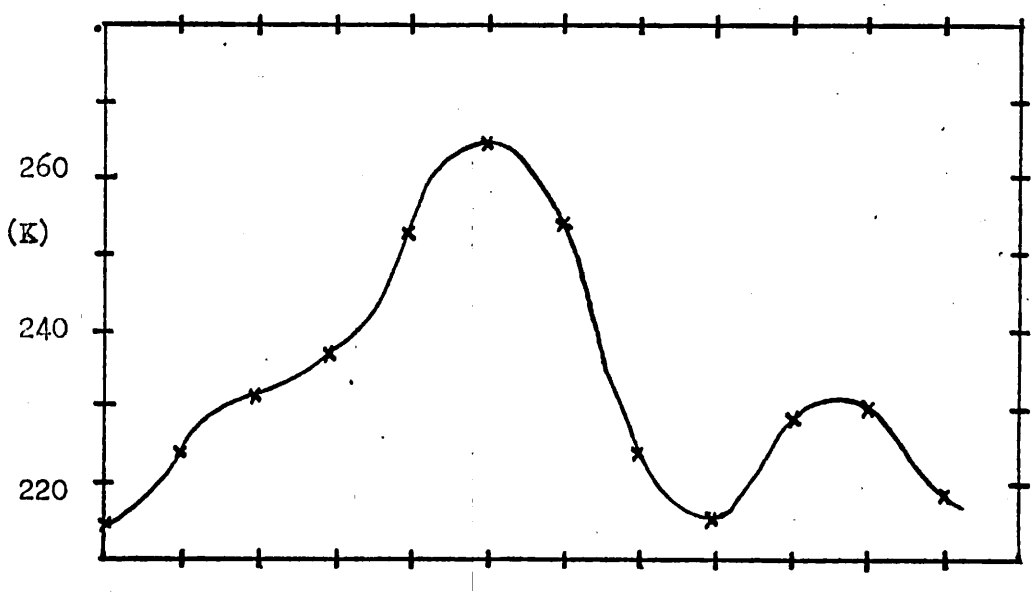

Fig. 2.5

105 km

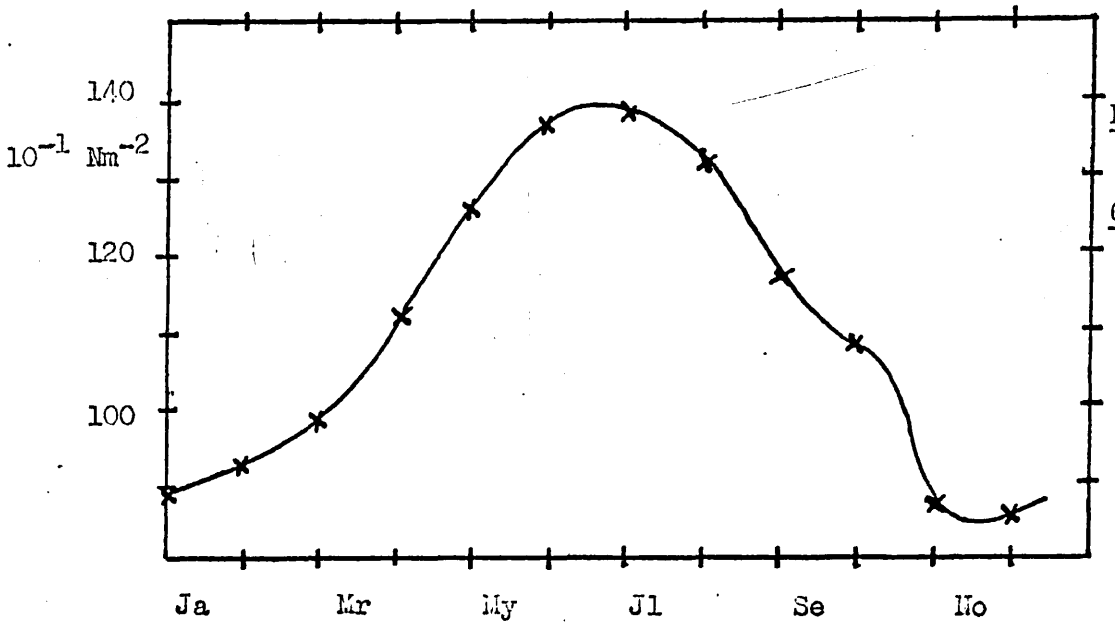

Fig. 2.6

65 km

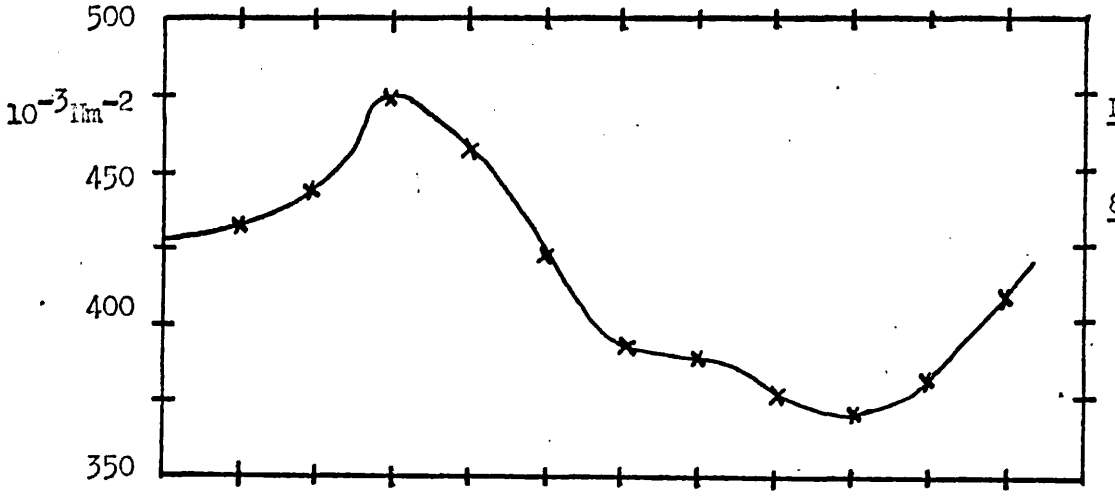

Fig. 2.7

85 km

SEASONAL VARIATION IN PRESSURE

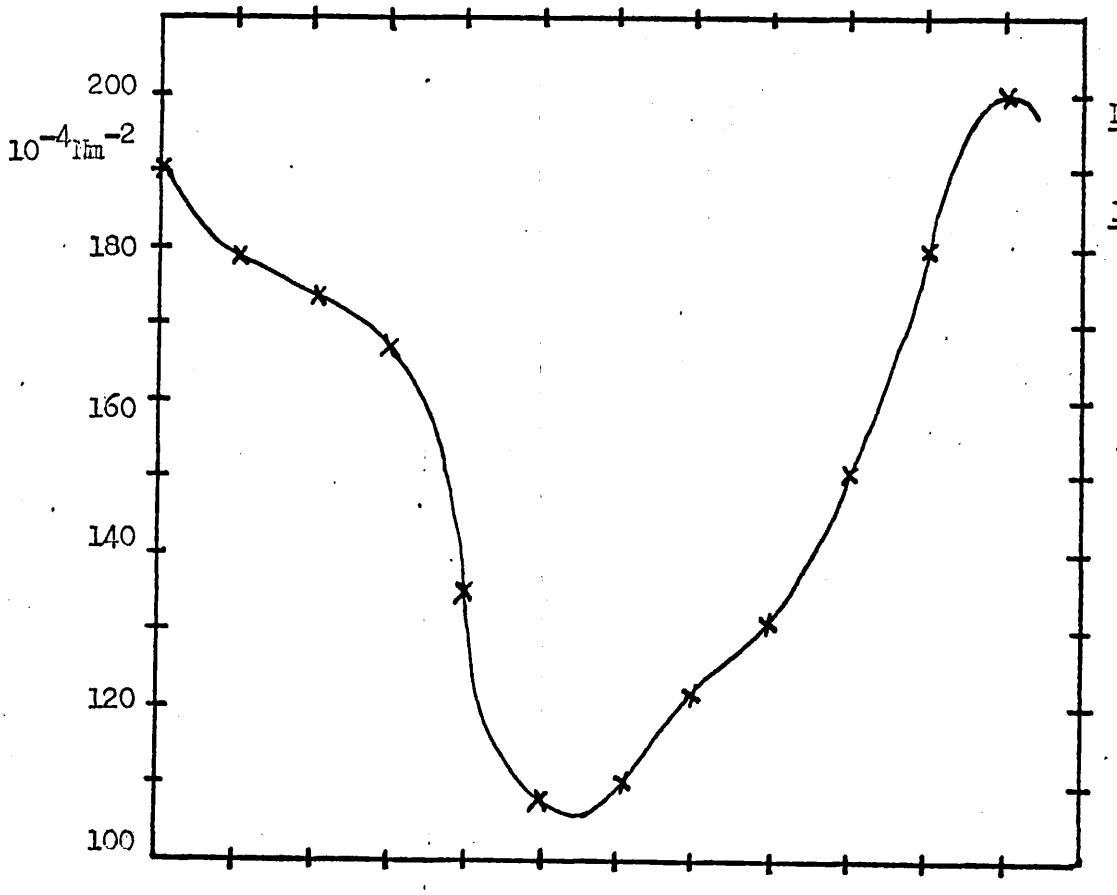

Fig. 2.8

105 km

The mass density model, which is not used in the present work, is calculated from:-

$$\rho = p\frac{M}{RT}$$

Groves points out that there is very little temperature data available for altitudes above about 95 km, and hence the models tend to be rather less certain than at lower heights.

Figs. 2.1 and 2.2 show the temperature and pressure profiles respectively for 1st March and 1st June. Figs. 2.3, 2.4, and 2.5 show the seasonal variation in temperature at 65, 85, and 105 km, Figs. 2.6, 2.7, and 2.8 giving the corresponding variations in pressure. The relative changes in pressure at 85 km suggest that it is nearer to an isopycnic level than the other two heights. Owing to such factors, however, as chemical interaction, non-uniform temperatures, and horizontal winds, the ideal isopycnic state, usually associated with altitudes of about 90 km, is never achieved in practice.

2.3 Composition.

2.3.1 Equilibrium.

The composition of the atmosphere is determined by three different types of equilibrium. Up to about 90 km there is photochemical equilibrium, whereby the production and loss processes of the constituents take place much more quickly than any diffusion effects. Between about 90 and 110 km there is considerable turbulence, which prevents any significant diffusive separation of the constituents. Above this height, however, the atmosphere is in diffusive equilibrium, i.e. the number density of each constituent falls off with increasing height at a rate which is proportional to the molecular weight of that constituent.

2.3.2 Molecular Oxygen and Nitrogen and Atomic Oxygen.

At heights above about 100 km it is possible to obtain number densities of molecular oxygen and nitrogen, and also atomic oxygen, from spectroscopic measurements aboard a rocket of the absorption of solar ultra violet lines as a function of height (Hinteregger and Watanabe, 1963). Another method, which can also be used below 100 km, is to measure the relative concentrations of the constituents in a rocket-borne mass spectrometer. With a knowledge of temperature and pressure, number densities of the constituents can then be calculated.

A major problem with the method is the loss of the highly reactive atomic oxygen by chemical processes inside the rocket, and Thomas (1971) has drawn attention to the consequent lack of data for this constituent at mesospheric heights. Profiles have been calculated, using vertical eddy diffusion considerations, by Colegrove et al. (1965), and Hesstvedt (1969).

Nicolet and Mange (1954) have pointed out that atomic oxygen is produced above about 90 km by the photo dissociation of molecular oxygen:-

$$O_2 + h\nu \rightarrow 2\,O$$

The energy is provided by solar radiation, including Lyman alpha, thus a diurnal variation in the production rate is to be expected. The $n(O)/n(O_2)$ ratio becomes increasingly large with increasing altitude.

The N_2 molecule, having a much smaller photo dissociation cross section than O_2, does not undergo this process to any significant extent.

2.3.3 Ozone.

Distributions of ozone have been deduced from rocket measurements of the absorption of solar X ray flux (Weeks and Smith, 1963), or by airglow emitted in the 80-100 km region (Reed, 1968). The reaction:-

$$O_3 + h\nu \rightarrow O_2 + O \quad (\lambda < 2900\,\text{Å})$$

is the major heating mechanism of the mesosphere. It will be seen also:-

(i) that the reaction must take place in the daytime,

(ii) that it is a source of atomic oxygen.

At night the following reaction becomes important:-

$$O_3 + O \rightarrow 2\,O_2 \quad ,$$

which is then a sink of atomic oxygen.

Thus there are two further reasons for expecting a diurnal variation in the atomic oxygen concentration. It is not unreasonable to suppose that there may well be a similar seasonal variation also.

2.3.4 Metastable Molecular Oxygen.

The excited state metastable oxygen molecule $O_2(^1\Delta_g)$ was suggested by Hunten and McElroy (1968) as an important source of electrons in the D Region, since it is heavily ionised by radiation in the 1027-1118 Å range. More recent work by Huffman et al. (1971) indicates, however, that electron production is less than previously supposed, owing to absorption of the radiation by carbon dioxide.

Hunten and McElroy also suggested the reaction:-

$$N + O_2(^1\Delta_g) \rightarrow NO + O \quad ;$$

thus further assisting electron production, by providing extra nitric oxide for ionisation by Lyman alpha.

The number density of $O_2(^1\Delta_g)$ above 70 km has been determined by Evans et al. (1968), using rocket experiments to measure dayglow emission at 1.27 μm in the transition:-

$$O_2(^1\Delta_g) \rightarrow O_2(^3\Sigma_g^-)$$

Below 70 km concentrations have been predicted by Gattinger and Vallance Jones (1966) from twilight observations of airglow.

The production reactions of the metastable oxygen molecule have been suggested by Green (1966) and Marr (1967):-

$$O_3(S_0) + h\nu^* \rightarrow O_3(S_1)$$

$$O_3(S_1)^* \xrightarrow{\text{BELOW } 3100\,\text{Å}} O_2(^1\Delta_g) + O(^1D)$$

$$O_3(S_1)^* \xrightarrow{\text{BELOW } 1690\,\text{Å}} O_2(^1\Delta_g) + O(^1S)$$

2.3.5 Nitric Oxide.

Nicolet (1945) suggested that the principal source of electrons in the D region is the ionisation of nitric oxide. For this reason it is crucial to have some knowledge of the NO profile.

Kistiakowsky and Volpi (1957) have used a photochemical technique to determine the NO profile from laboratory measurements of rate coefficients. Alternative methods to determine the profile have been:-

(i) From the variation in electron density during a solar cycle (Mitra, 1966);

(ii) From the diurnal variations in electron density (Mitra, 1968);

(iii) From NO^+ and O_2^+ measurements (Wagner, 1966);

(iv) From the simultaneous measurements of electron density and Lyman alpha flux (Smith, 1966b)

A rocket experiment by Barth (1966), which measured the NO γ band dayglow, yielded results over an order of magnitude greater than had previously been predicted. Hesstvedt (1969), using a theoretical model, took the effects of vertical eddy diffusion into account, and,

more recently, Strobel et al. (1970) have considered molecular diffusion also. Using a similar technique to that of Barth, Pearce (1969, and a private communication referenced by Thomas (1971)), and Meira (1971) have been able to confirm that Barth's figures were not an overestimate.

Meira's results are considered to be the best that have been obtained to date for undisturbed conditions. As they represent just two rocket flights in January and February, it is not possible to draw from them any conclusions regarding a seasonal variation. This clearly presents certain problems in the calculation of the seasonal variations in electron density profiles at mesospheric heights, and further reference to this point is made in Chapter 7.

Norton and Barth (1970) and Strobel et al. (1970) have reviewed the various processes governing the production and loss of nitric oxide. The more important of these are thought to be:-

PRODUCTION

(i) $N(^2D) + O_2 \rightarrow NO + O$

(ii) $N + O_2 \rightarrow NO + O$

(iii) $N + O_2(^1\Delta_g) \rightarrow NO + O$

(iv) $NO_2 + O \rightarrow NO + O_2$ [DAY]

LOSS

(v) $NO + h\nu \rightarrow N + O$

(vi) $NO + h\nu \rightarrow NO^+ + e$

(vii) $O_2^+ + NO \rightarrow NO^+ + O_2$

(viii) $N(^2D) + NO \rightarrow N_2 + O$

(ix) $NO + O \rightarrow NO_2$ [NIGHT]

(x) $NO + O_3 \rightarrow NO_2 + O_2$ [NIGHT]

Thomas (1971) has pointed out that reactions (iv) and (x) take place because of the increase in O_3 and decrease in O at lower heights during nighttime. Thus it is expected that below about 70 km there will be more nitric oxide by day than by night. The calculations of Strobel (1971) would be insensitive to changes in NO at such heights.

2.3.6 Water Vapour.

The concentration of water vapour in the mesosphere is calculated from heat exchange variation measurements aboard a rocket (Fedynsky, 1966). Hesstvedt (1968), using photochemical calculations, has considered the effect of vertical eddy transport, whilst Bowman et al. (1970) have shown that this transport compensates for the dissociation of water vapour in the mesosphere. The importance of water vapour lies in the formation of positive water cluster ions.

2.3.7 Positive Ions.

The observations of Narcisi and Bailey (1965), using a quadrupole mass spectrometer suggested that NO^+ and O_2^+ were the dominant ions above 83 km. Below that height, however, the principal ion had a mass of 37^+, interpreted as $H_3O^+.(H_2O)$. Similarly, the ion H_3O^+ was also found. Both these ions were observed to have a sharp cut-off at 82.5 km. The spectrometer detected also the ions of sodium, magnesium, calcium, and molecular nitrogen. In more recent measurements, Goldberg and Blumle (1970) found a cut-off some 4 km higher than that reported by Narcisi and Bailey.

Laboratory measurements had indicated the formation of water cluster ions in the reactions:-

(i) $H_2O^+ + H_2O \rightarrow H_3O^+ + OH$,

(ii) $H_3O^+.(H_2O)_n + H_2O + M \rightarrow H_3O^+.(H_2O)_{n+1} + M$ (n=0,1,2,....8)

but in fact the process is blocked by the reaction:-

(iii) $H_2O^+ + O_2 \rightarrow O_2^+ + H_2O$.

Fehsenfeld and Ferguson (1969) have therefore suggested the following alternative mechanism, where P is either NO or O_2 , and P^+ is the corresponding positive ion:-

(iv) $P^+ + P + M \rightarrow P^+.(P) + M$)
(v) $P^+.(P) + H_2O \rightarrow P^+.(H_2O) + P$) or
(vi) $O_2^+ + H_2O + M \rightarrow O_2^+.(H_2O) + M$

followed by for oxygen either:-

(vii) $O_2^+.(H_2O) + H_2O \rightarrow H_3O^+ + OH + O_2$, and then (ii) or
(viii) $O_2^+.(H_2O) + H_2O \rightarrow H_3O^+.(OH) + O_2$)
(ix) $H_3O^+.(OH) + H_2O \rightarrow H_3O^+.(H_2O) + OH$, and then (ii))

and for nitric oxide:-

(x) $NO^+.(H_2O)_n + H_2O + M \rightarrow NO^+.(H_2O)_{n+1} + M$, until:-)
(xi) $NO^+.(H_2O)_3 + H_2O \rightarrow H_3O^+.(H_2O)_2 + HNO_2$, and then (ii))

It is believed that ions up to $H_3O^+.(H_2O)_8$ can exist, but that they are difficult to detect because of their weak bonding, which leads to rapid breakup of the higher cluster ions when subjected to the rocket's shock wave, or the drawing-in voltage of the mass spectrometer.

Reid (1970) has suggested that the steep ledge generally observed in electron density profiles at about 85 km is caused by the sudden reduction in the water cluster ion concentrations, and that these might have very high dissociative recombination coefficients.

2.3.8 Negative Ions.

Most of the information regarding the concentration of negative ions has been obtained from theoretical models, using rate coefficients measured in the laboratory. On this basis, Fehsenfeld et al. (1967, 1969) have proposed the existence of the ions O^-, O_2^-, O_3^-, O_4^-, CO_3^-, CO_4^-, NO_2^-, and NO_3^-. Narcisi et al. (1969) in their direct measurements detected ions of mass 16^-, 35^-, 37^-, 62^-, and 76^-. Pack and Phelps (1966) have shown that the NO_3^- ion is likely to undergo hydration, becoming $NO_3^-(H_2O)_n$.

Below about 75 km the diurnal changes in O, O_3, NO, and NO_2 concentrations affect the concentrations of their corresponding ions, which in turn affect significantly the value of the effective electron loss coefficient, α, as shown in § 1.4.3. It seems reasonable to suppose that there may be a seasonal variation in this also.

CHAPTER THREE

ABSORPTION

3.1 Introduction.

3.1.1 Attenuation.

If an electromagnetic wave is propagated through an ionised medium, there will be three causes of attenuation:-

(i) An ordinary inverse square law effect;

(ii) An energy loss due to the interactions of the free electrons, accelerated by the wave's field, with neutral molecules, resulting in an increase in the electron temperature;

(iii) Scattering due to irregularities in the medium (an insignificant effect).

The present work will be concerned with (ii), known as absorption, and, in all calculations, allowance is made to remove the effect of (i).

According to Lambert's Law, if a wave of intensity I_0 is incident on a medium of thickness ds, and emerges with intensty I, then:-

$$I = I_0 \exp(-K\,ds),$$

where K is known as the Absorption Coefficient. It will be shown that K is not a constant, but a function of several parameters.

3.1.2 Units of Absorption.

The total absorption suffered by a ground-ionosphere-ground wave reflected at a height h is $2\int_0^h K\,ds$, the unit being the Neper, where the unit of the absorption coefficient, K, is Neper per unit distance. The absorption may alternatively be measured in terms of the Apparent Reflection Coefficient, ρ, such that:-

$$Ln\,\rho = -2\int_0^h K\,ds,$$

or measured in decibels:-

$$L\ (dB) = 8{\cdot}7 \times 2\int_0^h K\, ds\ .$$

Certain stations publish their data in terms of an "A" value, defined by:-

$$A = L\,(f + f_L)^2$$

where L is measured in dB, f is the wave frequency, and f_L the longitudinal component of the gyrofrequency. It will be shown in §4.4.1 that there is previous evidence to suggest that absorption in certain circumstances is proportional to $(f + f_L)^{-2}$ above about 2.0 MHz and away from any critical frequency. Thus the A value of absorption should be independent of the wave frequency.

3.1.3 Collision Frequency.

When the electromagnetic wave accelerates a free electron, there is no real energy loss because, in the absence of collisions, the electron will re-radiate the energy, causing merely a slight change of phase in the wave. The electrons, however, interact by a direct collision process with neutral molecules, and after the collision, their motion is random, and further energy must be supplied from the radio wave in order to restore their regular motion. The energy loss is dependent upon the relative magnitudes of the collision frequency and the wave and gyro frequencies.

The present work will be concerned with data up to an altitude of 110 km, and in this range it is possible to neglect interactions between electrons and positive and negative ions. The collision frequency, ν_M , of monoenergetic electrons is given by:-

$$\nu_M = \sum_i n_i \sigma_i v$$

where n_i is the number density of the i th neutral constituent, σ_i the velocity-dependent momentum transfer cross section,

and v the electron velocity. Provided the electron and neutral molecule temperatures are the same, then a knowledge of the neutral atmosphere temperature and composition, together with laboratory measurements of the cross-sections enable a profile of ν_M to be obtained.

3.2 The Appleton-Hartree Equation.

3.2.1 The Complex Refractive Index.

If a plane electromagnetic wave is travelling in the 1 direction, it can be represented by:-

$$E = E_0 \exp i(\omega t - k x_1) ,$$

where E = Electric intensity,

ω = Angular wave frequency,

t = Time,

k = Propagation factor $= \frac{2\pi}{\lambda} = \frac{n\omega}{c}$,

x_1 = Distance along the 1 axis,

λ = Wavelength,

c = Free space wave velocity,

n = Complex refractive index.

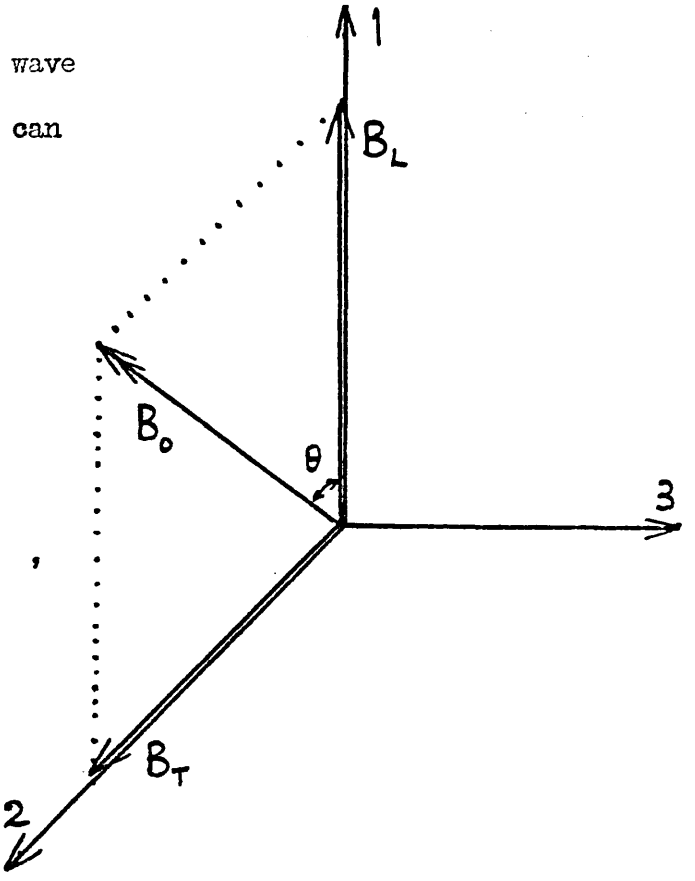

Appleton (1927) and Hartree (1931) showed that in the presence of an imposed magnetic field B_o, and free electrons of number density N(e), n may be found from:-

$$n^2 = 1 - \frac{X}{1 - iZ - \frac{Y_T^2}{2(1-X-iZ)} \pm \sqrt{\frac{Y_T^4}{4(1-X-iZ)^2} + Y_L^2}}$$

where:-

$$X = N(e)\, e^2/\epsilon_0 m \omega^2 ,$$

$$Y_{L,T,0} = e B_{L,T,0}/m\omega ,$$

$$\omega_L = e B_L/m ,$$

$Z = \nu_{eff}/\omega$,

e = Electronic charge,

m = Electronic mass,

ϵ_o = Free space permittivity

ν_{eff} = Effective electron collision frequency.

The relationship between ν_{eff} and ν_M will be explained in § 3.3.2.

3.2.2 Conditions for Reflection.

For reflection of a wave, the refractive index must be zero. It will be seen that this can occur only if the **imaginary part of the** equation is zero (i.e. $\omega \gg \nu_{eff}$). Thus if both real and imaginary parts of n are set equal to zero, the solutions obtained are:-

Positive Square Root:-

(a) $X = 1$

Negative Square Root:-

(b) $X = 1 - Y_o$ (if $f > f_H$), or

(c) $X = 1 + Y_o$ (if $f < f_H$), where $f_H = e B_o/2\pi m$.

There are two distinct modes of propagation. (a) represents the same condition for reflection as would be the case in the absence of the imposed magnetic field, and is therefore called the Ordinary Wave. (b) and (c) represent the Extraordinary Wave.

3.2.3 Critical (Penetration) Frequency.

The maximum value of electron density, $N_m(e)$, within a layer will determine whether a wave of given frequency will penetrate that layer, or be reflected by it.

For the ordinary wave at reflection, X = 1

$$N(e)\, e^2/\epsilon_o m\, \omega^2 = 1$$

$$N(e) = \epsilon_o m \omega^2/e^2 = 4\pi^2 \epsilon_o m f^2/e^2.$$

But $N_m(e) \geqslant N(e)$.

Thus, provided that:-

$$f \leq \frac{e}{2\pi}\sqrt{\frac{N_m(e)}{\epsilon_0 m}}$$

where f is the wave frequency, reflection will occur from the layer.

The critical frequency of the E region for the ordinary wave is given by:-

$$f_0E = \frac{e}{2\pi}\sqrt{\frac{N_m(e)_E}{\epsilon_0 m}}$$

A similar analysis will yield the value of the critical frequency, $f_x E$, for the extraordinary wave.

3.2.4 Quasi-Longitudinal and Quasi-Transverse Approximations.

One of two approximations may be used to simplify the Appleton-Hartree formula:-

(a) $Y_T^4 \gg 4(1-X)^2 Y_L^2$

The Quasi-Transverse mode approximates to the conditions applying where $\theta = 90^\circ$ or $X \approx 1$, although θ itself may be significantly less than 90°. An example occurs near reflection level for the ordinary component of a vertically incident wave.

(b) $Y_T^4 \ll 4(1-X)^2 Y_L^2$

The Quasi-Longitudinal mode approximates to the conditions applying where $\theta = 0^\circ$ and $X \not\approx 1$, for example for the ordinary component of a vertically incident wave, except near reflection level.

As the present work will be concerned with the absorption of the ordinary wave at vertical incidence, further use will be made of the QL approximation. Moreover, Ratcliffe (1959) has shown that if the effects of collisions are included, this approximation can still be satisfactory, even near reflection levels.

3.3 Evaluation of the Absorption Coefficient.

3.3.1 Use of the Appleton-Hartree Equation.

The complex refractive index may be divided into its real and imaginary parts as follows:-

$$n = (\mu - i\chi)$$

Substitution of this into the wave equation:-

$$E = E_0 \exp\left(i\omega t - \frac{\omega}{c} n x_1\right) \quad \text{, yields:-}$$

$$E = E_0 \exp i\left(\omega t - \frac{\omega}{c}[\mu - i\chi]x_1\right)$$

$$= E_0 \exp\left(-\chi \frac{\omega}{c} x_1\right) \exp i\left(\omega t - \mu\frac{\omega}{c} x_1\right)$$

The wave amplitude will decay exponentially with distance, and the absorption coefficient, K, is defined by:-

$$K = \frac{\chi\omega}{c}$$

It may be shown that application of the QL approximation to the complex refractive index formula yields:-

$$K \approx \frac{e^2}{2\epsilon_0 mc} \cdot \frac{1}{\mu} \cdot \frac{N(e)\,\nu_{eff}}{(\omega \pm \omega_L)^2 + \nu_{eff}^2}$$

The + and - signs refer to the ordinary and extraordinary waves respectively (although strictly the approximation cannot be used for the latter).

For the ordinary wave, μ will be given by:-

$$\mu^2 = 1 - \frac{e^2}{\epsilon_0 m} \cdot \frac{N(e)}{\omega^2}$$

3.3.2 Categories of Absorption.

Inspection of the above equation for K suggests three different categories of absorption:-

(i) Non-Deviative Absorption:

a Except near reflection level, where μ is significantly different from 1, K may be simplified to:-

$$K = \frac{e^2}{2\epsilon_0 mc} \cdot \frac{N(e)\,\nu_{eff}}{(\omega+\omega_L)^2+\nu_{eff}^2}$$

b At heights below about 60 km, where $\nu_{eff} \gg \omega$, the equation reduces to:-

$$K = \frac{e^2}{2\epsilon_0 mc} \cdot \frac{N(e)}{\nu_{eff}}$$

The collisions are so frequent here that the electron has not had the opportunity to acquire much energy, hence in the collision there is only a little energy to be lost, and K is theoretically independent of frequency.

(ii) Deviative Absorption:

This occurs near reflection level, where μ is significantly different from 1. For wave frequencies above about 2 MHz, and at those heights where $\omega \gg \nu_{eff}$, N(e) may be eliminated from the absorption equation, yielding:-

$$K = \frac{\nu_{eff}}{2c}\left(\frac{1}{\mu} - \mu\right)$$

3.3.3 Generalised Collision Statistics.

One of the assumptions made in the derivation of the Appleton-Hartree equation is that the collision frequency, ν_{eff} , is independent of electron energy. Phelps and Pack (1959) pointed out, however, that laboratory experiments, using nitrogen, indicated that the collision frequency was directly proportional to the electron energy. This result was confirmed for the case of molecular oxygen by Huxley (1959).

Assuming a Maxwellian energy distribution for electrons, Sen and Wyller (1960) generalised the Appleton-Hartree equation. This is of considerable importance in absorption since it increases the theoretical values of absorption by between 30 and 100 percent. This is because a few electrons with high energy can lose as much energy as many electrons with much less energy.

In the quasi-longitudinal case of the Sen and Wyller generalisation, the expression obtained for the absorption coefficient is:-

$$K = \frac{5}{4} \cdot \frac{1}{\mu} \cdot \frac{N(e)e^2}{\epsilon_0 mc\,\nu_M} C_{5/2}\left(\frac{\omega+\omega_L}{\nu_M}\right) .$$

The C Script integrals have been calculated by Burke and Hara (1963), according to the expression:-

$$C_p(x) = \frac{1}{p!} \int_0^\infty \frac{\phi^p \exp(-\phi)\, d\phi}{\phi^2 + x^2}$$

It may be shown that in the asymptotic limit if $\nu_m \gg \omega$, the classical Appleton-Hartree absorption equation can be used, by setting $\nu_{eff} = 3\nu_m/2$; or, if $\nu_m \ll \omega$, by setting $\nu_{eff} = 5\nu_m/2$, thereby simplifying the calculation of absorption.

3.3.4 Full Wave Theory.

In certain circumstances the whole Appleton-Hartree equation, and even its generalisation, using essentially the concepts of ray optics, is inadequate. It has been assumed that the properties of the medium do not alter appreciably over one wavelength but, in the case of low and very low frequency radio waves this is not the case. In particular, at **reflection** the wavelength of all radio waves will become infinite, if collisions are neglected. In this case, however, it has been shown that the ray theory will yield a more than adequate result except near a critical frequency.

Ratcliffe (1959) and Budden (1966) have studied the effects of the coupling between upgoing and downcoming waves. An analysis of the differential wave equations yields solutions that have no parallel in ray optics.

3.4 Implied Variations in the Absorption Coefficient.

Listed below are the variables which determine the value of K for a given time, altitude, and wave frequency. These are then traced back to the measurable parameters. It will be recalled that N(e) in addition determines the reflection level, which is the upper limit of the integral $\int_0^h K\, dh$.

The magnetic latitude will also affect the absorption, in its value of ω_L at a particular location.

ν_m		$N(e)$	
a	$n(N_2)$,	c	$\cos\chi$
	$n(O_2)$,	d	n(Ionisable constituents)
	$n(O)$	e	n(Absorbing constituents at greater heights)
b	Temperature	f	Solar fluxes at the different wavelengths
		g	Effective electron loss coefficient.

Diurnal Variation

c is the dominant cause, although the nitric oxide concentration is greater at low heights by day than by night, hence d will also be a factor. In addition, g varies at low heights because of the change in negative ion concentration between day and night. There is virtually no diurnal data for a, b, and e, and certainly not on an hour-by-hour basis. It is thought, however, that the effects of any variations of these would be insignificant compared with those of c.

Seasonal Variation

a, b, c, d, e, and possibly g are the causes of the seasonal variation. In addition, f varies slightly due to the inverse square law effect of the sun-earth distance. For a, the seasonal variations in the N_2, O_2, and O concentrations can be estimated if certain restrictive assumptions are made. These will be discussed in detail in §7.1.3.

The seasonal variation in $n(O_2)$ is needed again for e, because the Lyman alpha ionisation of NO depends on the amount of molecular oxygen present to absorb the radiation. It will be shown in Chapter 7 that certain Summer/Winter variations have been suggested by various authors for g, and nitric oxide (part of e), but no month-by-month values exist for either quantity.

Solar Cycle Variation

f is known to be a major cause, although Thomas (1971) has suggested that there may be changes in the concentration of nitric oxide and certain excited constituents. Thrane and Piggott (1966) were unable to find any correlation between ν_m below 110 km and solar epochs.

Groves (1969) has given a preliminary indication of possible density changes in the upper mesosphere and lower thermosphere by a factor of 1.5, but no definite evidence is yet available.

3.5 Experimental Methods.

3.5.1 Vertical Incidence Pulse Absorption.

This method, known as A1, is the standard method for measuring absorption. The lowest frequency which may be used to measure absorption at vertical incidence is $\sim$ 1.6 MHz, being governed by the amount of absorption suffered in the D region, and the signal/noise ratio of the transmitting and receiving system. The upper frequency, $\sim$ 6 MHz, is determined by the ability of the F region to reflect the wave (i.e. $< f_0F_2$).

Both deviative and non-deviative absorption will occur both on upward and downward journeys. In practice, aerial systems are usually designed so that only the ordinary component is received. In any case, the extraordinary component suffers $((f + f_L)/(f - f_L))^2$ times more absorption than the ordinary component.

Owing to fading, a statistical sample over a period is taken to find a mean amplitude. The time should be not less than ten minutes, and not more than about fifteen minutes, or the absorption itself will have changed. The calculation of L values from the strength of the reflected signals involves a knowledge of the receiver calibration factor, itself found from nighttime multiple reflection measurements. Inaccuracies have been shown by Piggott et al. (1957) to be caused by noise, interference,

pulse dispersion, pulse reflection, and scattering.

3.5.2 Relative Ionospheric Opacity, Riometer.

The A2 method of absorption measurement operates at 20-30 MHz, well beyond the penetration frequency f_0F_2, and measures the galactic cosmic noise flux. At higher frequencies there is too little absorption, while at lower frequencies there is too much man-made noise. The apparatus of Little and Leinbach (1958) scans a bandwidth of 100 kHz, finding the minimum noise level, in order to reject interference from radio stations.

It is assumed that the flux incident on the earth's atmosphere is constant from a given direction in space. The ratio of signal strength at a particular sidereal time to one at a similar time will give a measure of the relative ionospheric absorptions. Zero absorption is defined to occur on a night of low magnetic activity.

Most of the absorption occurs in the D and F_2 regions. Because of the low magnitude of absorption, $\sim \frac{1}{4}$ dB, it is not generally used at low latitudes, but is useful in the study of ionisation caused by particle precipitation in auroral polar regions, where the absorption would be too great to permit A1 measurements. Parthasarathy et al. (1963), using several frequencies, have been able to obtain a profile for N(e).

3.5.3 The Continuous Wave Oblique Incidence Method.

This method (A3) is theoretically the simplest means of measuring ionospheric absorption. A pen recorder is connected to the I/F stage of a radio receiver tuned to a distant radio station normally of frequency 0.01-5 MHz. As the ray path through the ionosphere is oblique, the theory is somewhat different from that for vertically incident waves.

It has been shown, however, by Martyn (1935) that, neglecting the imposed geomagnetic field, for an obliquely incident wave of frequency

f, reflected at a true height h, there exists an equivalent vertical frequency f_v , reflected at the same true height, sharing the same virtual height h', and suffering the same absorption as the obliquely incident wave. The relationship between them is given by:-

$$f = f_v \sec \phi_o$$

A disadvantage of the method is that it is not always possible to distinguish between the several different paths by which the composite wave has travelled; and for an unambiguous analysis of the measurements, the receiver should be carefully calibrated. It is important also that the transmitter power should be constant.

In order to calculate the absorption in dB, ideally the signal strength should be compared with that on a night when there is a strongly reflecting Es layer present. Since this does not occur very frequently, Schwentek (1965) has suggested a means of determining the approximate Es signal strength by extrapolating the graphs of the diurnal variation.

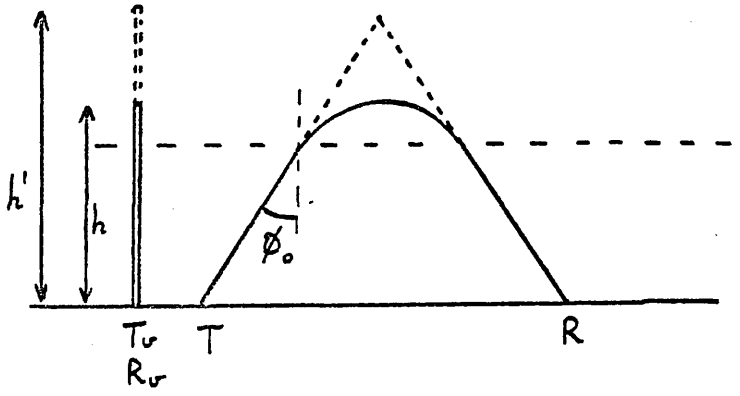

The Equivalence Theorem of Martyn

for plane earth and plane ionosphere

CHAPTER FOUR

PREVIOUS EXPERIMENTAL WORK

4.1 Superimposition of Temporal Variations.

Owing to a constantly changing ionosphere, due to such causes as winds and turbulence, there is a large random variation in the amount of absorption suffered by a radio wave at any one time. There are, in addition, superimposed on each other, diurnal, seasonal, and solar cycle variations in absorption. If any one of these three variations is to be observed, then the effects of the other two must be eliminated, and a sufficient number of measurements taken to minimise the effect of the random variation.

4.2 Solar Cycle Variation.

Using data for mean monthly noon absorption at 4 MHz (A1) at Cambridge (52.2°N 0.1°E) and Slough (51.5°N 0.6°W) for the period 1935-1952, Appleton and Piggott (1954) found that for each individual month, i there was a reasonably linear relationship between absorption L, and sunspot number R of the form:-

$$L = a_i + b_i' R$$

where the constants a_i and b_i' were found by the method of least squares. Alternatively, the equation may be expressed as:-

$$L = a_i(1 + b_i R)$$

Appleton and Piggott obtained the following values for a_i and b_i :-

i	Jan.	Feb.	Mar.	Apr.	May	Jun.	Jul.	Aug.	Sep.	Oct.	Nov.	Dec.
a_i (dB)	10.4	11.3	12.2	12.2	13.0	12.2	13.0	13.0	12.2	9.6	8.7	8.7
$10^3 \times b_i$ (R^{-1})	9.2	7.0	7.5	11.3	10.9	13.2	11.1	8.5	8.8	8.9	8.3	9.6

In a similar analysis of data at Ibadan (7.4°N 3.9°E), Skinner and Wright (1964) reported the following values for $10^3 \times b_i$ at 2.4 MHz:-

2.7 3.1 2.9 2.4 2.2 2.2 1.9 2.3 2.7 2.2 3.2 2.9

Its mean annual value of 2.6×10^{-3} compared with the corresponding value of 3.5×10^{-3} at 5.7 MHz, and agreed well with the value of 3.0×10^{-3} obtained by Skinner (1956) for Singapore (1.3°N 103.8°E). The values tended to be larger at Southern solstice than at Northern solstice or equinoxes. The larger overall values at Slough were ascribed to increased E and F region absorption in temperate latitudes. Because of this, and also the fact that the percentage of D region absorption is smaller at 5.7 MHz than at 2.4 MHz, it was proposed that there is more sunspot control over the E region than over the D region.

Bibl et al. (1965), from observations of twelve month running means of noon absorption at Freiburg (48.1°N 7.6°E) have considered the relative variation of the deviative and non-deviative components (as defined by Bibl and Rawer (1951)), with changes in sunspot number. They found that although the deviative absorption was the more dependent upon solar activity, if R became greater than 160, no further increase in absorption of this type occurred.

From vertical incidence measurements at Waltair (17.7°N 83.3°E) during 1963 and 1964, Rao and Rao (1968) obtained from monthly values of b, annual means of value 4.14×10^{-3}, 8.44×10^{-3}, and 9.58×10^{-3} for 2.0, 2.5, and 3.0 MHz respectively. Although these results are internally consistent with the conclusion drawn by Skinner and Wright (1964), they are overall somewhat higher than previous observations. Since in this case only two years' measurements have been examined, both of low solar activity, the results are not as statistically significant as those in the above references.

In an analysis of a and b, using twelve month running means of absorption at Freiburg, de Bilt (52.1°N 5.2°E), Kokubunji (35.7°N 139.5°E), and Monte Capellino (44.6°N 9.0°E), Higashimura et al. (1969) found that a increased steadily from 24.0 dB at de Bilt to 28.5 dB at Kokubunji. No such dependence was found for b, whose values were found to be nominally constant at $(4.3 \pm .2) \times 10^{-3}$. (This method precludes an evaluation of the

seasonal variation.)

4.3 Diurnal and Seasonal Variations in Absorption.

4.3.1 Some Theoretical Considerations.

Appleton and Piggott (1954) employed equations devised by Appleton (1937), in order to compare their experimental data with theoretical values of the total absorption. Assuming that there was a single Chapman layer with no deviative absorption, Appleton showed that for the ordinary component:-

$$\int_0^h K\,dh \quad \propto \quad \cos^{3/2}\chi/(\omega+\omega_L)^2$$

if the effective electron loss coefficient, α, is independent of pressure; or, if α is proportional to pressure:-

$$\int_0^h K\,dh \quad \propto \quad \cos\chi/(\omega+\omega_L)^2$$

Jaeger (1947) considered the absorption suffered by a wave either transmitted through or reflected by a Chapman layer. For a vertically incident wave, and neglecting the geomagnetic field, the total absorption within the layer varies according to:-

$$-Ln\,\rho \quad \propto \quad \cos\chi\ F(f/f_o)$$

where F is an analytic function of f, f_o, and $\cos\chi$, whose values have been tabulated by Jaeger. This function takes the form of an integral, whose limits are determined by whether f is greater than or less than f_o, in which case reflection will not take place within the layer, but at some higher level.

Bibl and Rawer (1951) and Bibl et al. (1962) have shown that absorption can be expressed in terms of its non-deviative and deviative components:-

$$L_{(f)} = A/(f \pm f_L)^2 \quad + B\ F(f/f_o E)$$

and where the measurements of several frequencies are available, the constants A and B can be found graphically ("Spider's Web Nomogram").

Piggott (1964) has pointed out, however, that certain of the assumptions made in calculating $F(f/f_oE)$, for example the profiles of ν , and α , and the use of the QL approximation for deviative absorption, tend to make the method unreliable.

4.3.2 Presentation of Results.

In measurements of absorption as a function of another quantity, x, a choice exists as to which parameters shall vary and which shall remain fixed. Below are listed the different possibilities:-

	x	Variable	Fixed	Type
(i)	χ	Time	Date, f	Diurnal
(ii)	χ	Time, f	Date, (f/f_oE)	Diurnal
(iii)	χ	Date	Time, f	Seasonal
(iv)	Date	Time	χ , f	Seasonal

(v) As (i) or (iv), but "Daytime Absorption", L_D' , caused by solar radiation is calculated from:-

$$L_D' = L_{OBSERVED} - L_{(\chi=90°)}$$

It will be shown how these different methods can yield information about different aspects of the ionosphere. The fixed time is usually local noon. Because there is a diurnal variation superimposed upon the seasonal variation, the results of methods (iii) and (iv) will have quite different meanings, and, as such, they cannot be readily compared.

4.3.3 Previous Results.

The value of the exponent in the $\cos\chi$ relationship was first investigated experimentally by Appleton (1937). Using (iii), he obtained the result $n = 0.8$. For the diurnal variations (i), Best and Ratcliffe (1938) obtained the value 1.5, but Taylor's (1948) value was 0.87 . The results of various authors indicated a decrease in the value of n

with increasing frequency. Appleton and Piggott (1954), reviewing the various values, suggested 0.7 as a mean for sunspot minimum conditions, and 0.75 for sunspot maximum.

Beynon and Davies (1955) in their analysis of absorption measurements of types (i), (ii), (iii), and (iv) made at Swansea (51.6°N 4.0°W), concluded that in the months March - October both diurnal and seasonal variations in absorption could be represented by:-

$$L = A + B\,F(f/f_{oE})\cos\chi$$

where the term A varies with solar activity, and F is the Jaeger function. In the remaining four months, because of anomalously high absorption by day, the above formula was only suitable for diurnal variations.

Skinner and Wright (1964) investigated the absorption at Ibadan (7.4°N 3.9°E) by methods (i) and (iii) for six frequencies from 2.0 to 7.5 MHz. They found that the $\cos^n\chi$ law was obeyed only approximately. The mean seasonal value for n at 2.4 MHz was found to be 0.9 at sunspot maximum and 1.6 at sunspot minimum. They showed also a seasonal variation in the diurnal value of n.

Bibl et al. (1965) from a long term series of observations at Freiburg (48.1°N 7.6°E), reported that the diurnal variation was caused mainly by non-deviative absorption, and that in the diurnal variation there existed greater absorption in the evening than at the time of equal χ in the morning. They suggested also that the seasonal variation might be produced by the systematic variation in height of the E region.

Davies (1965) has drawn attention to a decrease in n at high latitudes, and to some evidence suggesting a small decrease in equatorial regions also.

In a survey of A3 absorption measurements, Lauter (1966) has pointed out that if diurnal results for low frequencies are calculated by method (v), then values of n between 1.3 and 1.5 are obtained.

Kotadia and Patel (1969) have investigated the effects of lunar variation on radio waves at different frequencies over a period of nine years. They conclude that the effect of lunar variation in absorption is semi-diurnal at solar maximum, but diurnal at sunspot minimum. The semi-diurnal variation affects h'E, and seems to affect the absorption particularly if the wave frequency is close to f_0E. The maximum lunar variation is $\sim \pm$ 0.5 percent.

4.3.4 Diurnal Deviations from the $\cos^n \chi$ Law.

An analysis of Appleton and Piggott's diurnal data indicated that maximum absorption occurred in general about twenty minutes after local noon. It had previously been shown by Appleton (1953) that the time of occurrence of peak electron density in any layer suffers a delay on that of peak electron production by an amount given approximately by:-

$$\tau = 1/2\alpha N(e)$$

the effect being analagous to the relaxation time in a plasma.

Nitzsche (1967) has shown that diurnal data (i) for oblique incidence absorption, L'_t, at Neustrelitz (53.3°N 13.1°E) is given by:-

$$L'_t = L_0 \cos^n \chi_{t-\tau}$$

and a logarithmic plot of L'_t as a function of $\cos \chi_{t-\tau}$ will yield, with suitable choice of τ, an excellent straight line. The values obtained are:-

2614 kHz	395 km		2775 kHz	220 km
n	(Min.)		n	(Min.)
1.00	25	Spring	1.00	18
0.64	40	Summer	0.64	40
0.55	10	Autumn	0.78	15
0.59	15	Winter	0.50	20

The large Summer delay tends to suggest a reduction in α at this season, especially in view of the increase in N(e).

4.3.5 Seasonal Deviations from the $\cos^n\chi$ Law.

In an analysis of Winter Anomaly, Beynon and Jones (1965a) indicated the presence of a lag in the seasonal variation in absorption, similar to the diurnal delay, so that a plot of Log L against Log ($\cos\chi$) did not yield a straight line of slope n, but became instead a loop. They suggested that the cause was meteorological rather than geomagnetic in origin, and showed that certain meteorological parameters yielded similar curves when so plotted.

Certain authors, such as Wakai et al. (1969) and Higashimura et al. (1969) have found the least squares straight line, although a loop is quite clearly present in the data that they exhibit.

Lauter and Mitzsche (1967) have shown semi-annual variations in absorption (iv) for a low sun height ($\cos\chi = 0.2$), with minima, of different magnitudes, in April and October.

4.4 Further Experimental Absorption Results.

4.4.1 The Variation of Absorption with Frequency.

Both of the equations derived by Appleton (1937) for the total absorption, imply that it is proportional to $1/(f + f_L)^2$. Appleton and Piggott (1954) investigated the experimental validity of the relationship over a range from 1.2 to 5.5 MHz, by measuring the absorption at noon on certain fixed days. Except below about 2.0 MHz and near the critical frequencies, a straight line was obtained for a plot of $L^{-\frac{1}{2}}$ against f, with a frequency intercept of -1.2 MHz, compared with the theoretical value for f_L of 1.16 MHz.

Reference has already been made to the frequency-dependent function of Beynon and Davies (1955). Skinner and Wright (1956, and 1964) have pointed out that a $1/(f + f_L)$ relationship holds for the absorption measurements at Ibadan. A similar dependence was found by Yasuda (1963)

at Kokubunji (35.7°N 139.5°E). Rao et al. (1962) obtain a $1/(f + f_L)^m$ relationship for Delhi (28.6°N 77.2°E), with values of m ranging from 1.1 to 2.4 .

Whitehead's (1957) formula for absorption at Slough (51.5°N 0.6°W) and Cambridge (52.2°N 0.1°E) is:-

$$L = B/(f + f_L)^2 + C$$

where B and C show different seasonal variations. The results of the present work appear to confirm the need for a seasonal variation in frequency dependence.

The relative accuracies of the various empirical formulae in certain limited conditions have been compared by Jain and Setty (1968).

4.4.2 Winter Anomaly and Sudden Stratospheric Warmings.

The worst deviation from a linear relationship between Log L and Log ($\cos\chi$) is to be found in the Winter months, for which the absorption is anomalously high. The Winter Anomaly is not uniform but on certain groups of days particularly high absorption will occur. Appleton and Piggott (1954) have shown that the effect does not occur near the equator, being a maximum at mid latitudes. Appleton and Piggott have suggested that it is caused neither by magnetic activity nor by changes in the intensity of solar radiation.

Thomas (1962) has shown that at any one time the area over which the effect is observed is of the order of 10^6 km^2. Gregory (1965) suggested that it might be caused by vertical transport of ionisable constituents.

A possible relation with a lower altitude phenomenon, known as a Sudden Stratospheric Warming (Stratwarm), was first investigated and shown to exist by Bossolasco and Elena (1963a,b). In a stratwarm, the temperature at the 10 mb (30 km) level rises suddenly by up to 50° C

for a period of about a week over an area of similar size to that of Winter Anomaly, and is accompanied by a dramatic change in the upper stratospheric structure and circulation pattern.

The superposed epoch analysis of Shapley and Beynon (1965) indicated that an 18° C increase in the 10 mb temperature resulted in a 25 percent increase in ionospheric absorption at 1 MHz. Belrose (1967) has detected changes in the VLF phase height and increases in absorption when stratwarms occur.

Mawdsley (1961) and Sechrist (1967) have proposed that the Winter Anomaly might be caused by an enhancement of the nitric oxide concentration, itself produced by a mesospheric warming, related perhaps to a corresponding stratospheric warming.

Beynon and Jones (1965b) have indicated a statistical relationship between stratospheric warmings and increases both in the maximum virtual height of reflection from the E region, and in f_0F_2.

CHAPTER FIVE

THE PRESENT EXPERIMENTAL WORK

5.1 Equipment.

The experimental work was carried out on the top floor of a building in central London (51.5°N 0.1°W). The equipment consisted of two HRO-M radio receivers, and two 1 ma F.S.D. pen recorders operating at 1 inch per hour. The recorders were connected to an amplified signal of the I/F stage of the output, the circuit diagram for this modification being shown in Fig. 5.1 .

Owing to both intermittent fading of the radio signal, and also occasional electrical interference, it was initially found very difficult to determine the mean reading on the paper chart at any one time (Fig. 5.2). The capacitance was increased from 1 μF to 5 μF, and the improvement can be seen in Fig. 5.3 , although this did result in the system having a time constant of about fifteen minutes. Consequently, as with A1 measurements, the value of signal strength read from the paper chart for a particular time represented an average value for a period round about that time. As noon measurements of absorption were being taken, and as absorption changes rapidly only at sunrise and sunset, this was of no importance.

The aerial for each receiver was at a height of approximately 15 m above ground level, pointing in the direction of the transmitting stations. At frequent intervals each receiver was calibrated, using a Marconi TF. 144G signal generator.

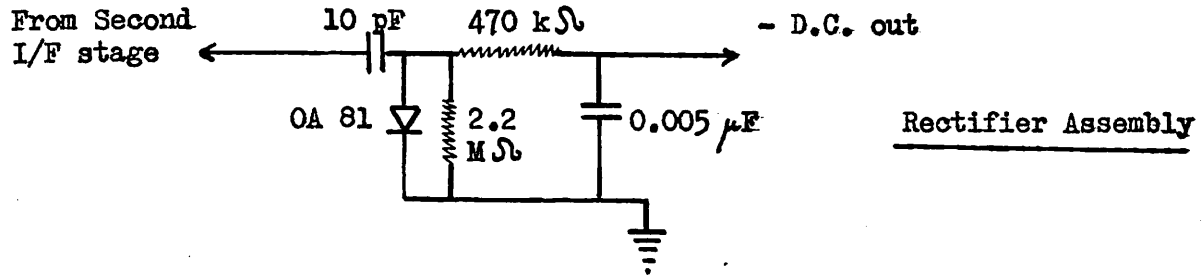

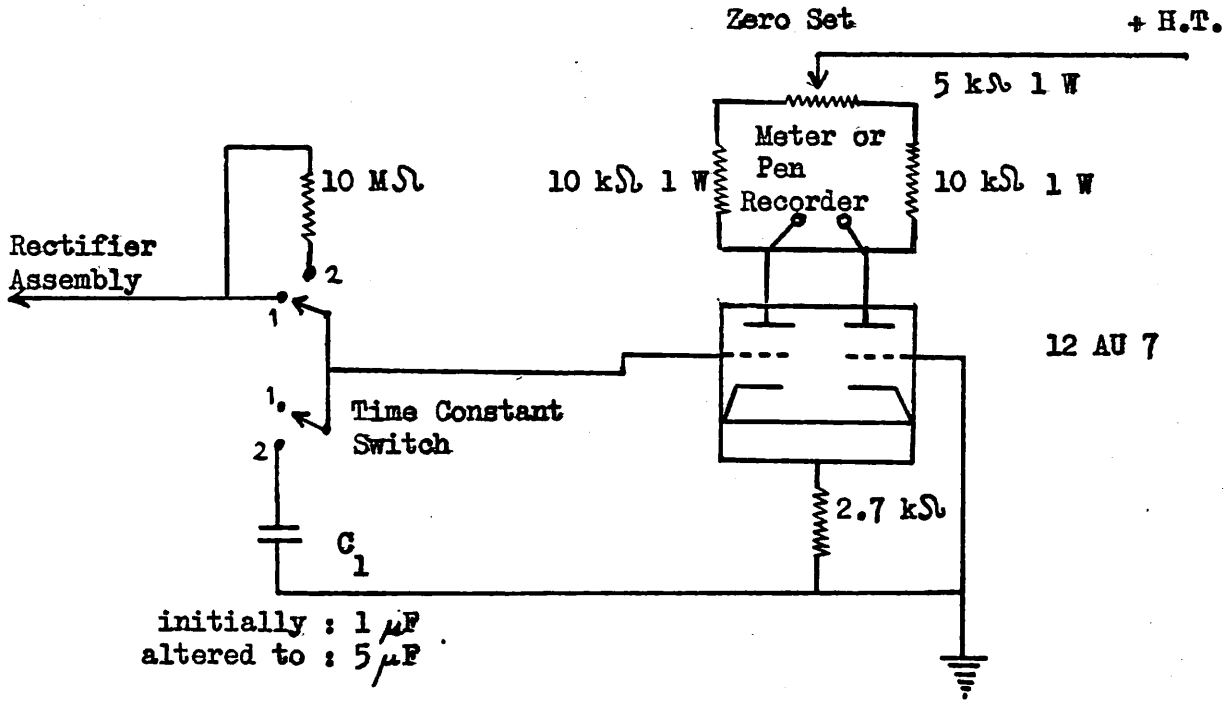

Amplification Circuit with Output for Meter or Pen Recorder

Fig. 5.1

Modification to HRO-M Radio Receivers

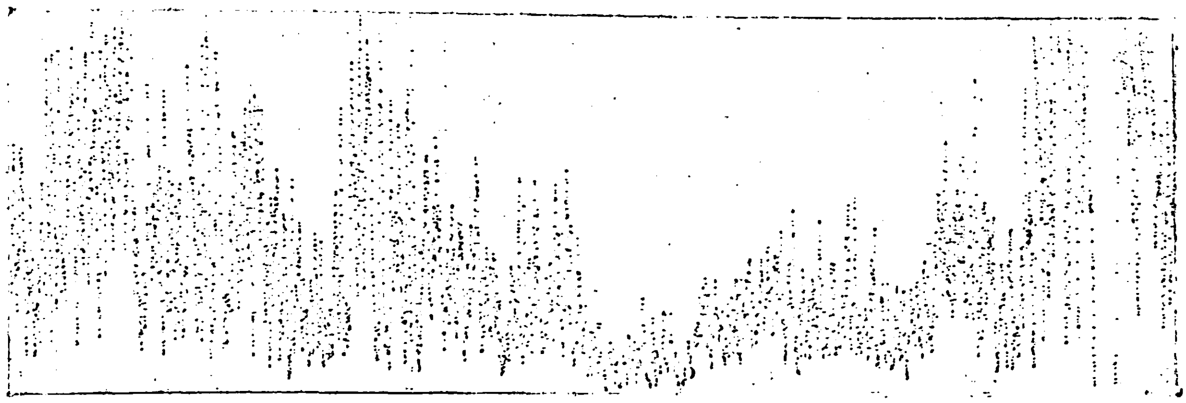

Fig. 5.2 Paper Chart ($C_1 = 1\mu F$)

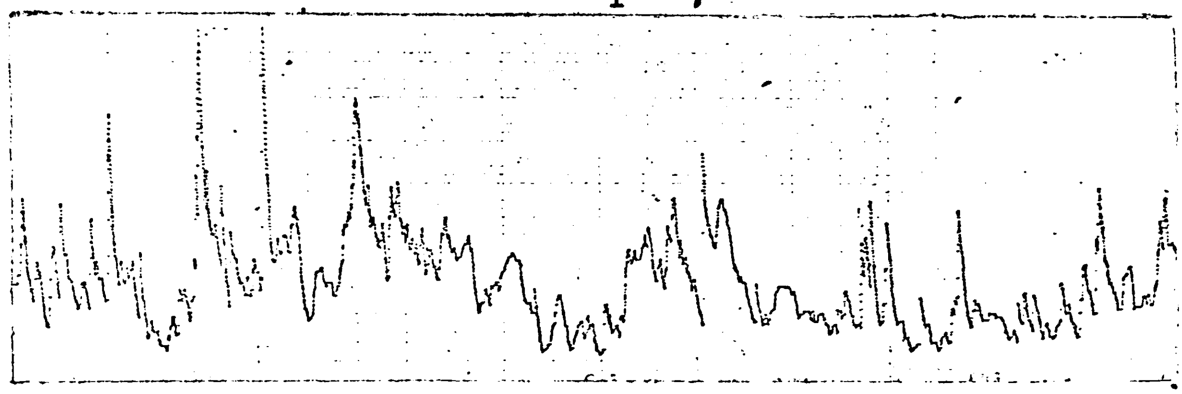

Fig. 5.3 Paper Chart ($C_1 = 5\mu F$)

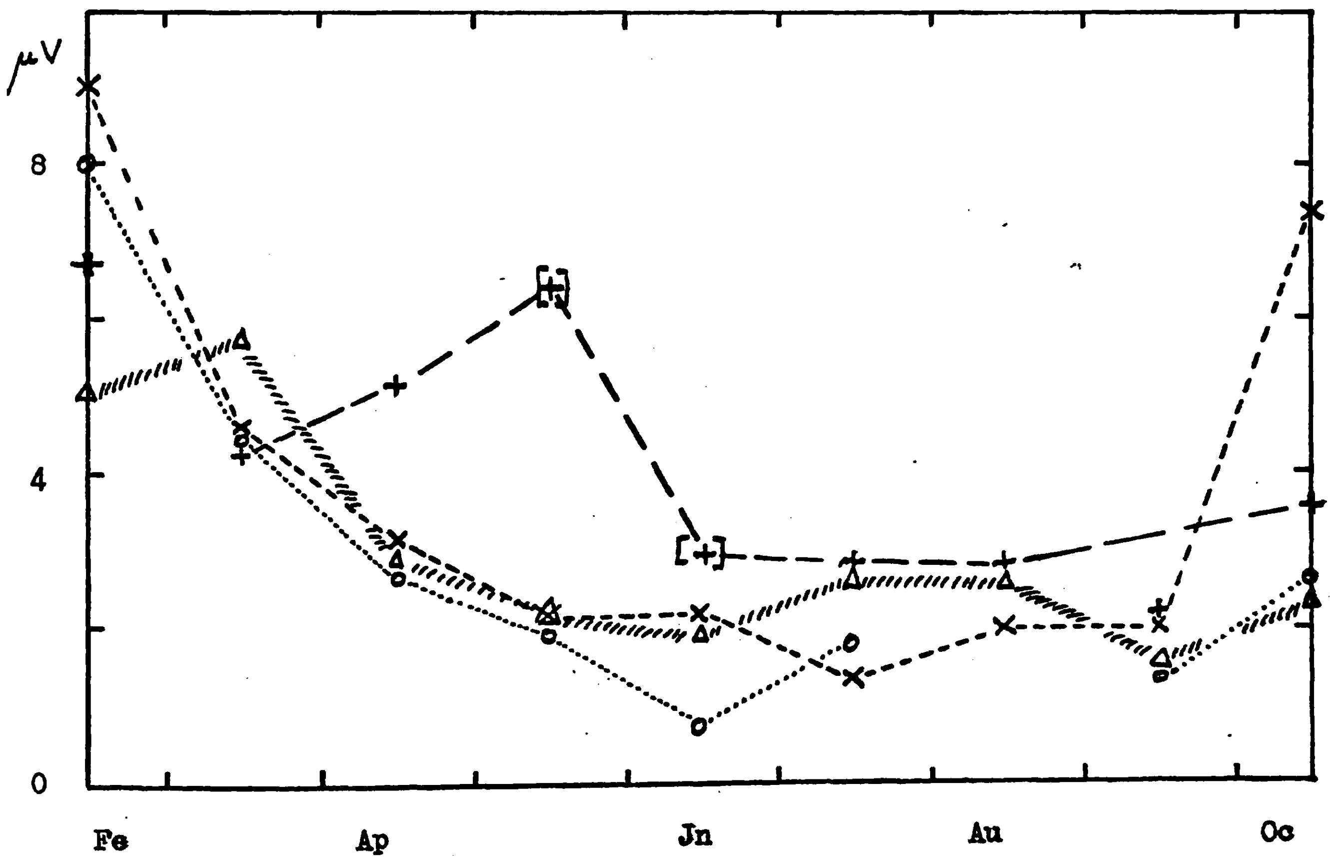

Fig. 5.4 Seasonal Variation in Noon Signal Field Strengths

1969		1970
- - - - - -×	Luxembourg (RX 1)	..........o
— — —+	Strasbourg (RX 2)	////////////Δ

[ ] Potentially unreliable value; see text.

5.2 The Method.

Receiver 1 was tuned to Radio Luxembourg (49.6°N 6.1°E) at a transmitting frequency of 1.434 MHz, and Receiver 2 to Radio Strasbourg (48.6°N 7.9°E) at 1.277 MHz. The horizontal transmission distances are 500 and 650 km, corresponding to equivalent vertical frequencies of approximately 500 kHz and 300 kHz respectively.

Periodically the R/F gain control was adjusted so that the reading of the pen recorder was approximately in the middle of the chart at midday, to facilitate interpretation of the charts.

From the charts and the calibration data were found the monthly median values of the field strengths of the signals detected by the receivers. The taking of monthly medians further reduces the possibility of electrical interference affecting the result.

5.3 The Results and Discussion.

The results are given in the table below. A ÷ sign against a value indicates that the monthly median is based upon only a small number of daily values due to technical reasons.

	Feb.	Mar.	Apr.	May	Jun.	Jul.	Aug.	Sep.	Oct.	
					1969					
RX 1	9.0	4.6	3.2	2.3	2.3	1.4	2.1	2.1	7.5	μV
RX 2	6.7	4.3	5.2	÷6.4	÷3.0	2.9	2.8	2.2	3.6	
					1970					
RX 1	8.0	4.5	2.8	2.0	0.9	1.8	÷ -	1.4	2.7	μV
RX 2	5.1	5.8	3.0	2.3	2.0	2.7	2.7	1.5	2.5	

These results are shown plotted in Fig. 5.4 .

It will be seen that in 1969 the peak absorption occurred in about mid-July for RX 1 and about mid-September for RX 2. 1970 is rather more difficult to judge for RX 1 because of the missing data. It would seem, however, that for both stations there is a peak of absorption in June and another in about September. It may be significant that for all four measurements, the September absorption is rather higher than might be expected from a simple $\cos^n\chi$ law.

The results of these, and other oblique incidence measurements will be further discussed in §7.6 .

CHAPTER SIX

THE ANALYSIS

6.1 List of the Stations.

The monthly median values of noon absorption at the following stations were examined:-

SLOUGH (51.5°N 0.6°W) A1

Freq. MHz / Year	2.0	2.4	2.8	3.2	4.0	4.8
1947	X	X	X	X	X	X
1948	X	X	X	X	X	X
1949	X	X	X	X	X	X
1950	X	X	X	X	X	X
1951	X	X	X	X	X	X
1952	X	X	X	X	X	X
1953	X	X	X	X	X	X
1954	X	X	X	X	X	X
1955	X	X	X	X	X	X

FREIBURG (48.1°N 7.6°E) A1

Freq. MHz / Year	1.725	2.05	2.44	2.90	3.45	4.10	4.88	5.80
1956	÷	X	÷	X	÷	X	÷	÷
1957	X	X	X	X	X	X	X	÷
1958	X	X	X	X	X	X	X	X
1959	X	X	X	X	X	X	X	X
1960	X	X	X	X	X	X	X	X
1961	X	X	X	X	X	X	X	÷
1962	X	X	X	X	X	X	X	
1963	X	X	X	X	X	X	÷	
1964	X	X	X	X	X	X		
1965	X	X	X	X	X	X		
1966	X	X	X	X	X	X	÷	
1967	X	X	X	X	X	X	X	
1968	X	X	X	X	X	X	X	
1969	X	X	X	X	X	X	X	

DE BILT (52.1°N 5.2°E) A1

Freq. MHz / Year	1.95	2.30	2.60	2.90	3.20
1958	X	X	X	X	X
1961	X	X	X	X	X
1962	X	X	X	X	X
1963	X	X	X	X	X
1964	X	X	X	X	X
1965	X	X	X	X	X
1966	X	X	X	X	X
1968	÷	÷	÷	÷	÷
1969	÷	÷	÷	÷	÷

PORT STANLEY, FALKLAND ISLANDS (51.7°S 57.8°W) A1 2.6 MHz

≒ 1950, 1951, 1952, 1955, 1957, 1959, 1960

KOKUBUNJI (35.7°N 139.5°E) A1 2.4 MHz

≒ 1957, 1958, 1959, 1960, 1961, 1962, 1963, 1964, 1965.

IBADAN (7.4°N 3.9°E) A1 2.0, 2.4, 3.05, 4.0, 5.8 MHz

≒ 1954, 1955, 1956, 1958.

LINDAU (51.7°N 10.1°E) DAN Norddeich Radio 2.614 MHz A3 ($f_v \approx$ 1.5MHz)
(Reflection Point 52.7 N 10.1 E)

≒ 1957, 1958, 1959, 1960, 1961, 1962, 1963, 1964, 1965.

A ≒ sign denotes that absorption measurements were plotted on a long term basis, and an X indicates that in addition they were analysed on a year by year basis. Where a year by year examination did not take place, it was for one or more of the following reasons:-

(i) One or more months' measurements were unavailable;

(ii) It was visually clear that no reasonable curve could be fitted for the seasonal variation;

(iii) There were insufficient measurements of a similar type with which to compare the results.

Individual years' measurements were also analysed for the following stations (frequencies in MHz):-

1958, 1959	Alma Ata (43.2°N 76.9°E)	A1 2.2, 3.0
	Ashkabad (37.9°N 58.3°E)	A1 2.2, 3.0
	Kuhlungsborn (54.1°N 11.8°E)	A3 0.245, 1.178
1958	Moscow (55.5°N 37.3°E)	A1 2.2, 3.0
1959	Murmansk (69.0°N 33.0°E)	A1 2.2, 3.0
1964, 1965	Aberystwyth (52.4°N 4.1°W)	A1 1.95, 3.50
	Kokubunji (35.7°N 139.5°E)	A1 2.00, 2.40
	Rugen (54.4°N 13.3°E)	A1 3.86
	Akita (39.7°N 140.1°E)	A3 2.5

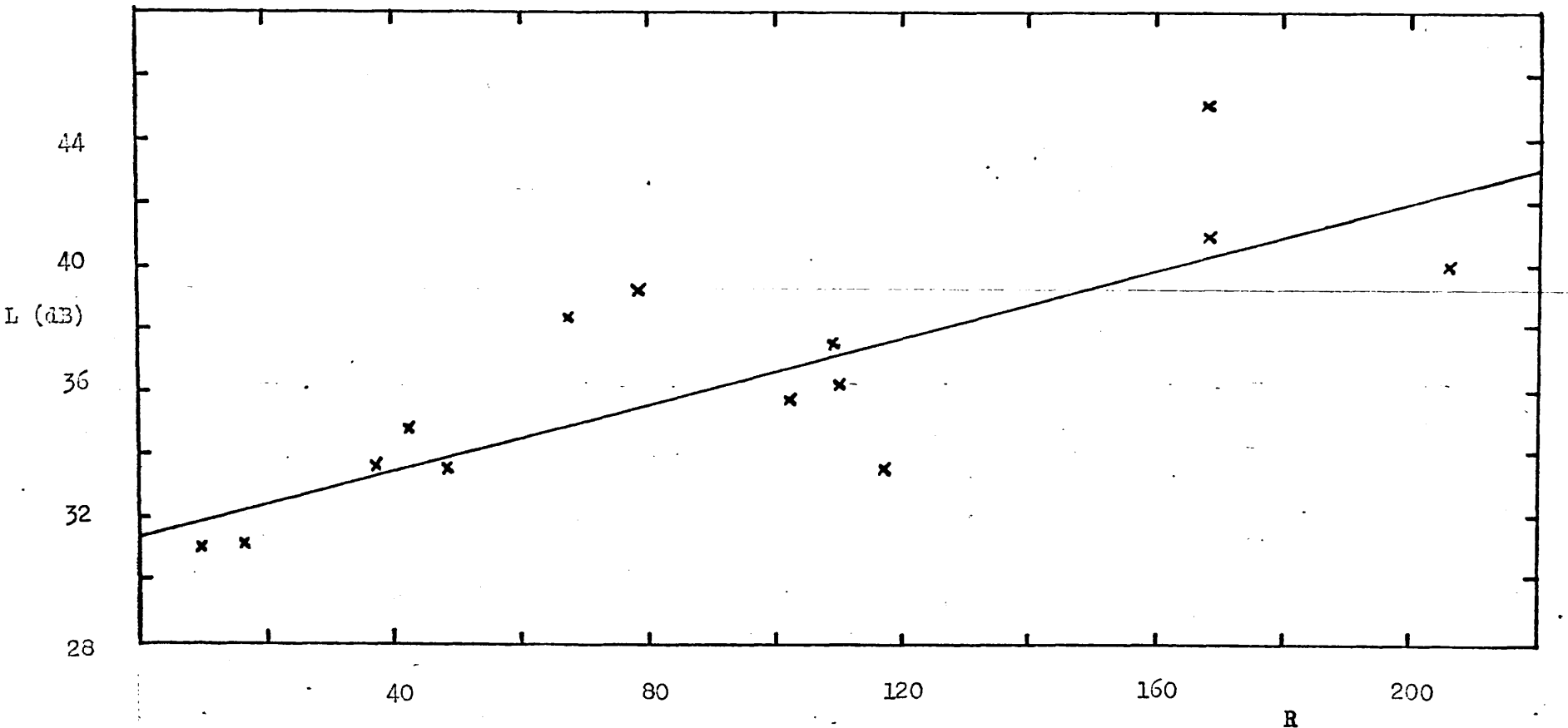

Fig. 6.1

The variation of absorption, L, with sunspot number, R .

(Freiburg, June, 2.44 MHz)

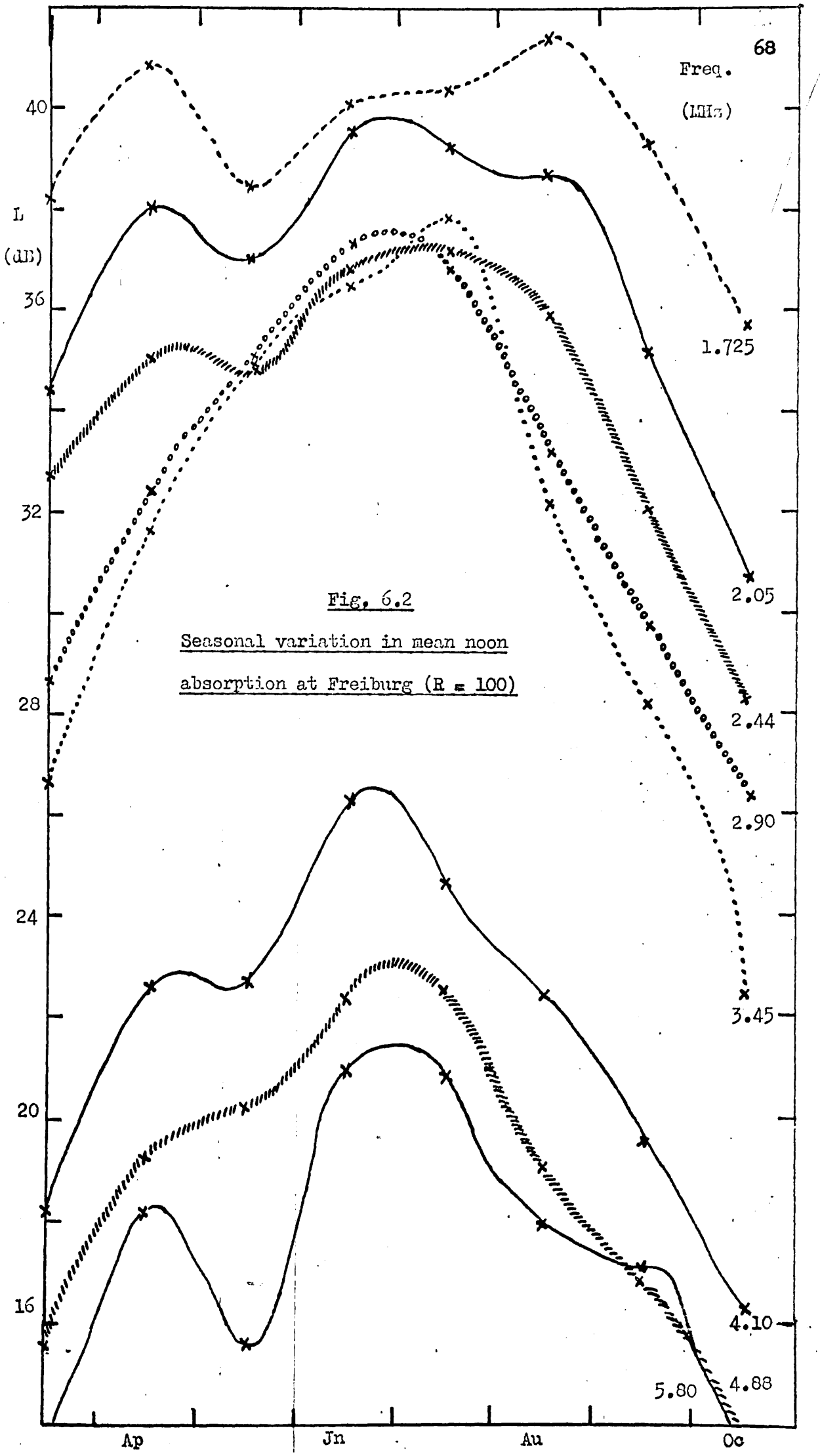

Fig. 6.2

Seasonal variation in mean noon absorption at Freiburg (R = 100)

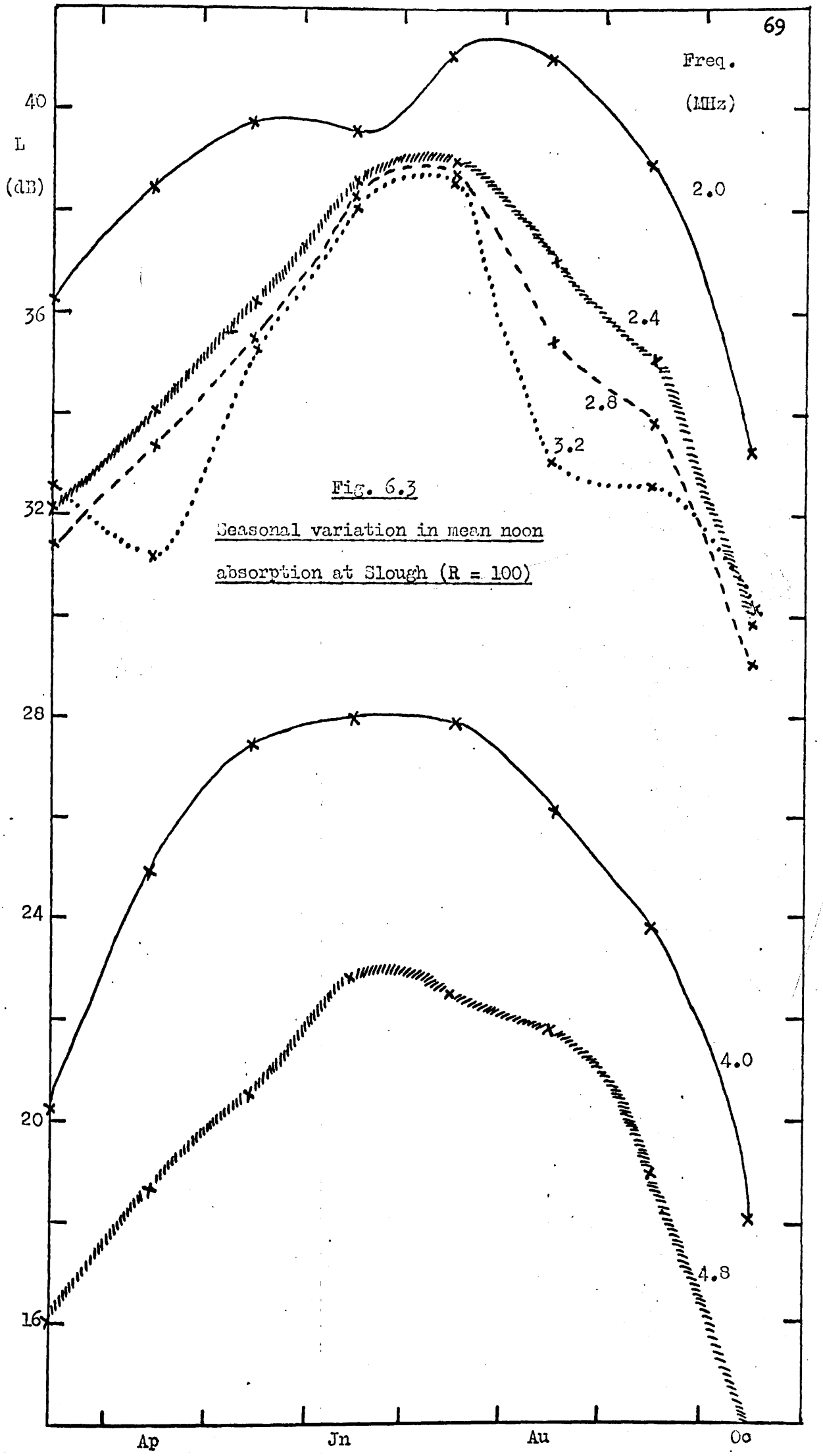

Fig. 6.3

Seasonal variation in mean noon absorption at Slough (R = 100)

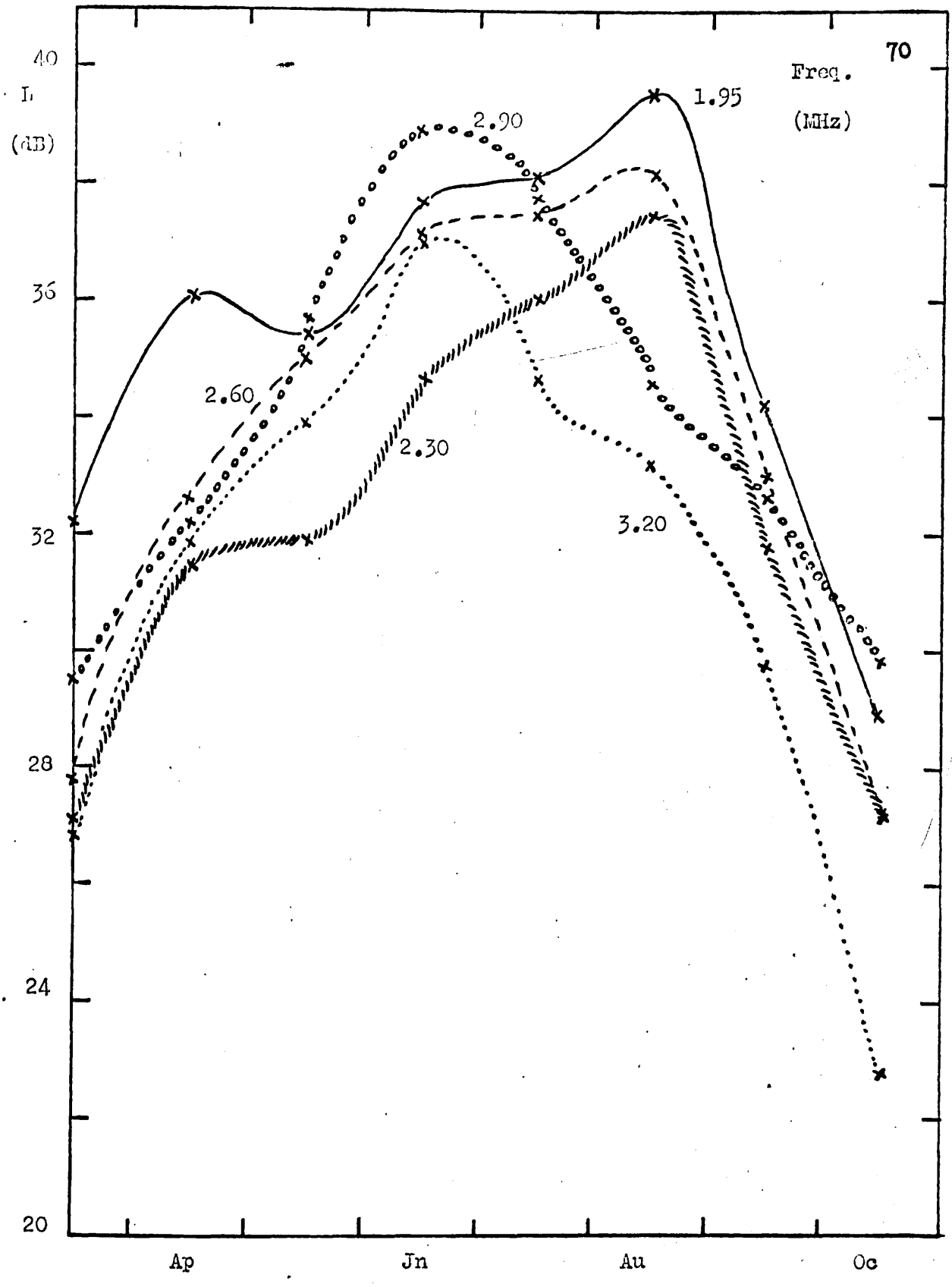

Fig. 6.4

Seasonal variation in mean noon absorption at de Bilt (R = 100)

1964, 1965,)(Lindau (51.7°N 10.1°E) A3 2.614
)(
1966, 1967)(Neustrelitz (53.3°N 13.1°E) A3 2.614, 2.775 .

6.2 The Choice and Reduction of Data.

Because of atmospheric turbulence, and other random variations in signal strength, it is necessary to take the monthly median values of absorption. A choice exists in an analysis of a seasonal variation whether to take monthly values with constant solar zenith angle, or those at the same time of day (noon). The latter course was adopted because there were more measurements of this type available, and, in addition, the use of constant χ values involves, in the Summer months, the taking of absorption measurements near sunrise and sunset, when the absorption itself is changing rapidly during the sampling period.

In order to reduce further the effects of random variations, and to eliminate the effect of varying sunspot number, where several years' measurements were available, preferably a whole solar cycle or longer, they were treated by the method of Appleton and Piggott (1954), described in §4.2 . The "mean" absorption L_i in the i th month for a particular arbitrary sunspot number R is defined by:-

$$L_i = a_i + b'_i R$$

The values of R chosen were 0 (very low), 100 (medium-high), and 175 (very high solar activity). a_i represents the absorption for zero sunpot number, while b'_i is equivalent to the response of the ionosphere to a change in solar flux. A typical graph of this type is shown in Fig. 6.1 .

Measurements were also analysed on a year by year basis, and in this case the following approximate sunspot correction was applied:-

$$L_i^* = L_i + b'_i (\bar{R} - R_i)$$

where L_i^* is the "corrected" absorption to a mean sunspot number $\bar{R}$, and

L_i the uncorrected absorption value for a sunspot number R_i .

The method depends upon the availability of values of b'_i , or in their absence, corresponding values taken from another station of equivalent frequency, for which several years' measurements are available. One cannot rely, however, on these values being the same from station to station, and it will in fact be shown in § 7.8.2 that the long term analysis of Freiburg, Slough, and de Bilt yielded somewhat different values of b'_i for each station. Because there were measurements for more years than at Slough or de Bilt, the values of b'_i of Freiburg were used for those stations for which their own values could not be calculated.

6.3 Seasonal Variation in Absorption.

6.3.1 Preliminary Observations.

Figs. 6.2, 6.3, and 6.4 show the mean seasonal variation in absorption at R = 100 for Freiburg, Slough, and de Bilt. A clear departure from any direct $\cos^n\chi$ relationship is immediately noticeable. One effect which does not appear to have been commented upon in the open literature is the subsidiary maximum at the lower frequencies in April (or May in the case of Slough).

6.3.2 The Investigation of the Lag in Absorption.

In order to measure the difference between the times of maximum absorption and maximum $\cos\chi$, the following procedure was adopted:-

The "best fit" polynomial of degree N was found for the eight monthly absorption values (calculated by one of the methods described in §6.2). The measurements for November to February inclusive were not incorporated so as to avoid the complication of anomalously high Winter values in the curve-fitting process. The data both in this analysis, and in the "model" calculations, described in Chapter Seven, corresponded

to the middle of the month, rather than the first day of it.

The curve thus generated was then automatically scanned at half-monthly increments by the computer to find the approximate date of maximum absorption. To determine the date more exactly, the curve was differentiated and tested by means of the Newton-Raphson method for the position of zero gradient.

Denoting y as the absorption in dB, and x as the month (2.5 represents mid-March, i.e. 2.5 months of the year completed, etc.), the computer was programmed to determine the least squares coefficients, A_n, in a polynomial of degree N given by:-

$$y = F(x) = \sum_{n=1}^{n=N+1} A_n x^{n-1}$$

N being an integer whose upper limit was eight.

If an initial approximation for the x value of the maximum (i.e. where $dy/dx = 0$) is x_j, the Newton-Raphson gives an improved approximation of:-

$$x_{j+1} = x_j - F'(x_j)/F''(x_j) ,$$

$$F'(x) = dy/dx = \sum_{n=2}^{n=N+1} A_n (n-1) x^{n-2}$$

$$F''(x) = d^2y/dx^2 = \sum_{n=3}^{n=N+1} A_n (n-1)(n-2) x^{n-3}$$

This process was repeated until there was good agreement between x_j and x_{j+1}, i.e.:-

$$|(x_j - x_{j+1})| < 0.005$$

The "Delay" was calculated as being the number of months that the turning point in absorption occurred after the corresponding turning point in Cos χ.

6.3.3 The Degree of the Polynomial.

The choice of the degree of the polynomial used depended to a considerable extent upon the type of data being analysed, and this fell into three categories:-

a Mid-latitude data on a long term basis,

b Low latitude data on a long term basis,

c Mid-latitude data for individual years.

a In an initial analysis, a program was prepared for fitting a polynomial of degree two, but the absorption could not adequately be defined by such a curve. In subsequent analyses, therefore, a computer library subroutine, permitting polynomial degrees up to eight, was used instead. As a check on the validity of the subroutine, it was used initially for degree two. This gave results identical to those found in the early analysis.

A polynomial of degree three might well be unreliable also, because, even neglecting Winter anomaly, turning points are to be expected three months before the start and two months after the end of the data being investigated. This implies three turning points altogether, whilst a degree three polynomial can accommodate only two such points. In practice this polynomial was even less useful than might otherwise have been expected, owing to the presence of the subsidiary maximum during April or May.

It might be argued that in order to obtain as good a fit as possible, a polynomial of degree (N - 1) should be used for the N data points, in this case eight. However, despite the previous smoothing of the data, a random variation might still be present. In view of this, the inevitable smoothing introduced by a lower degree polynomial is then actually desirable. Consequently some compromise value for the degree of the polynomial was required.

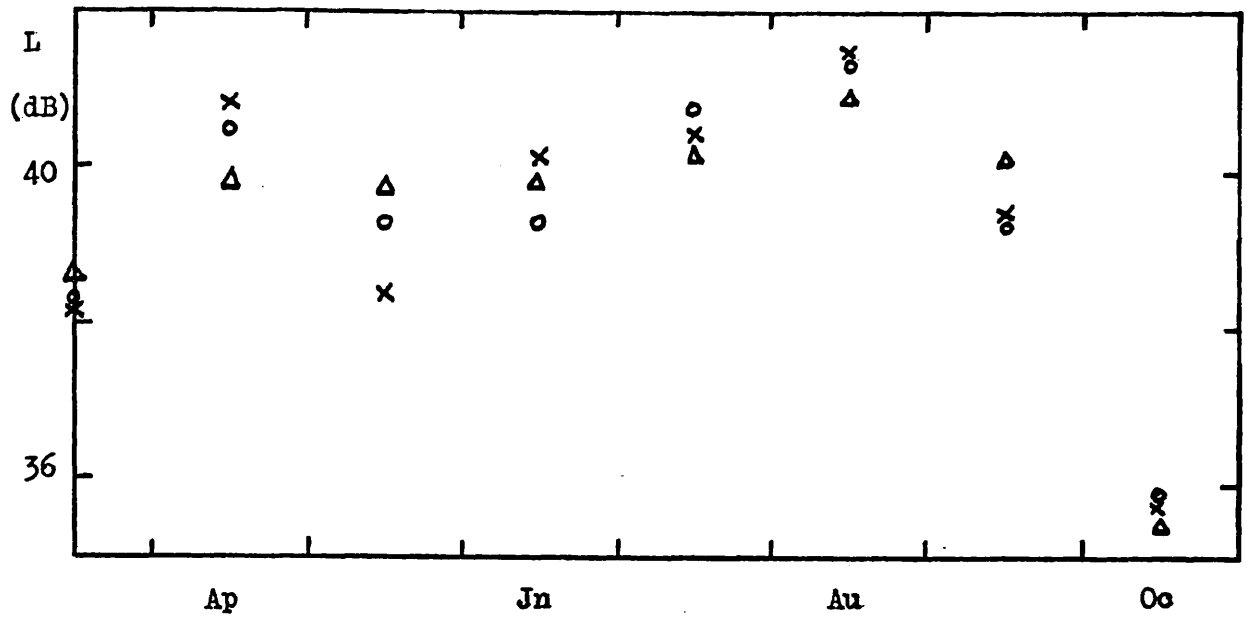

Fig. 6.5 A Comparison of the Seasonal Variation in "Raw" Absorption Data with that yielded by its Least Squares Polynomials. (1.725 MHz, R=100, Freiburg, Fig. 6.2)

× Raw data
Δ Degree 4
o Degree 5

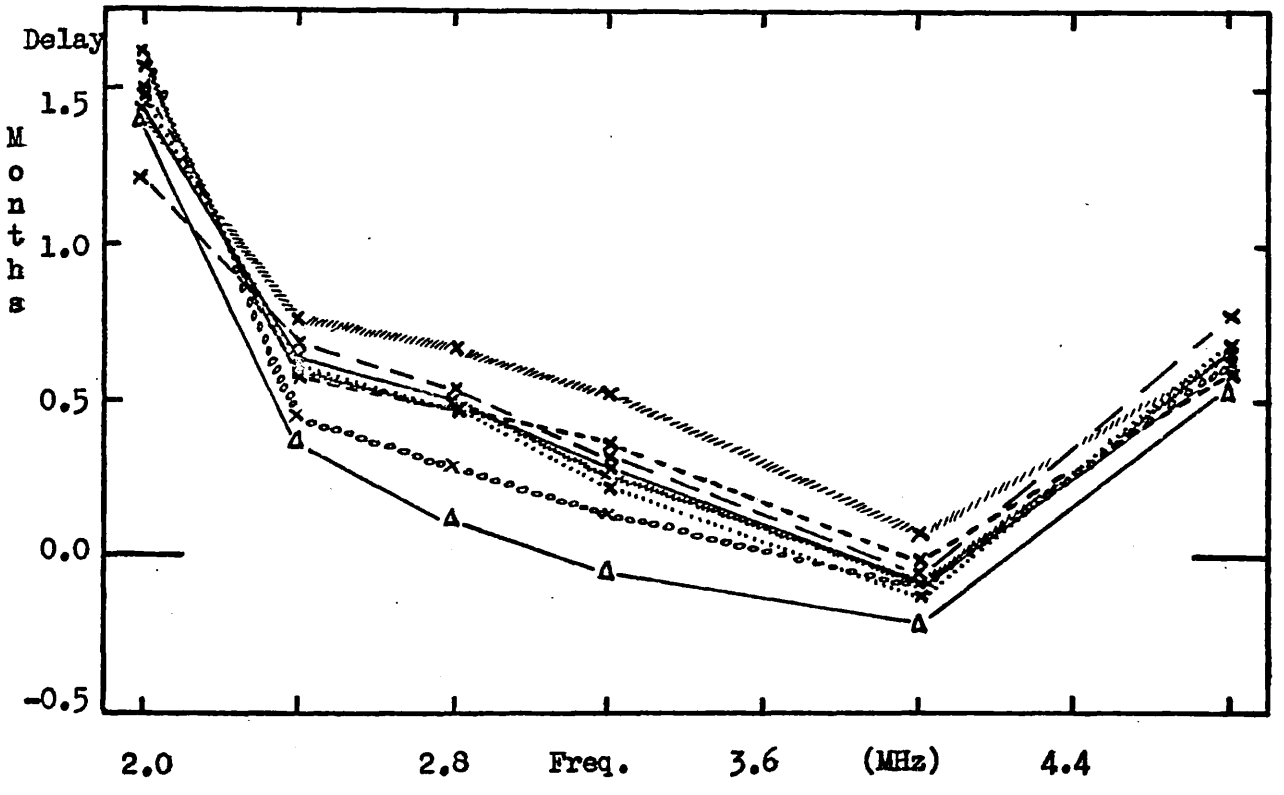

Fig. 6.6 "Delay" Values obtained from the Slough Absorption Data shown in Fig. 6.3

..... April data omitted
-------- May data omitted
— — — June data omitted
~~~~~~~~~~ July data omitted
~~~~~~~~~~ August data omitted
oooooooooo September data omitted
——— Full data included

× Degree 4
Δ Degree 5

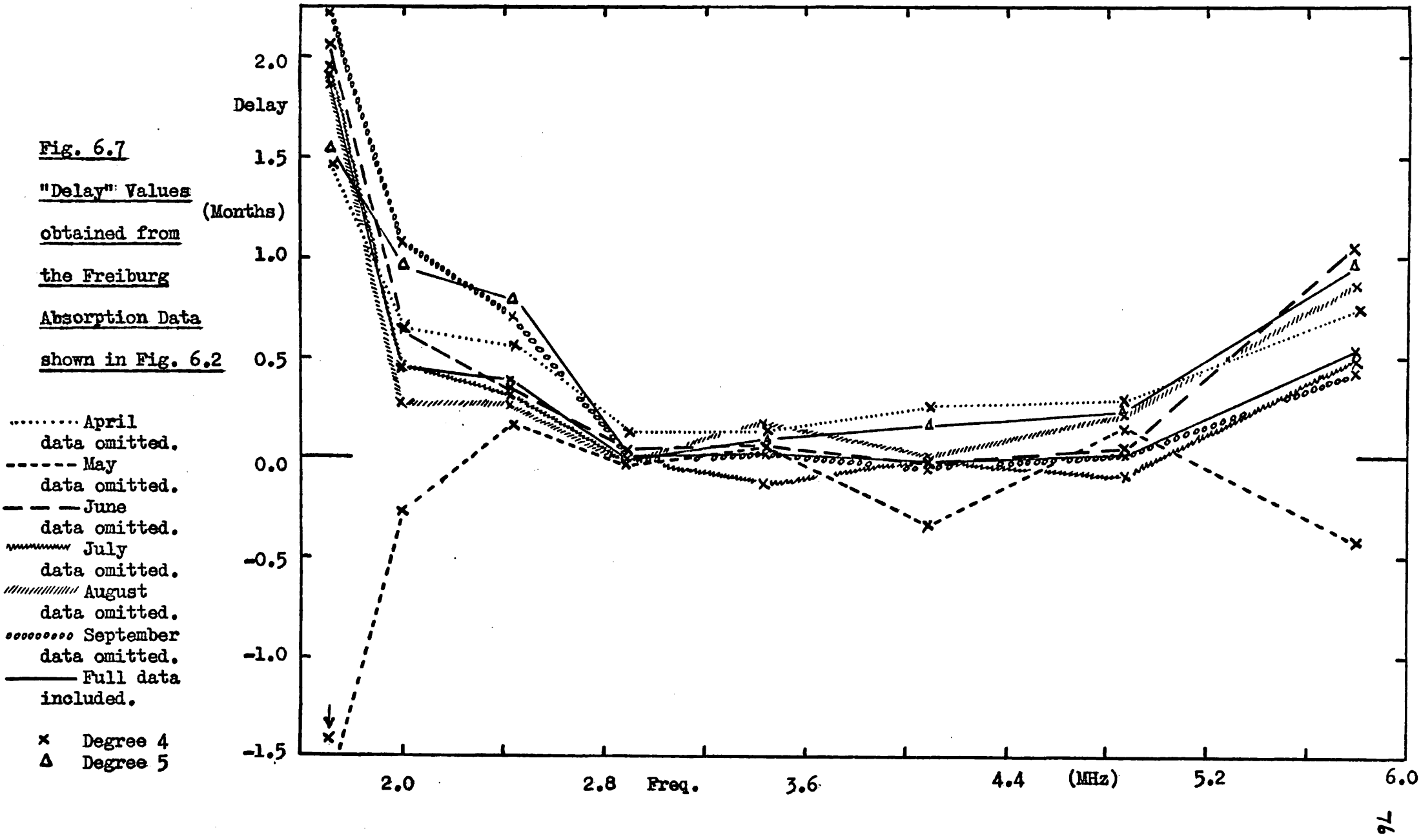

Fig. 6.7

"Delay" Values obtained from the Freiburg Absorption Data shown in Fig. 6.2

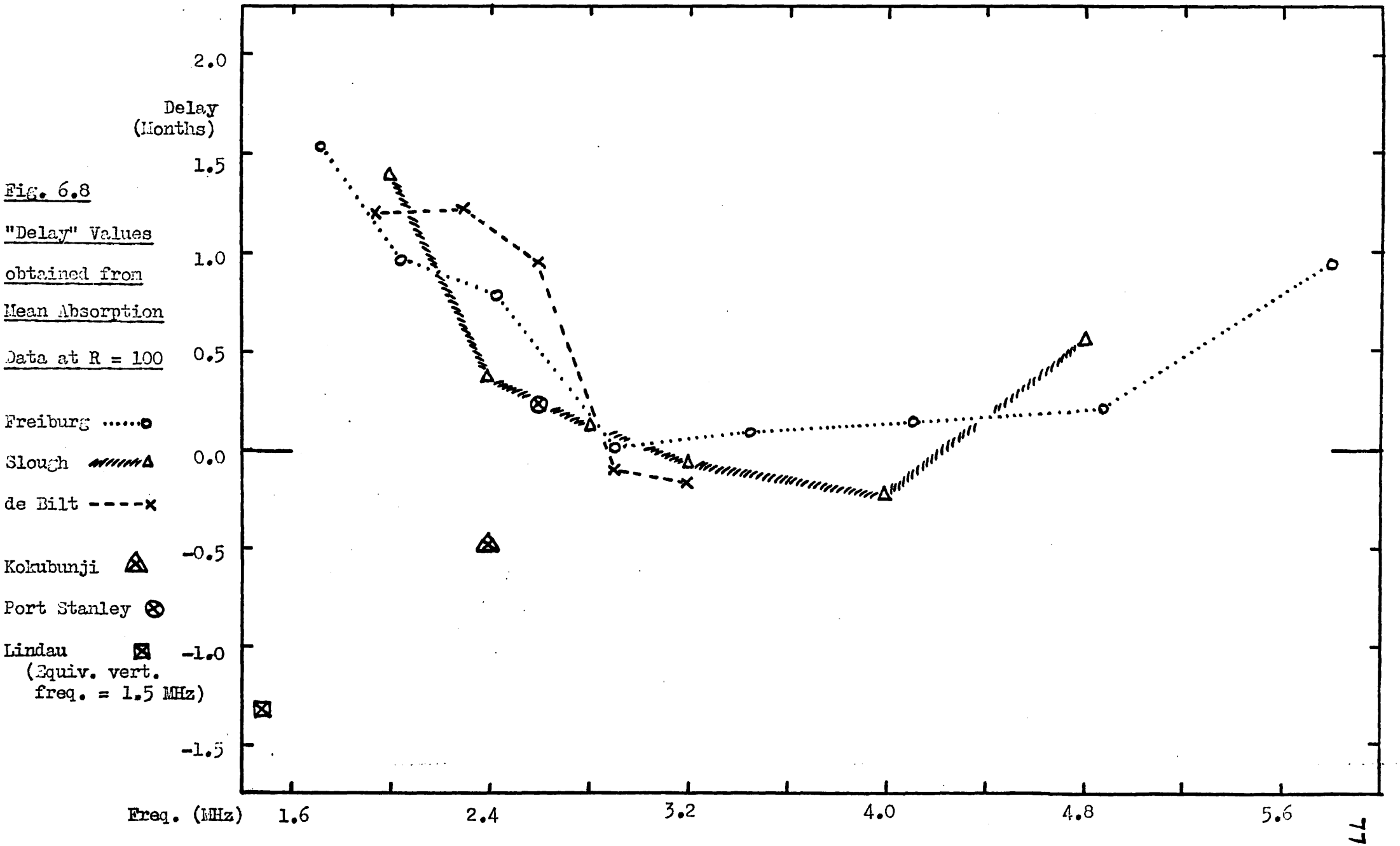

Fig. 6.8

"Delay" Values obtained from Mean Absorption Data at R = 100

Polynomials of degrees four and five were in general reasonably consistent with each other, and so it was decided to use both of these in the main analysis, whilst degree five was finally chosen for comparison with the results obtained from the theoretical model. Fig. 6.5 shows a comparison of "raw" absorption data with its corresponding least squares polynomials.

b The problem at low latitudes is somewhat more complicated, as $\cos\chi$ now has two peaks in the year, one sometime around March, the other around September (the precise times depending on the latitude), while two troughs occur, one each in June and December. These four turning points indicate that a polynomial of degree five is needed. Winter anomaly is not present in equatorial regions, so data throughout the year may be used.

In order to define more clearly the December trough, the absorption values for January and February were placed both at the beginning of the year and at the end (i.e. fourteen data points altogether). Results were obtained for degrees six, seven, and eight.

c Measurements of absorption for individual years were clearly less reliable than mean results of a group of years, which had already undergone a certain amount of smoothing in the drawing of the L / R graphs (or its equivalent calculation on the computer). Some smoothing could be accomplished by the choice of a lower degree of polynomial for the curve fitting. However, in this case, if there were anomalously high absorption in any one month, the effect would be to centre the one and only peak at that point.

On the other hand, a higher degree of polynomial could accommodate two peaks, in which case a scan for the peak could be carried out over a fairly narrow range of dates around the Summer solstice. In some cases it was impossible to decide which was the "genuine" peak

and which the anomalous one, whilst in others the computer chose what, from a visual assessment, appeared to be the wrong one. In the subsequent interpretation of the results for polynomials of degrees four and five, delays of less than $-2\frac{1}{2}$ or greater than $+2\frac{1}{2}$ months were clearly unacceptable, as were delays found from ill-defined curves.

6.3.4 The Computing.

The analysis of absorption measurements was carried out on the University of London Atlas computer, using EXCALF autocode. The calculation of theoretical values of absorption, to be described in Chapter Seven, was carried out on the University of London C.D.C. 6400 and 6600 computers, which only came into operation during the course of the present work, and were much faster than the Atlas computer. FORTRAN IV (FUN compiler) was used as the programming code.

6.3.5 The Results.

Figs. 6.6 and 6.7 show "Delay" values plotted as a function of wave frequency at Slough and Freiburg for R = 100. In order to check the reliability of the curve fitting process in finding the time of maximum absorption, the curve was re-computed eight times using a polynomial of degree four, but systematically omitting each month in turn from the eight data points. The one set of somewhat inconsistent delay values at Freiburg was obtained when May's absorption value was withheld. This had the effect of accentuating the April peak, so that it became the dominant one. Overall, however, these results, together with the "complete" data for degrees four and five, suggest that the method is satisfactory, and give an indication of its limits of accuracy.

Fig. 6.8 shows the Delay values for degree five at R = 100 for Freiburg, Slough, de Bilt, Port Stanley, Lindau, and Kokubunji. The results of the first three stations would appear to show a consistent trend, whilst that of Port Stanley suggests that a similar effect occurs in Summer in the Southern hemisphere.

The significance of the results for Lindau, Kokubunji, and equatorial stations, together with the results for R = 0 and R = 200, and the data for individual years, will be discussed in Chapter Seven.

CHAPTER SEVEN

THE EVALUATION OF A THEORETICAL ABSORPTION MODEL, AND ITS USE IN A DISCUSSION ON THE DELAY EFFECT IN ABSORPTION

7.1 The Production of the Model.

7.1.1 The Aim.

In order to find a possible explanation for the asymmetric seasonal variation in ionospheric absorption, theoretical values of midday absorption at a latitude of 50°N for R = 0, 100, and 175, were calculated on a month by month basis using model atmospheres, and incorporating wherever possible seasonal variations in the parameters.

7.1.2 The Sources of the Values of Parameters used in the Calculation.

A " + " indicates the availability of monthly data.

Temperature + , and Pressure +	Groves (1970)
Solar zenith angles +	URSI Station Manual (1957)
Sun / Earth distance + , for solar flux correction factors	Astronomical Ephemeris (1970) H.M.S.O.
U.V. flux for $O_2(^1\Delta_g)$ ionisation	Hall and Hinteregger (1970)
All other solar fluxes	Swider (1969)
$n(O)/n(O_2)$ ratio at 120 km +	Mayr and Mahajan (1971) (Fig. 7.1)
$n(N_2)$, $n(O_2)$	Norton and Barth (1970)
n(O) (Fig. 7.2)	Norton and Barth (1970), Hesstvedt (1969)
$n(O_2(^1\Delta_g))$ (Fig. 7.3)	Evans et al. (1968)
Galactic cosmic ray electron production rates	Webber (1962)
Lyman Beta molecular cross sections	Samson and Cairns (1964)

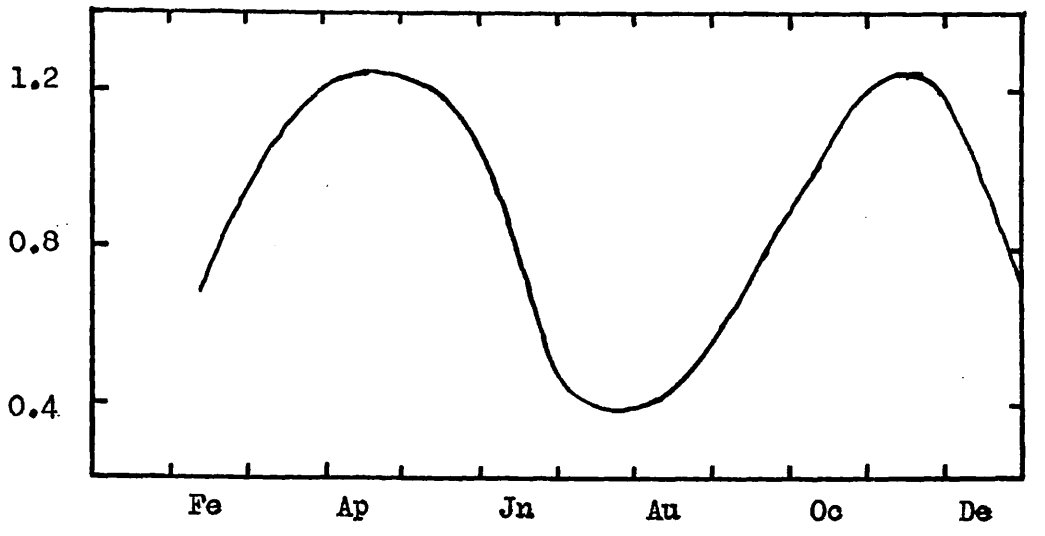

Fig. 7.1 Seasonal Variation in $n(O)/n(O_2)$ at 120 km, mid Northern Latitude. (Mayr and Mahajan, 1971)

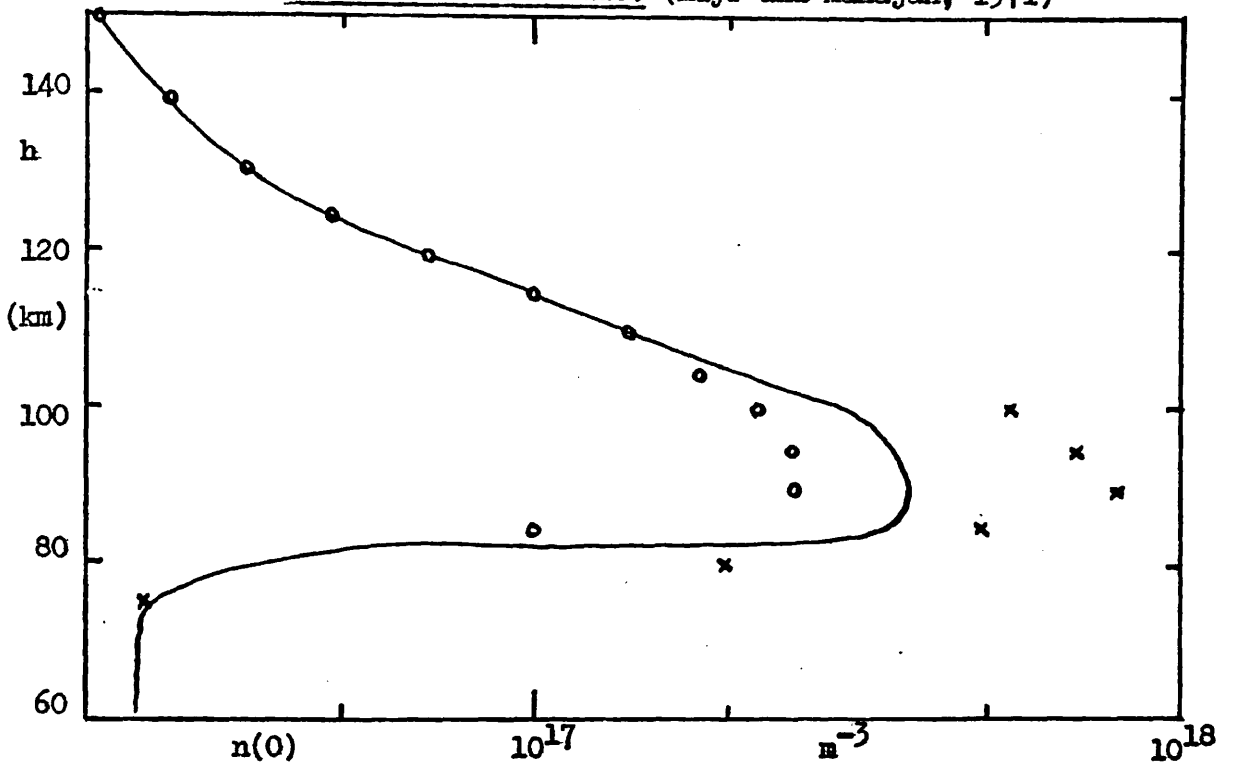

Fig. 7.2 Mean Annual Atomic Oxygen Profile

o Norton and Barth (1970) × Hesstvedt (1969)

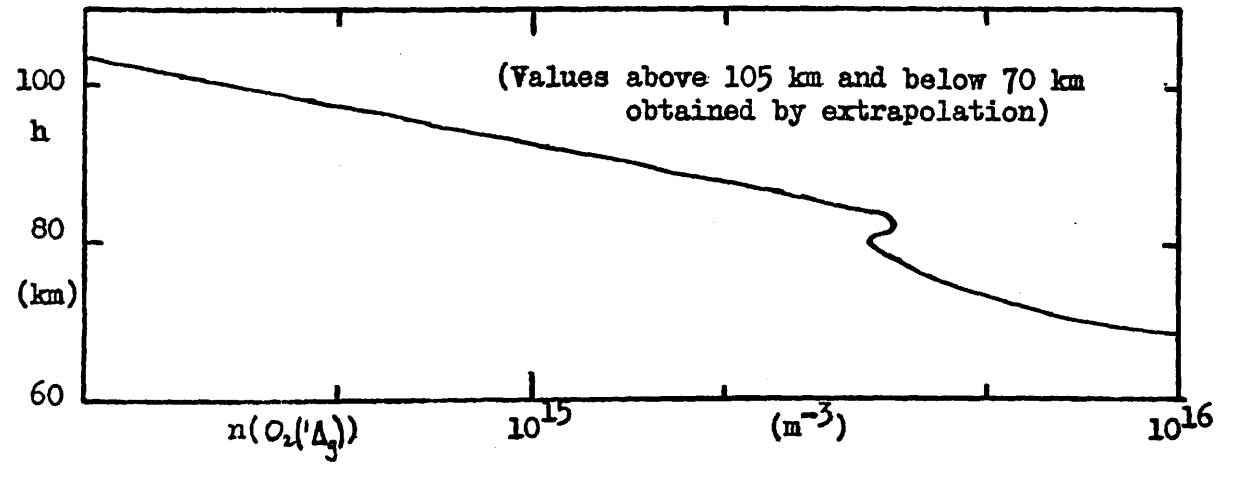

Fig. 7.3 Metastable Molecular Oxygen Profile (Evans et al., 1968)

Lyman Alpha Cross Sections:-

Photo absorption for (O_2)	Lee (1955)
Photo absorption for (H_2)	Ditchburn et al. (1954)
Photo ionisation for (NO)	Watanabe et al. (1967)
30-120 Å absorption cross sections	Snider (1969)
2-10 Å absorption cross sections	"
Ionisation efficiencies	"
$O_2(^1\Delta_g)$ Ionisation cross sections	Clark and Wayne (1970)
Absorption cross section for (O_2)	Huffman et al. (1971)

A number of models for the nitric oxide concentration and the effective electron loss coefficient will be subsequently described in more detail.

7.1.3 Seasonal Variation of Molecular Oxygen, Atomic Oxygen, and Molecular Nitrogen Concentrations.

With the data available for mean annual $n(O_2)$, $n(O)$, and $n(N_2)$ profiles, monthly temperature and pressure profiles (at 5 km intervals) up to 110 km, and proposed monthly values of $n(O)/n(O_2)$ at 120 km, the following procedure was adopted:-

a Graphs of the temperature and pressure data corresponding to the first day of the months March - November were drawn for each height, so that values corresponding to the middle of the months March - October could be interpolated from them. This comprised the basic temperature and pressure data input to the computer, from which, for each month, values at 1 km intervals in the range 65-110 km were interpolated.

b Insofar as atmospheric pressure in the range 40-110 km is concerned, molecular oxygen and nitrogen are dominant throughout, whilst atomic oxygen is insignificant below about 85 km.

One may write:-

$$n(O_2) + n(N_2) + n(O) = \rho/kT$$

and in those ranges where atomic oxygen is of any significance, its concentration may be considered to vary according to:-

$$n(O) = a_1 a_2 \, n(O_2)$$

where a_1 is a function of height only (i.e. a mean annual ratio). while a_2 will in general be a function both of season and height. The only information available in the literature for a_2 is given for a height of 120 km by Mayr and Mahajan (1971), and is shown in Fig. 7.1 . In the absence, therefore, of any other seasonal data for atomic oxygen, it was decided to use the a_2 values throughout the range 110-85 km, below which a seasonally constant profile was used. Further, one may write:-

$$n(N_2) = a_3 \left[n(O_2) + n(N_2) + n(O) \right]$$

where a_3 is a function of height and season. There is no evidence to suggest a large seasonal variation in a_3 , although it is not unreasonable to suppose that there may be a small one. In the absence of other data, therefore, a_3 was taken as a function of height alone. It is for this reason that, in calculating the pressure values used in the present work, Groves (1970) found it necessary to assume a mean molecular weight as a function of height alone.

Solution of the equations yields:-

$$n(N_2) = a_3 \cdot \rho/kT$$

$$n(O_2) = \frac{(1 - a_3)}{(1 + a_1 a_2)} \cdot \rho/kT$$

$$n(O) = \frac{(1 - a_3) \cdot a_1 a_2}{(1 + a_1 a_2)} \cdot \rho/kT$$

The absence of temperature and pressure data on a seasonal basis at heights of 115 and 120 km would normally have meant a seasonally invariant optical depth at 110 km. To avoid this, the proportional seasonal variation at 110 km of atomic and molecular oxygen and molecular nitrogen has been superimposed upon their respective mean annual values.

Because the mean $n(O)/n(O_2)$ ratio at 120 km of Mayr and Mahajan does not agree with the single ratio of Norton and Barth's (1970) results at that altitude, the relative seasonal change is retained, but the absolute values of the ratio are changed to conform with Norton and Barth's results, which are used both above and below this altitude.

It was found desirable to increase a_3 for all months in the range 65-110 km by an average of three percent. This change was made because otherwise the molecular oxygen would have absorbed too much of the Lyman alpha radiation, and this in turn would have resulted in insufficient radio wave absorption. Below 85 km, where n(O) is insignificant, an x percent change in $n(N_2)$, causes a 4x percent change in $n(O_2)$, a similar change in the electron production rate, and a 2x percent in electron density and hence in the absorption coefficient.

In the absence of any firm evidence, no attempt was made to adjust the density for varying solar activity in the manner suggested tentatively by Groves (1969).

7.1.4 The Computing.

7.1.4.1 Evaluation of the Optical Depth and Electron Production Rate.

The evaluation of the optical depth and electron production were carried out in the subroutine OPDEP. The subroutine was called once for each process (Lyman beta, nine ranges of soft X rays, five ranges of hard X rays, nine ranges of ionisation of $O_2(^1\Delta_g)$, and Lyman alpha).

It was assumed that in all cases there was zero optical depth at 150 km, as the increase in optical depth between 150 km and 140 km was insignificant. Counting downwards:-

The optical depth at the i th height

= the optical depth at the (i - 1) th height +

(the height interval × Sec χ ×

$\sum_{j=1}^{j=N}$ (Absorption cross section of j th species of molecule

Average number density of j th species at the (i - 1) th and i th heights))

$N \leq 4$, and in the case of X rays, the "total ozygen molecule concentration" is considered as $(n(O_2) + 0.5n(O))$, as shown by Henry (1967).

The heights were 150, 140, 130, 120, 115 km, then 110-65 km at 1 km intervals, followed by 60, 55, 50, 45, 40 km. The intervals were chosen with the aim of making as good use as possible of the data available. On the other hand, the use of 0.5 km intervals would have required greater computer resources, with a consequent slower turnround of programs. As it was, several arrays of variables were used for a number of different parameters in the course of the program, which had the effect of minimising the necessary "memory" store. Once the optical depth had reached forty, the calculation was terminated, as electron production rates at lower altitudes for this particular process would be negligible.

The electron production rate for a particular process at the i th height

= (Average annual sun-earth distance/sun-earth distance for month)^2

× Average annual incident solar flux for the process

× exp(- optical depth)

× $\sum_{j=1}^{j=M}$ (Ionisation cross section of the j th species ×

its number density at the i th height)

$M \leq 2$.

The electron production rate thus generated for each process was aggregated with the electron production rates of the other processes for the height and month concerned. After the addition of the galactic cosmic ray electron production rates, the electron density was calculated in the usual way, using the values of electron loss coefficient to be discussed later..

7.1.4.2 Calculation of Mono-Energetic Collision Frequencies.

Using the cross sections of Banks (1966), Rangaswamy (1969) obtained the following equation for the mono-energetic collision frequency of electrons with neutral particles:-

$$\nu_M = \left(n(N_2).9{\cdot}605.T + n(O_2).\sqrt{T}(121 + 2{\cdot}61\sqrt{T}) + n(O).187{\cdot}2\sqrt{T}\right)\times 10^{-18}$$

where T is the temperature of the neutral atmosphere, provided that thermal equilibrium exists between electrons and neutral particles. Evans (1967) has shown that this is in fact the case in the D and lower E regions.

Thrane and Piggott (1966) have pointed out, however, that calculated collision frequencies of this type have a Winter maximum above 90 km, whereas measurements suggest that the opposite is the case. No satisfactory explanation has yet been found for this discrepancy.

7.1.4.3 Evaluation of Script Integrals.

Integrals of the type:-

$$C_{5/2}(x) = \frac{1}{(5/2)!}\int_0^\infty \phi^{5/2}\exp(-\phi)\,d\phi/(\phi^2 + x^2)$$

where ϕ is a dummy variable, needed in the Sen and Wyller (1960) method of evaluating the absorption coefficient, are evaluated numerically, using either the Trapezoidal Rule or Simpson's Rule. Although tables of these integrals have been prepared by Burke and Hara (1963), it was

found more satisfactory to evaluate the integral each time it was required.

The trapezoidal rule was adopted because it facilitated a gradual increase in $\delta\phi$, which was required for reasons a and b below:-

$$x = \frac{\omega + \omega_L}{\nu_M}$$

At 60 km with a wave frequency of 2.0 MHz:-

$$x^2 = \left(\frac{2\pi \times 3.2 \times 10^6}{1.9 \times 10^7}\right)^2 \approx 1 .$$

or at 105 km with a wave frequency of 3.2 MHz:-

$$x^2 = \left(\frac{2\pi \times 4.4 \times 10^6}{7.5 \times 10^3}\right)^2 \approx 1.4 \times 10^7$$

In the function:-

$$f(\phi) = \phi^{5/2} \exp(-\phi)/(\phi^2 + x^2)$$

the term $\exp(-\phi)$ will increasingly predominate once ϕ becomes greater than unity. Thus, initially, at $\phi = 0$, $\delta\phi$ needs to be very small, and a value of 0.003 was taken in this case. If $\delta\phi$ is kept constant at this value throughout the integration, two problems arise:-

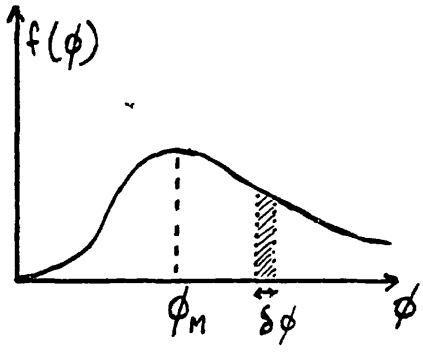

a Approximately 3×10^{62} separate areas would need to be summed, requiring considerable computing time.

b As ϕ increases, $f(\phi).\delta\phi$ rapidly diminishes, and the area of each further step becomes increasingly insignificant compared with the area that has already been summed. As the computer can normally store only fourteen significant figures, the area of each of the remaining strips will be lost in rounding errors. The important point here is that although the area of one strip might be insignificant, the area of a group of strips need not necessarily be.

x	ϕ_M
$\to 0$	$\to 0.5$
$1/\sqrt{3}$	1.0
1.5	1.5
$\sqrt{12}$	2.0
$\to \infty$	$\to 2.5$

The problems were overcome by increasing $\delta\phi$ by a constant factor of 1.17 for each successive strip. Thus the early part of the curve was scanned at small intervals of ϕ, whereas when $f(\phi)$ approached a simple exponential decay, $\delta\phi$ was increasing to compensate for this. One thousand strips were generated, enabling the integral to be evaluated up to $\phi = 2 \times 10^{68}$.

Using test data, a number of typical script integrals were calculated for comparison with the values obtained by Burke and Hara (1963). In no case was there a discrepancy of greater than 0.5 percent, and in view of the large uncertainties in the values of the other parameters, this was considered to be perfectly adequate.

7.1.4.4 Evaluation of K , and $\int K\,dh$.

The following expression was used for the absorption coefficient:-

$$K = \frac{5}{4} \cdot \frac{1}{\mu} \cdot \frac{N(e)e^2}{\epsilon_0 m c \nu_M} \cdot C_{5/2}\left(\frac{2\pi f + \omega_L}{\nu_M}\right)$$

the refractive index μ being given by:-

$$\mu^2 = 1 - \frac{e^2}{4\pi^2 \epsilon_0 m} \cdot \frac{N(e)}{f^2} = 1 - 80.5\, N(e)/f^2$$

At reflection, μ is zero; hence the necessary electron density for reflection, $N'(e)$ is given by:-

$$N'(e) = f^2/80.5 \quad \text{, and hence:-}$$

$$\mu = \sqrt{\left(1 - N(e)/N'(e)\right)}$$

The absorption in the interval between the i th and (i - 1) th heights for the incident wave, plus the absorption between the (i - 1) th and i th heights for the **reflected wave, was calculated from:-**

$$\Delta L\ (dB) = 8{\cdot}7 \times 2 \times \frac{5}{4} \times \frac{e^2}{\epsilon_0 m c} \times \left(\frac{1}{0{\cdot}5(\mu_i + \mu_{i-1})}\right)$$

$$\times \frac{(N_i(e) + N_{i-1}(e))}{(\nu_{m_i} + \nu_{m_{i-1}})}$$

$$\times\ 0{\cdot}5 \left(C_{5/2}\left(\frac{2\pi f + \omega_L}{\nu_{m_i}}\right) + C_{5/2}\left(\frac{2\pi f + \omega_L}{\nu_{m_{i-1}}}\right)\right)$$

$$\times\ (h_{i-1} - h_i) \times F$$

F being a fraction equal to 1.0 except at reflection. If:-

$N_{i-1}(e) \geqslant N'(e)$, then:-

$F = (N'(e) - N_i(e))/(N_{i-1}(e) - N_i(e))$, and

$\mu_{i-1} = 0$. An estimate of the height of reflection was obtained from:-

$$h = h_i + F.(h_{i-1} - h_i)$$

and if reflection had not taken place by 110 km, the reflection height was set equal to zero to indicate that, because of this, it had not been possible to calculate the total absorption, and also that the wave frequency was above f_0E.

The total absorption was then obtained by summing the individual absorption values over the intervals from 40 km to the height of reflection.

7.1.5 The Choice of Profile for the Effective Electron Loss Coefficient.

The absorption coefficient is proportional to the electron density, and inversely proportional to the refractive index, itself a function of electron density. In addition, the height of reflection is a function of the electron density.

Since the electron density is given by:-

$$N(e) = \sqrt{\varepsilon q/\alpha}$$

a small increase in the profile of the effective electron loss coefficient can therefore cause a considerable change in the calculated value of total absorption, although it is not always possible without calculation to know in which direction this change will take place.

At present, however, there is very little data for α under undisturbed conditions, none of it being on a seasonal basis. Profiles summarised by Mitra (1968) must be discarded because of their use of a production rate based on what are now considered as unacceptably low concentrations of nitric oxide.

Reid's (1970) determination of α, using Barth's (1966) NO profile, and including a steep ledge in α at around 87 km, was used in the preliminary model calculations. It yielded values of total absorption 50 percent too low, with a large proportion of it occurring above the ledge, with the result that there was virtually no reduction in absorption with increasing frequency. The profile extended only to 93 km, which required an extrapolation of a further 17 km for use in the present work.

A recent determination of α by Hall (private communication), which simultaneously measured the electron density and absorption of Lyman alpha and 2-10 Å X rays, provided confirmation of the ledge.

These results ought, therefore, to be more reliable and have in fact yielded in the model, absorption values much closer to those obtained by experiment. Hall's measurement also tends to be unreliable above about 90 km, because it neglects the effects of ionising radiations in in the range 30-120 Å , and the reflection heights obtained in the model were inconsistent with those calculated from R.R.E. incoherent scatter data (Taylor, private communication). Since in general at reflection height, electron production rates due to the ionisation of nitric oxide are of minor importance, adjustment of the effective electron loss coefficient to yield satisfactory reflection heights was carried out before the final choice of profile for NO was made, after which further slight adjustments were necessary.

It is quite possible that α varies seasonally, and preliminary reports by Folkested et al. (1972 a, b) suggest that evidence for such a variation has been found. In their investigation of mesospheric nitric oxide concentrations during a polar cap absorption event, Narcisi et al. (1972) have reported that the molecular ion / water cluster ion ledge, normally found at 87 km, occurred at 73 km during the day, and 77 km at sunset. From this it was inferred that under undisturbed conditions also, the height of the ledge might vary diurnally, and hence quite possibly seasonally as well.

Provided that reflection heights are not affected, the lowering of the height of the ledge would increase the absorption, with the lower frequencies being increased by a relatively greater amount than that of the higher frequencies. Thus if the variation of Cos χ is considered, midday may be analagous to Summer, and the time near sunset to Winter, the Summer absorption would be increased relative to that in Winter.

Moreover, Folkestad (1970) has indicated that the D region water vapour content in Winter is lower than that in Spring and Autumn.

Fig. 7.4

Profiles of Effective Electron Loss Coefficient

——— Hall (private communication)

— — — Upward extrapolation of ———

This combined profile will be referred to as "H1".

..... "Corrected" profile: "H2"

Reid (1970)

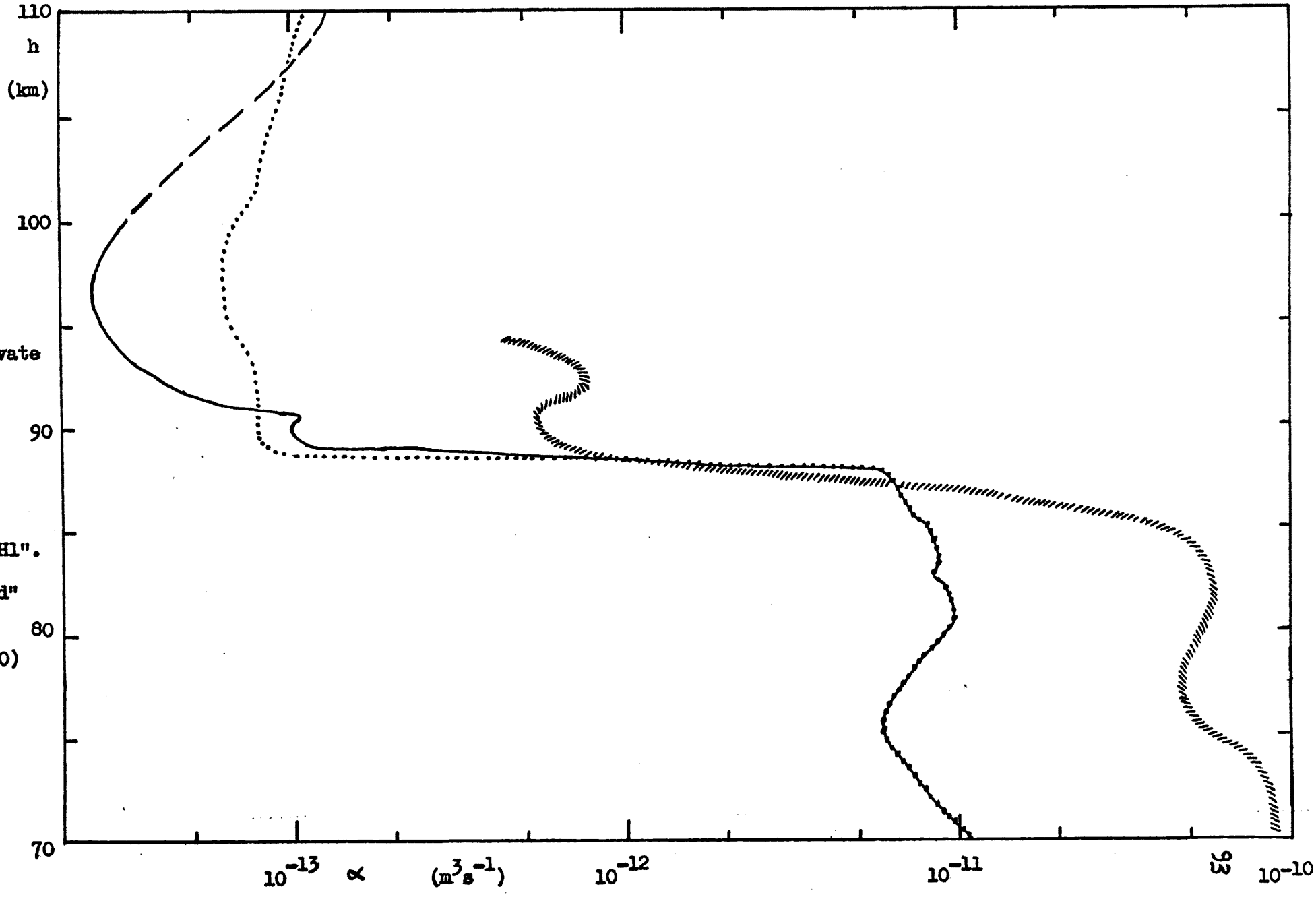

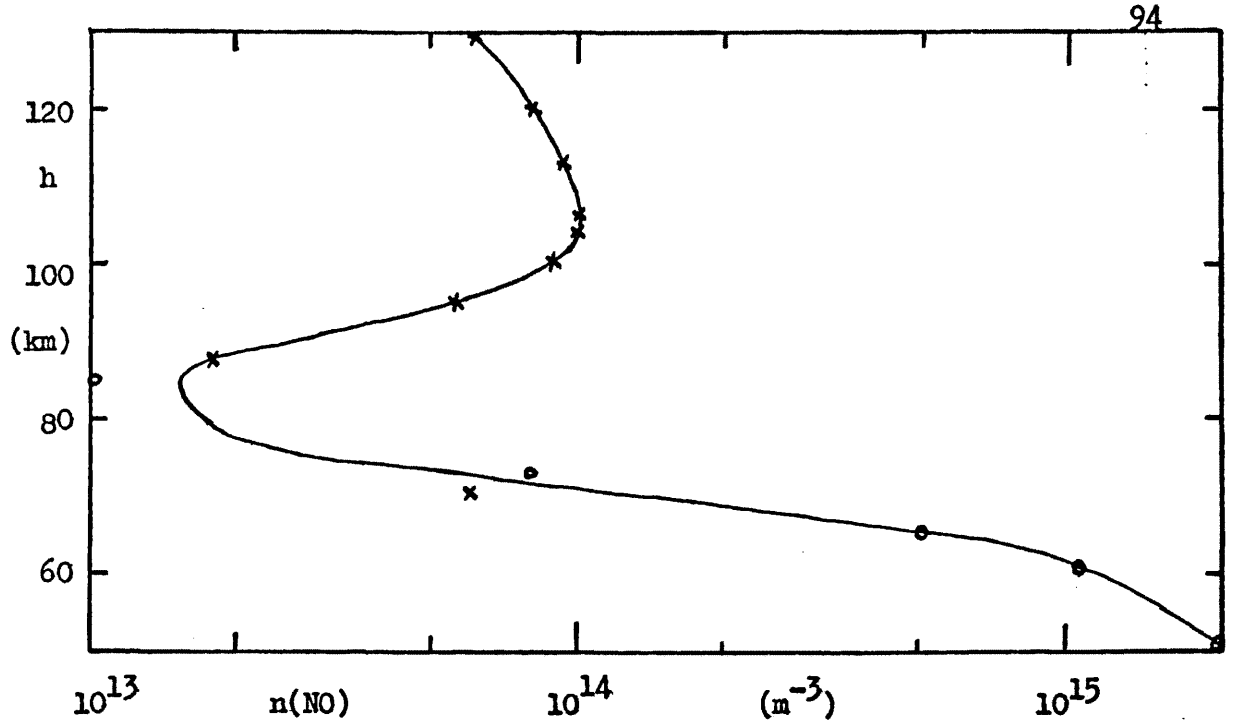

Fig. 7.5 Initial Nitric Oxide Profile "M/H"

× Meira (1971) o Hesstvedt (1969)

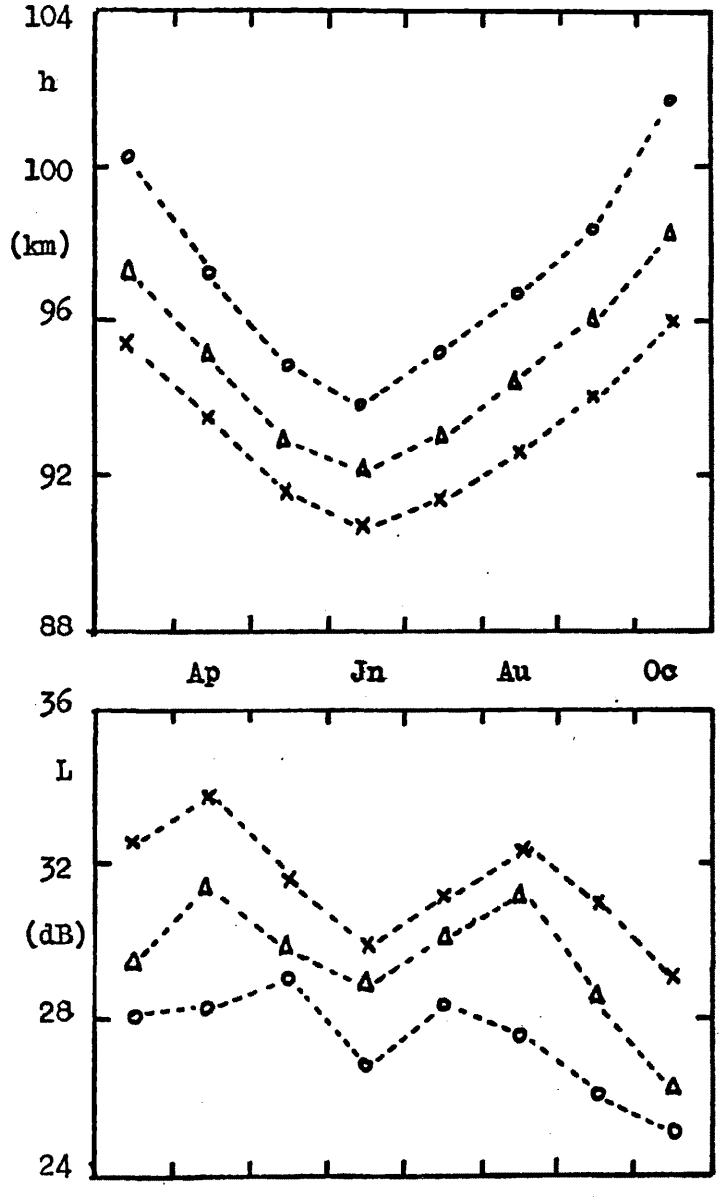

Fig. 7.6

Preliminary Reflection Heights and Absorption Values obtained from Model for R = 100

(NO) profile : M/H

∝ profile : H2

× 2.0 MHz Δ 2.4 MHz

o 2.9 MHz

Note on all Figs. showing results obtained from the Model. Except where otherwise stated, the values of Cos χ for Freiburg have been used.

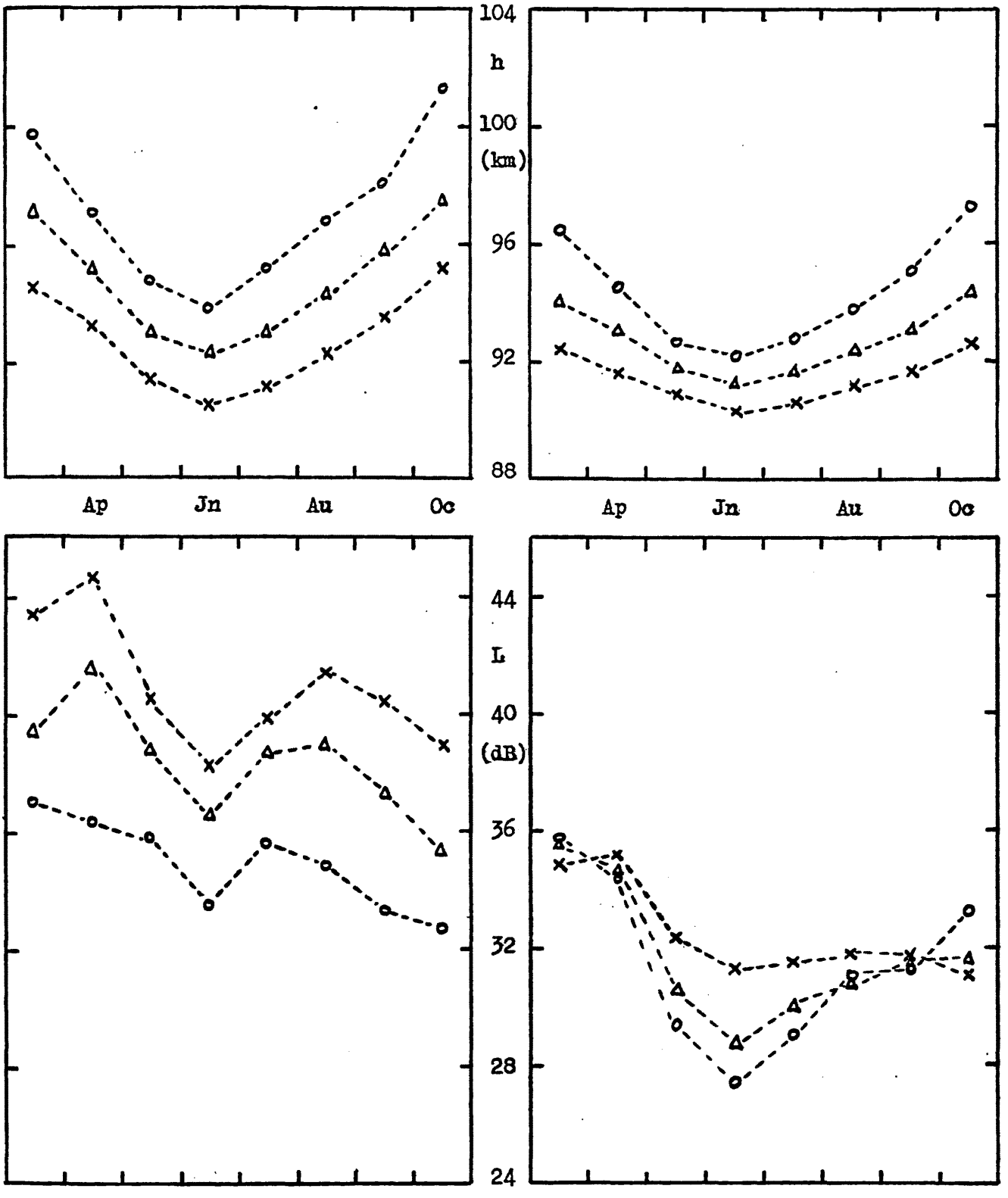

Fig. 7.7

(NO) profile : 2 x (M/H)

∝ profile : H2

Fig. 7.8

(NO) profile : 2 x (M/H)

∝ profile : H1

Preliminary Reflection Heights and Absorption Values obtained from Model for R = 100

× 2.0 MHz Δ 2.4 MHz o 2.9 MHz

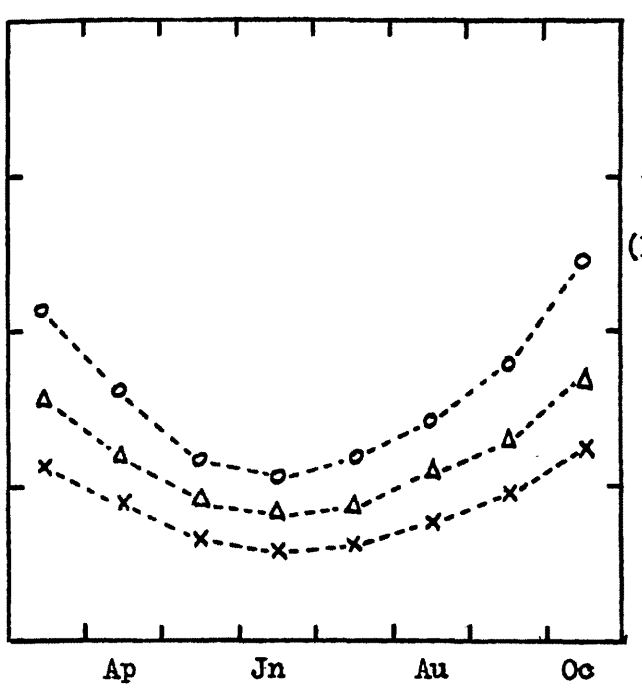

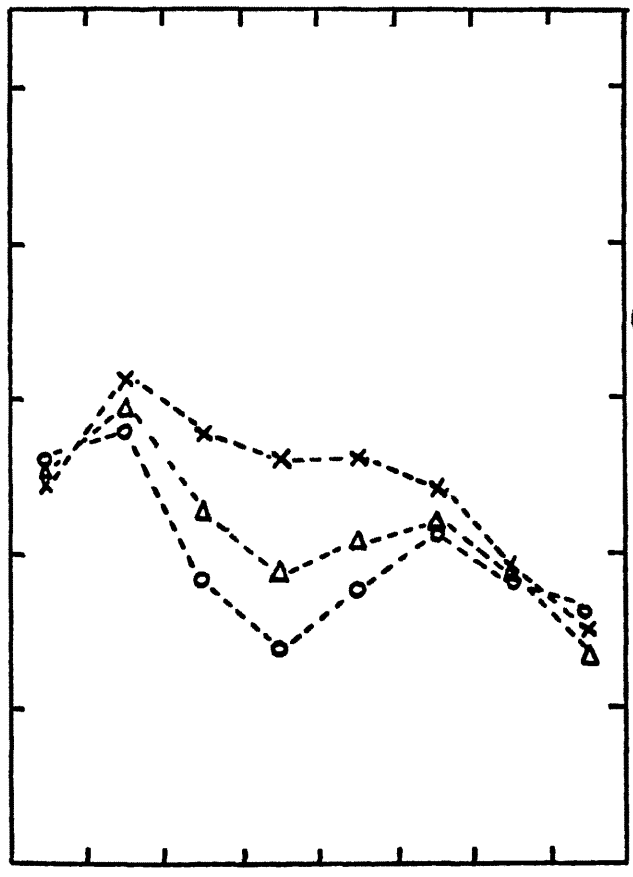

Fig. 7.9

(NO) profile : $2.8 \times \cos\chi \times (M/H)$

α profile : H1

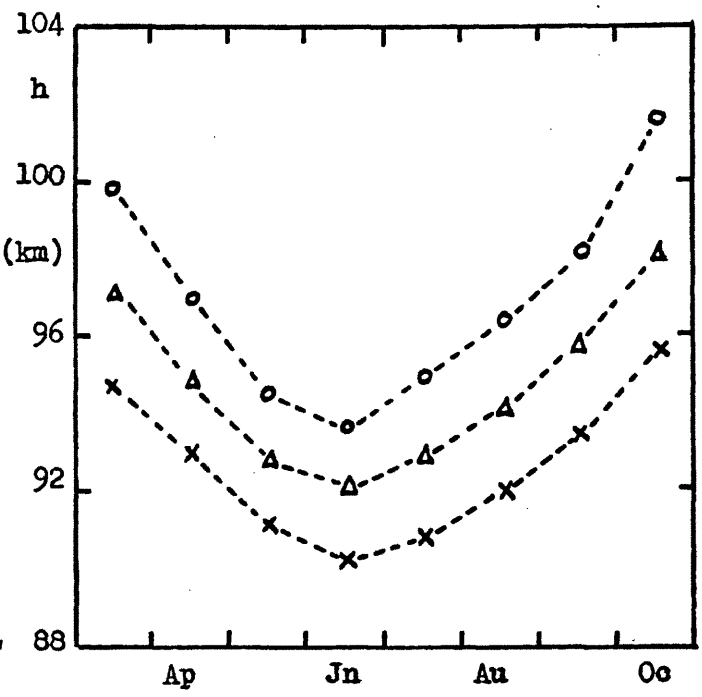

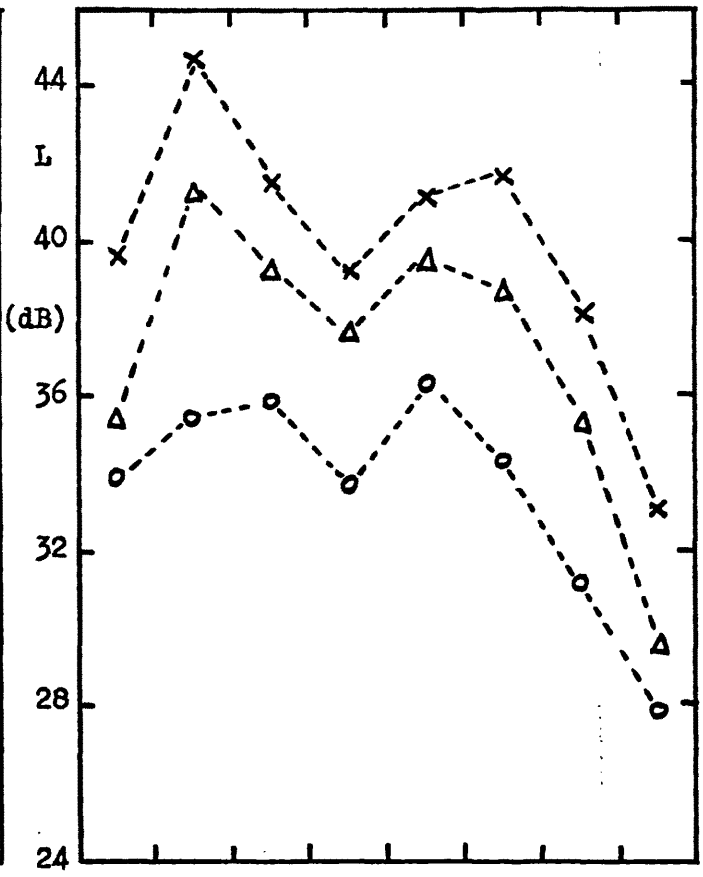

Fig. 7.10

(NO) profile : $2.8 \times \cos\chi \times (M/H)$

α profile : H2

Preliminary Reflection Heights and Absorption Values obtained from Model for R = 100

× 2.0 MHz Δ 2.4 MHz o 2.9 MHz

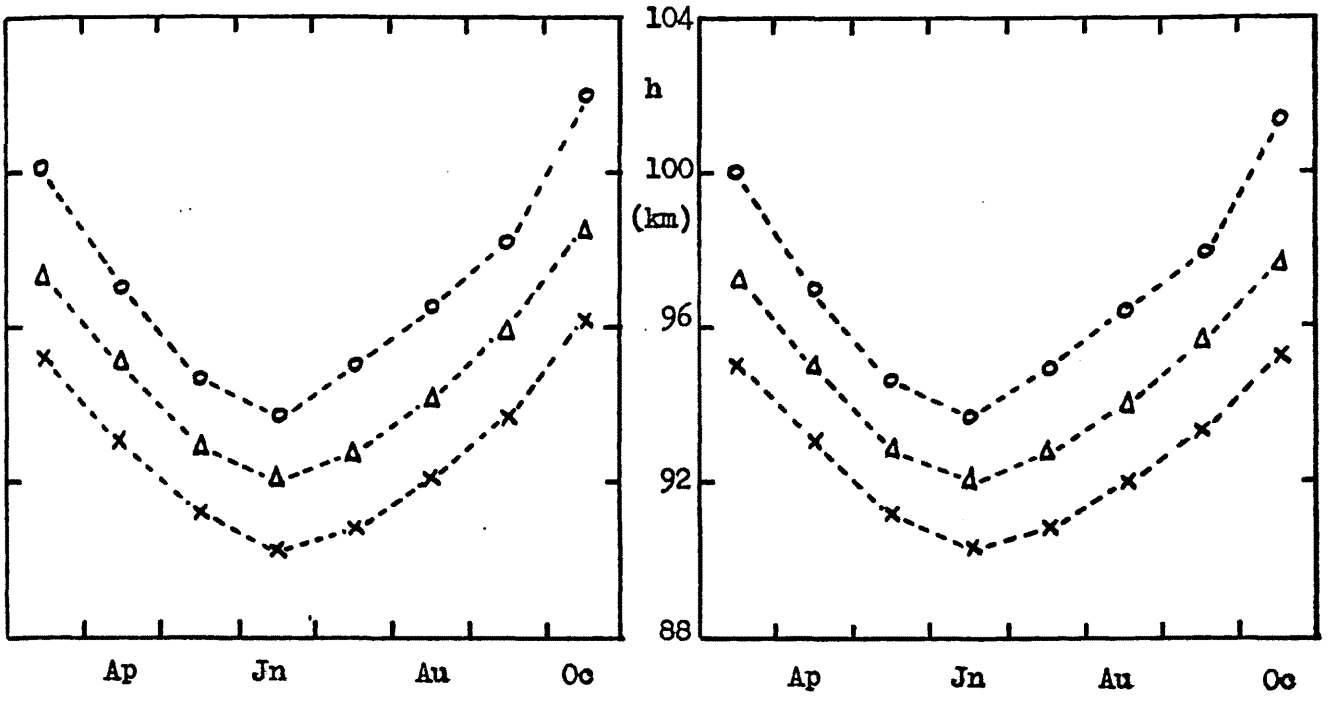

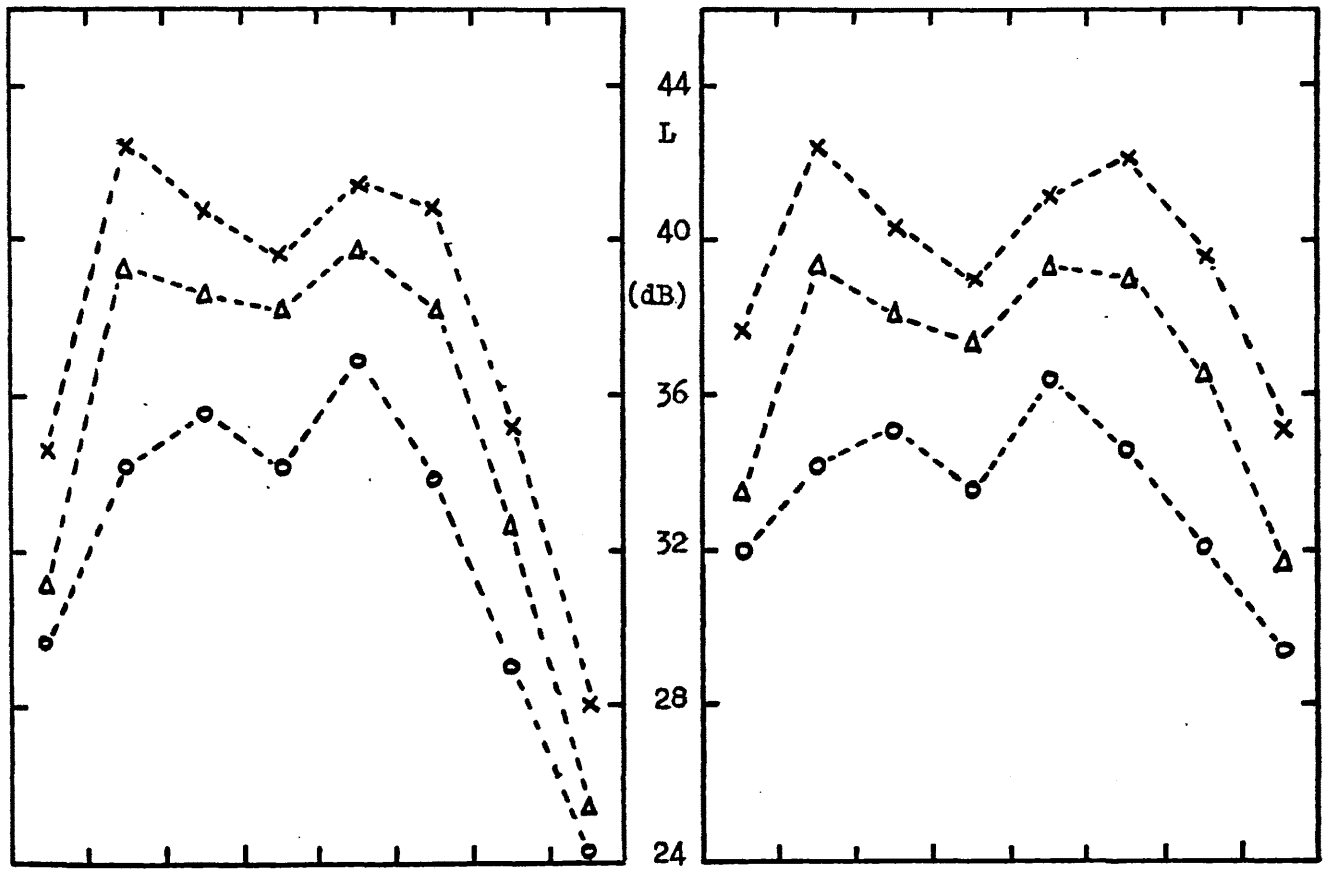

Fig. 7.11

(NO) profile : $3.0 \times \cos^2\chi \times (M/H)$

profile : H2

Fig. 7.12

(NO) profile : $2.8 \times \cos\chi_{(\text{Month} - \frac{1}{2})}$

profile : H2 $\times (M/H)$

Preliminary Reflection Heights and Absorption Values obtained from Model for R = 100

× 2.0 MHz Δ 2.4 MHz o 2.9 MHz

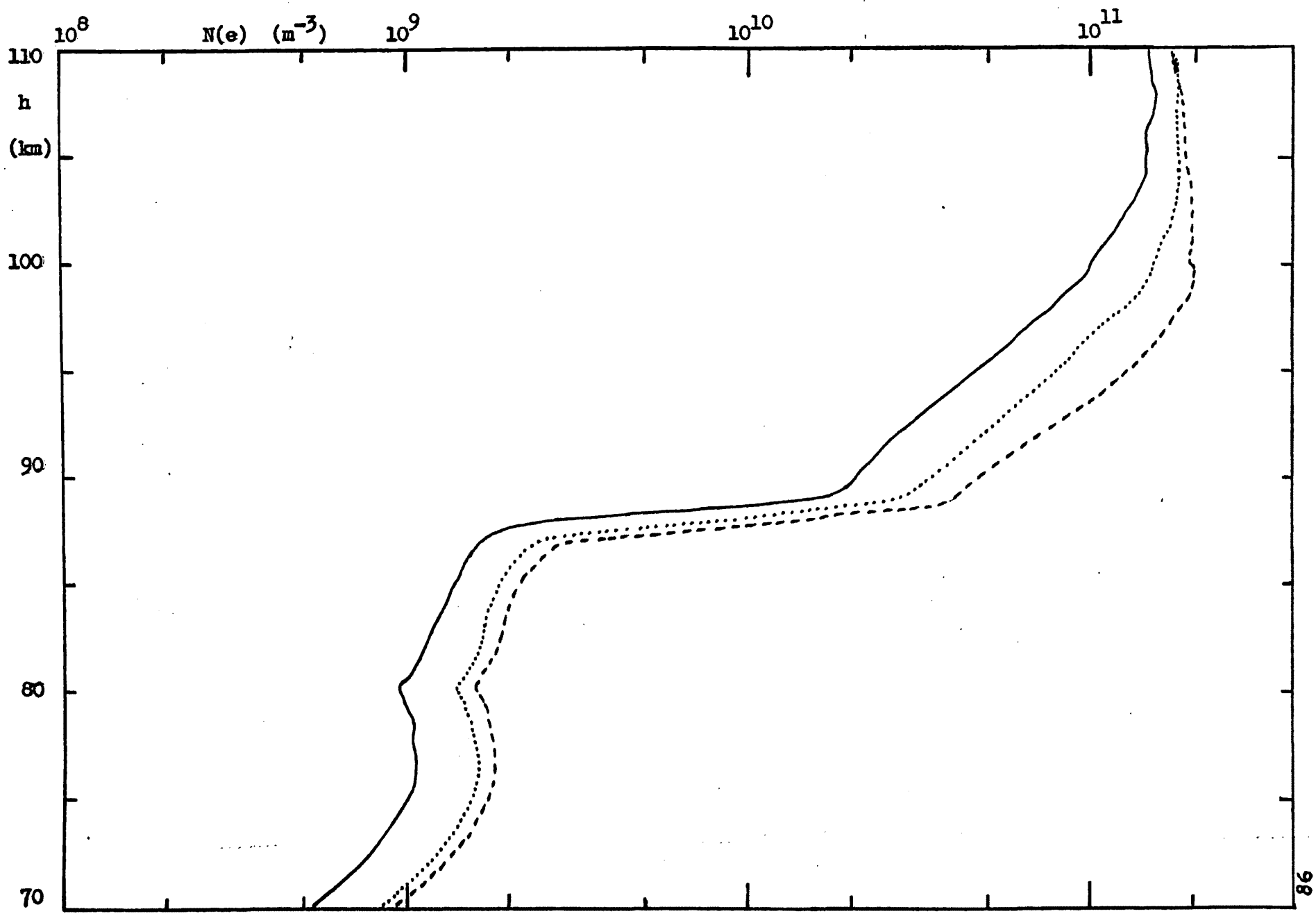

Fig. 7.13a

Model Electron Density Profiles at R = 100

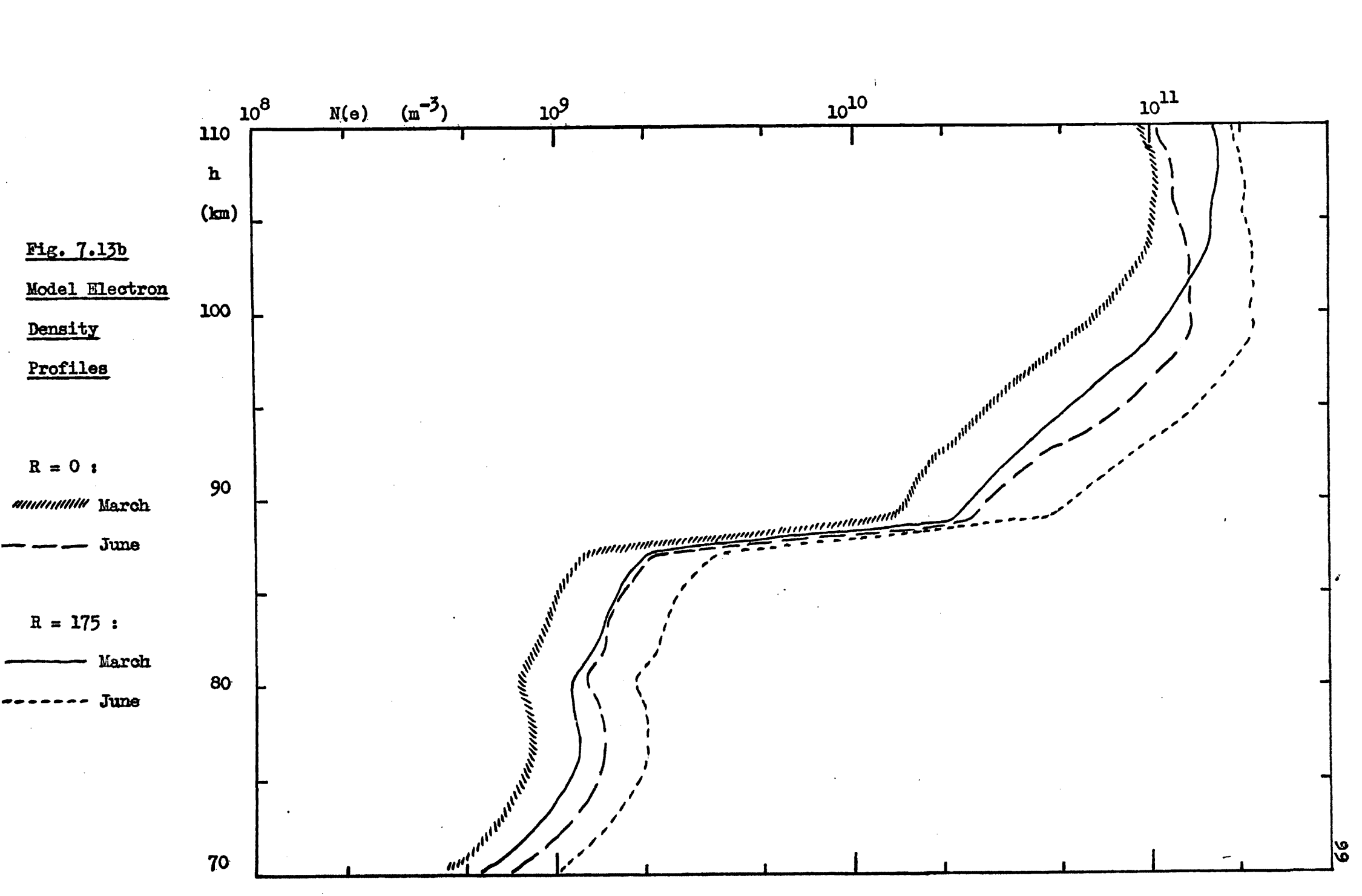

Fig. 7.13b

Model Electron Density Profiles

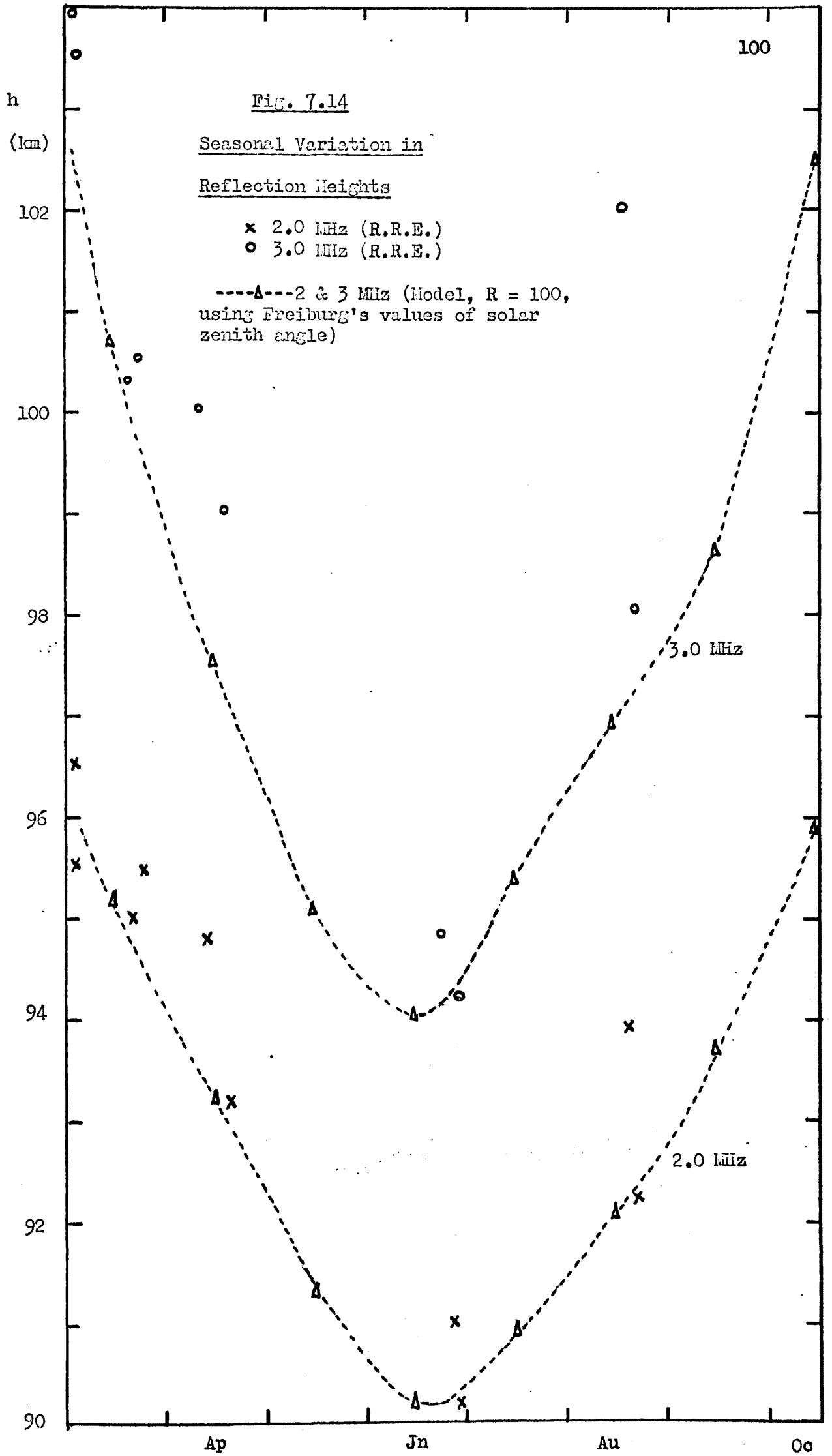
Fig. 7.14
Seasonal Variation in
Reflection Heights
× 2.0 MHz (R.R.E.)
o 3.0 MHz (R.R.E.)
----Δ---2 & 3 MHz (Model, R = 100, using Freiburg's values of solar zenith angle)
h
(km)
100
102
100
98
96
94
92
90
3.0 MHz
2.0 MHz
Ap
Jn
Au
Oc

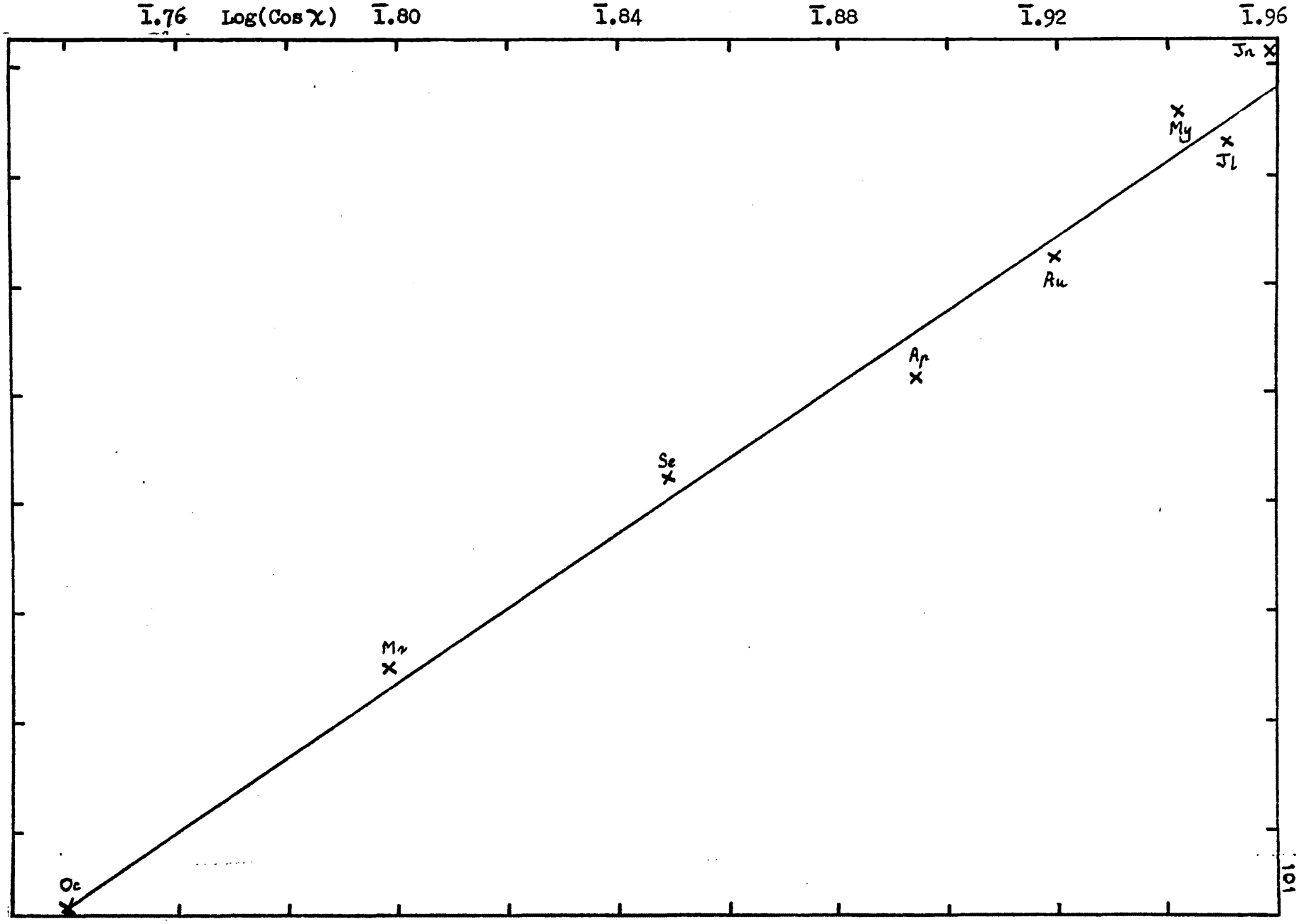

Fig. 7.15

The Logarithm of the Maximum E Region Electron Density, computed by the Model, plotted as a Function of the Logarithm of Cos χ

(R = 100)

Bardsley and Biondi (1970) have suggested that on theoretical grounds the dissociative recombination coefficient should be inversely proportional to the square root of temperature.

In the absence of any further definite data, however, a seasonally invariant effective loss coefficient was adopted. In any case, in the height range 65-85 km, an increase in α is, from the computing point of view, exactly equivalent to a corresponding decrease in n(NO). It was therefore felt unnecessary at this stage to invoke any seasonally changing profile for α, when the equivalent necessary adjustment in absorption could be obtained without this complication, by varying the nitric oxide profile.

Hall's profile for α had to be extrapolated downwards from 70 km. For the sake of consistency, it was decided not to use those values for the lower ionosphere obtained by Larson and Houston (1969) using a method similar to that of Hall, but whose value at 70 km was one and a half orders of magnitude smaller. For the same reason, the data of Johannesen et al. (1972) available only between 83 and 86.5 km, could not be used, despite its greater detail within that range.

Fig. 7.4 shows the profiles of α obtained by Reid, and Hall. Also shown is Hall's profile after correction, which was used in subsequent calculations in the present work.

7.1.6 The Choice of Profile of Nitric Oxide Concentration.

In initial calculations, the nitric oxide profile of Meira (1971) was used, merging into that of Nesstvedt (1969) below 70 km. This is shown in Fig. 7.5. After subtraction of Rayleigh scattering, the profiles of Barth (1966) and Pearce (1969) can be brought quite well into line with those of Meira. In addition, Narcisi et al. (1972) have obtained rocket measurements during a PCA event which yield further confirmation of Meira's profile.

Ferguson has pointed out, however, that Meira's results are not really sensitive to mesospheric nitric oxide because the concentration profile is calculated from the differential of the integrated (1, 0)γ dayglow emission profile, whose major contribution comes from NO above 95 km. Strobel (1972) has argued the need for a technique of measurement of NO that is sensitive at mesospheric heights; while Narcisi et al. have pointed out that until this is available, no seasonal measurements of concentrations will be possible, because the uncertainties in the measurement will probably be greater than the seasonal variation.

It will be seen from Figs. 7.6 - 7.8 that the use of seasonally invariant NO profiles and the α profiles of Hall both before and after the correction described in §7.1.5, resulted in quite unacceptable absorption minima in June. Rather than vary the α profile, it was decided instead to retain the Meira / Nesstvedt NO profile, but to multiply it by a factor which was a function of the month concerned. Figs. 7.9 and 7.10 show the effect on absorption of such a profile proportional to Cos χ, before and after the correction of α respectively. Figs. 7.11 and 7.12 show the effect of profiles proportional to $\cos^2\chi$, and $\cos\chi_{(\text{Month} - \frac{1}{2})}$ i.e. with half a month's delay. Although there has been some improvement, the June value of absorption is still less than that in either May or July.

A very large number of models were then run, in order to find what seasonal variation in the above factor was needed to produce as good an agreement as possible with the experimental results, both as a function of season and of wave frequency. These factors were found to be:-

Mar.	Apr.	May	Jun.	Jul.	Aug.	Sep.	Oct.
1.2	1.5	2.0	3.1	2.7	2.2	1.6	1.1

Although the figure for June in particular may seem rather high, it will be remembered that the seasonal change in electron density below 87 km,

arbitrarily assigned here to changes in n(NO) may in fact be partly or wholly due to changes in α.

Recent theoretical work by Shimazaki and Laird (1972) suggests that at 70 km the ratio of Summer to Winter concentrations of NO is four. Between about 80 km and 105 km, however, their Winter value is in excess of their Summer one. Strobel (1972), Swider (1972), and Donahue (1972) all point out, however, that below about 80 km Meira's values may be too high to be compatible with the observed concentrations of NO^+.

It may be seen, therefore, that considerable uncertainty in the concentration of nitric oxide still exists, and the justification for the present suggested seasonal variation is in the nature of the results that it produces. It is not in any way claimed to be the unique solution, but as one possible solution that may be found using the other parameters at present available.

7.2 Tests on the Model.

7.2.1 Electron Density Profiles and Critical Frequency Variations.

The model's electron density profiles at R = 100 for March, June, and August are shown in Fig. 7.13a. The March and June profiles, each for R = 0 and R = 175 are shown in Fig. 7.13b. Comparison has already been made in Figs. 1.1 and 1.2 with various experimental profiles. Fig. 7.14 shows a comparison of the calculated reflection heights for 2.0 and 3.0 MHz with those obtained from the R.R.E. data (Taylor, private communication).

Two further tests were applied to the model's electron density profiles. In those cases where the wave had failed to be reflected (indicated by a zero in the "Reflection Height"), the wave frequency was greater than f_0E. This value of f_0E was then compared with the value obtained from the empirical relationship:-

$$f_0E = 0.9\left[(180 + 1.44\,R)\cos\chi\right]^{0.25}$$

The results are shown in the following table:-

de Bilt					Freiburg				
Cosχ	Month	R	$f_o E$ (MHz) Model	Empir.	Cosχ	Month	R	$f_o E$ (MHz) Model	Empir.
.484	Oct.	0	< 2.70	2.75	.550	Oct.	0	< 2.80	2.84
.583	Mar.	0	< 2.90	2.88	.638	Mar.	0	<3.00	2.96
.652	Sep.	0	<3.00	2.96	.707	Sep.	0	<3.10	3.02
.756	Apr.	0	<3.10	3.05	.784	Apr.	0	<3.15	3.10
.786	Aug.	0	<3.15	3.10	.829	Aug.	0	<3.20	3.14
.833	May	0	<3.25	3.15	.872	May	0	<3.35	3.18
.860	Jul.	0	<3.25	3.18	.894	Jul.	0	<3.25	3.20
.874	Jun.	0	<3.30	3.19	.908	Jun.	0	<3.35	3.36
.484	Oct.	100	<3.25	3.18	.550	Oct.	100	<3.40	3.32
.583	Mar.	100	<3.45	3.32					
.484	Oct.	175	<3.40	3.43					

The results for Slough are almost identical to those for de Bilt.

At reflection $\mu = 0$, therefore:-

$$f_o^2 E = k N_m(e)_E \quad \text{(where } k = e^2/4\pi^2\epsilon_o m \text{)}, \text{ and hence:-}$$

$$k N_m(e)_E = 0.81[(180 + 1.44R)\cos\chi]^{0.5}$$

Thus, for a given sunspot number, a logarithmic plot of $N_m(e)_E$ as a function of Cosχ might be expected to yield a slope of 0.5 .

The figure obtained from the graph (Fig. 7.15) was 0.68 , 36 percent too high (Beynon and Brown, 1959). It seems to imply that the value of α , chosen for a particular altitude so as to cause a certain frequency to be reflected in a particular month, will not necessarily be the correct value in other months. Alternatively, this high figure may be caused by incorrect temperature or pressure data, or incorrect mixing ratios of the various constituents. This is believed to be the first calculation of its type to determine the seasonal variation in electron density in the E region.

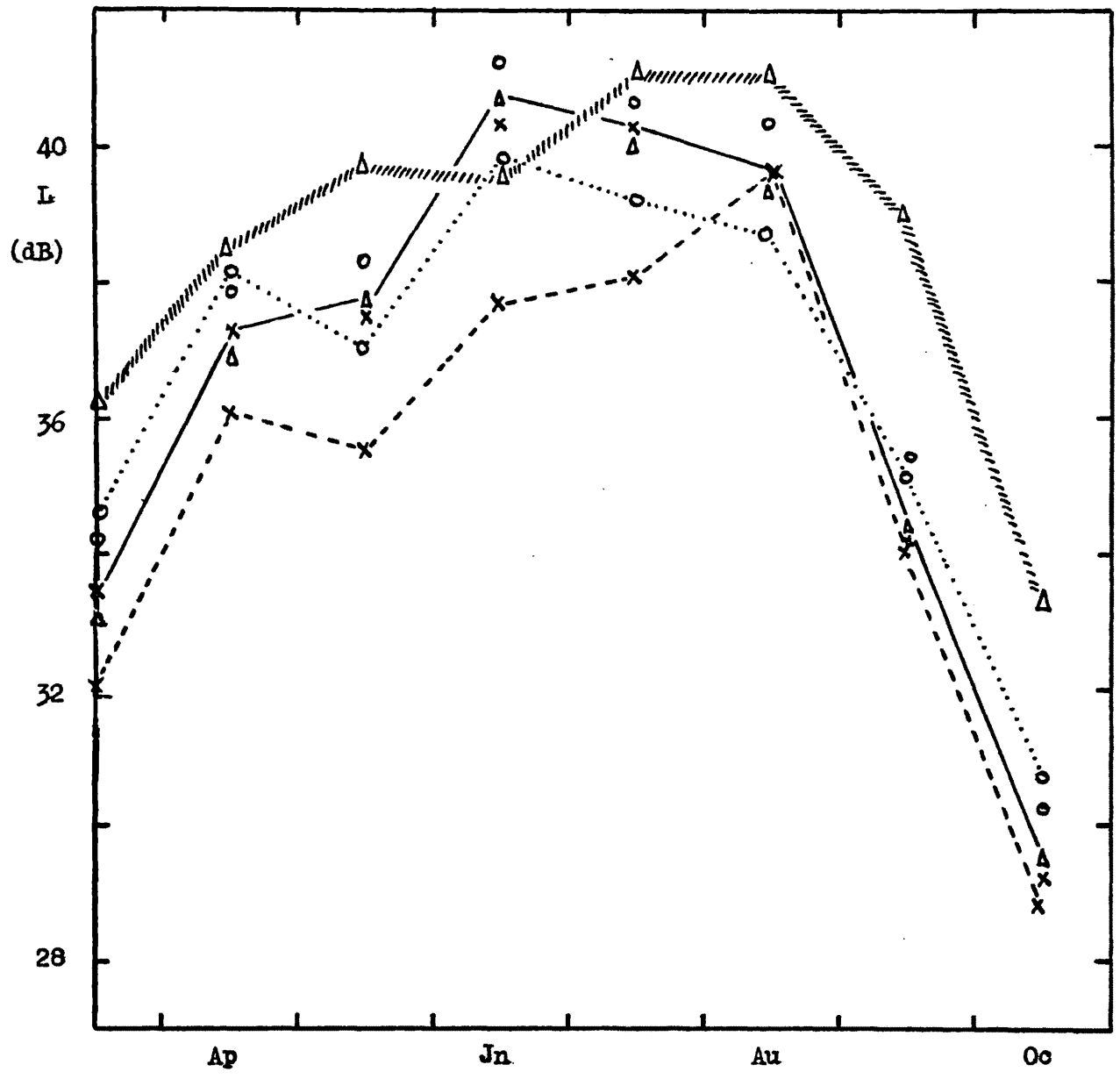

Fig. 7.16

Seasonal Variation in Absorption at R = 100

- – – – –x de Bilt, 1.95 MHz)
- ////////////Δ Slough, 2.00 MHz) Mean experimental data
- ·····o Freiburg, 2.05 MHz)

Δ
——— x Model values of absorption, corresponding to the above experimental results.
o

Note on Figs. 7.16 - 7.18 and 7.22 - 7.27

For reasons of clarity, only one line has been drawn between the model values. In each case this joins the medians of the three values.

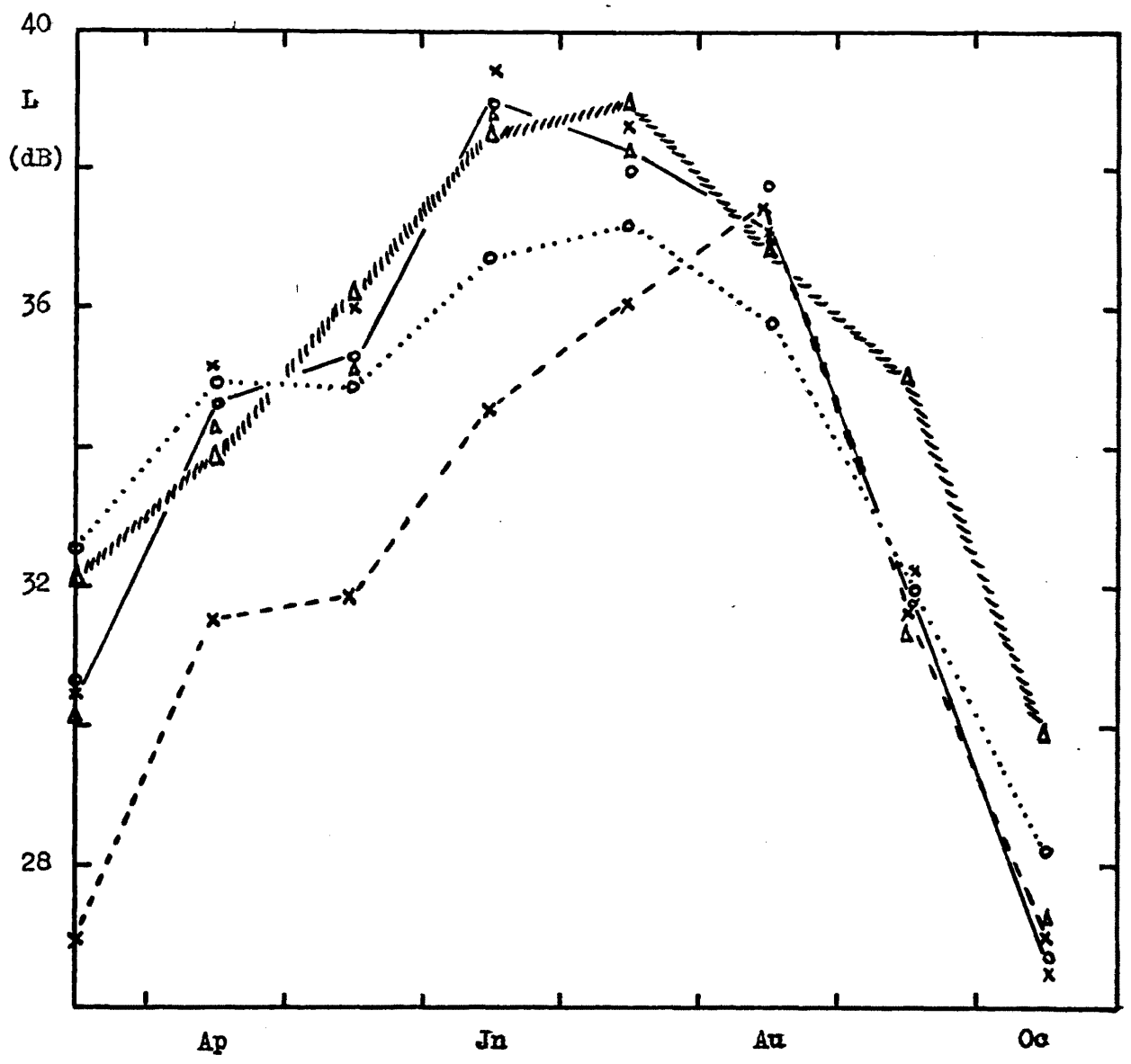

Fig. 7.17

Seasonal Variation in Absorption at R = 100

-----x de Bilt, 2.30 MHz)
Slough, 2.40 MHz) Mean experimental data
.....o Freiburg, 2.44 MHz)

Model values of absorption, corresponding to the above experimental results.

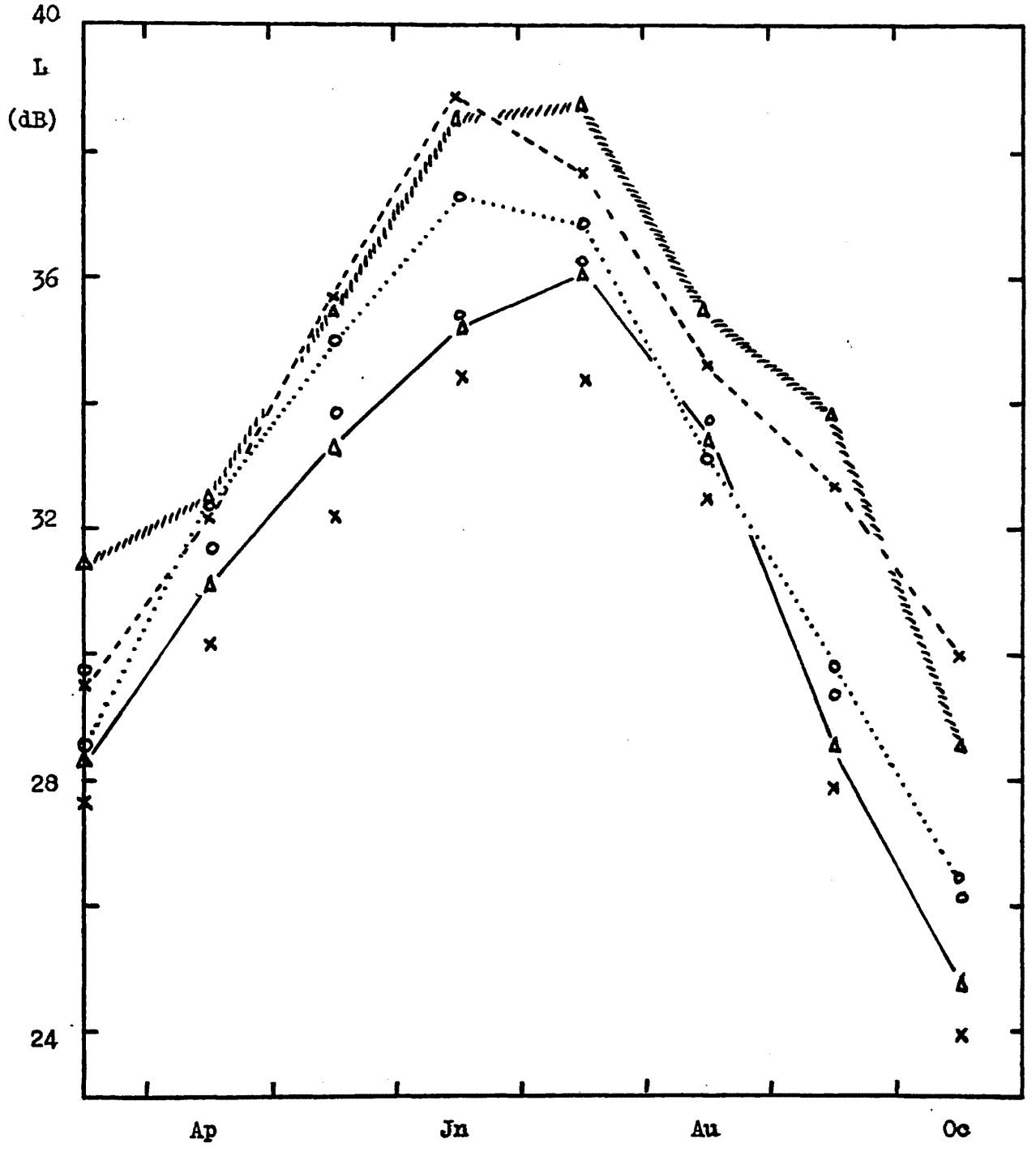

Fig. 7.18

Seasonal Variation in Absorption at R = 100

Slough, 2.80 MHz)
de Bilt, 2.90 MHz) Mean experimental data
Freiburg, 2.90 MHz)

Model values of absorption, corresponding to the above experimental results.

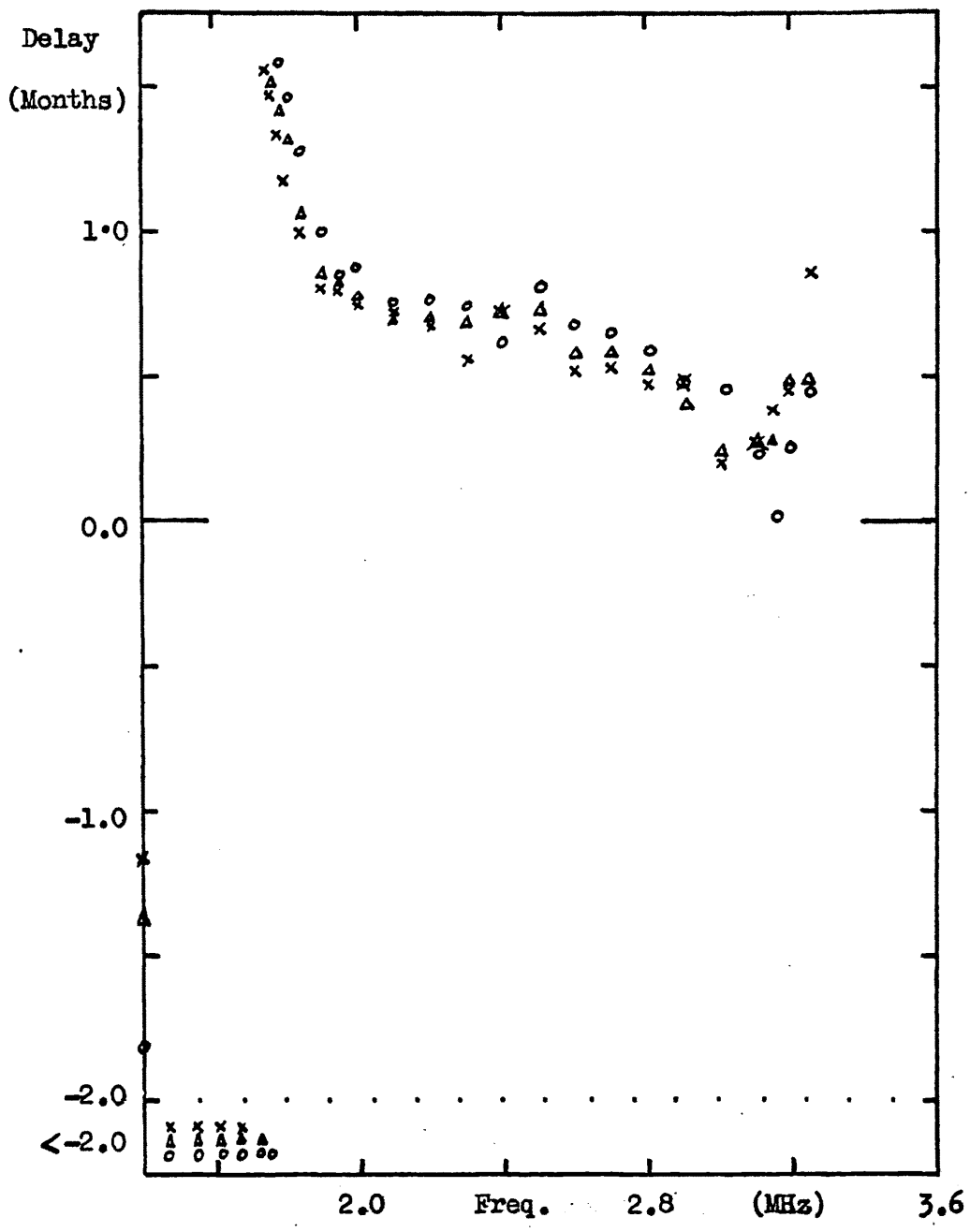

Fig. 7.19

"Delay" Values obtained from the Absorption Model at R = 100

Δ Slough

× de Bilt

o Freiburg

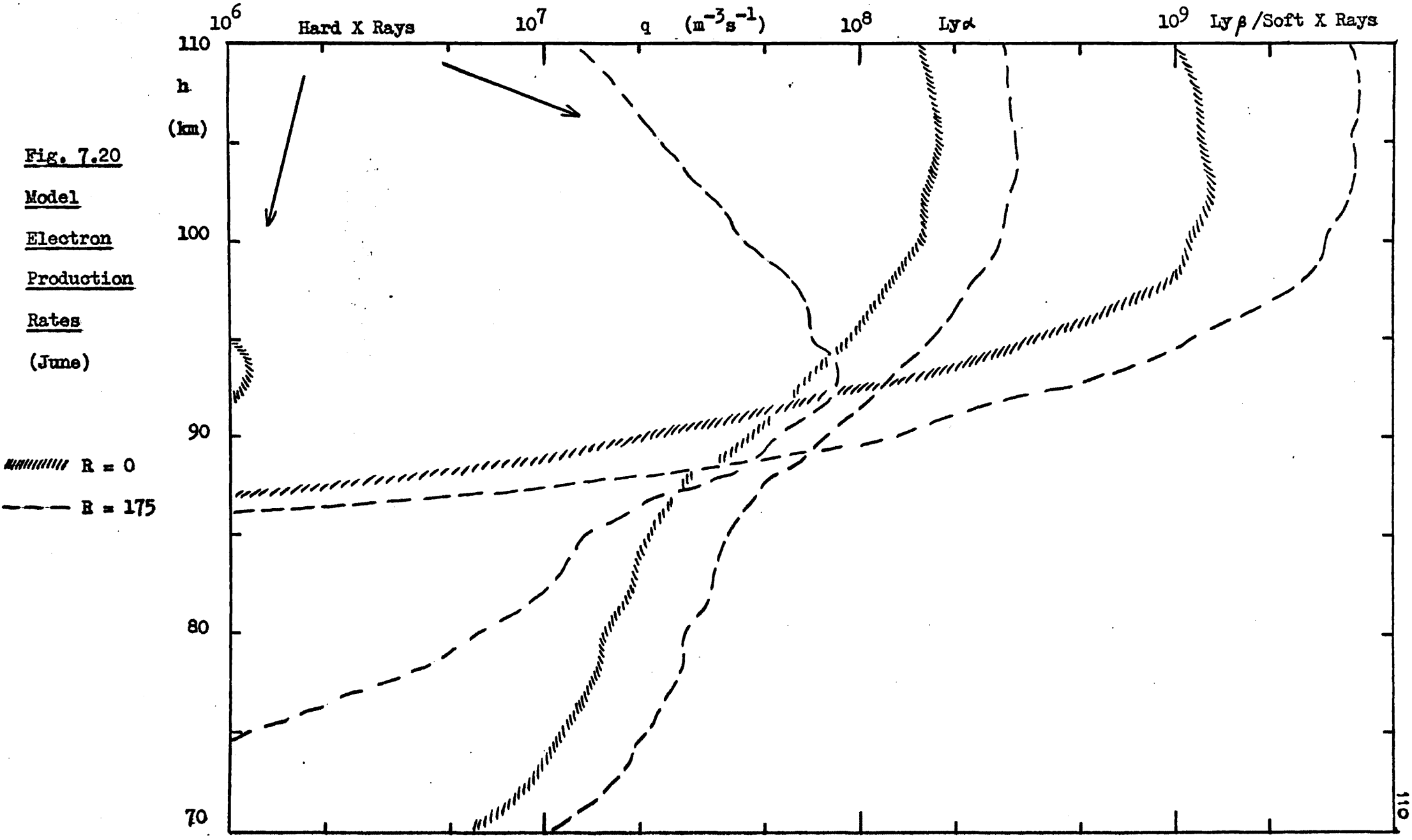

Fig. 7.20 Model Electron Production Rates (June)

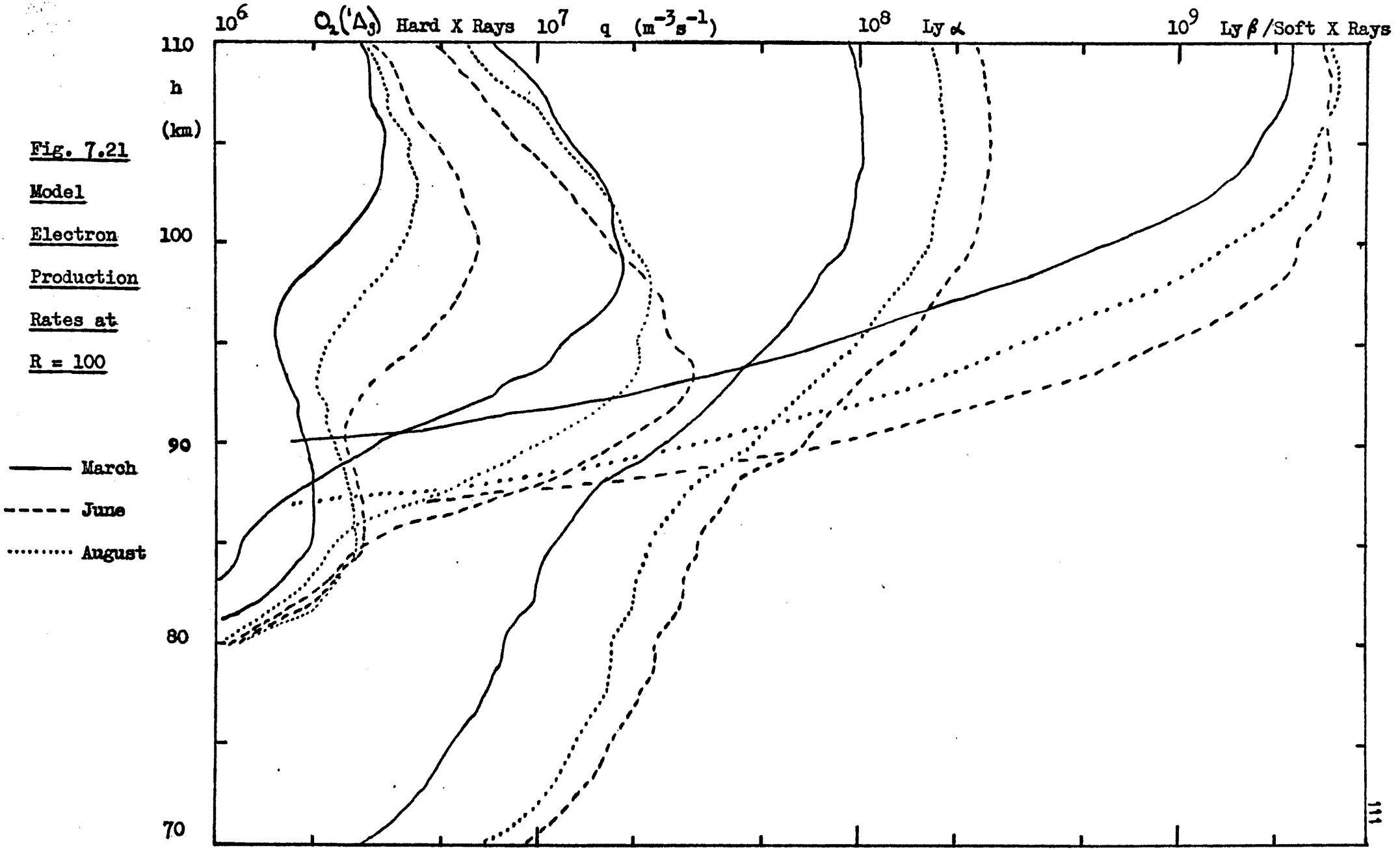

Fig. 7.21 Model Electron Production Rates at R = 100

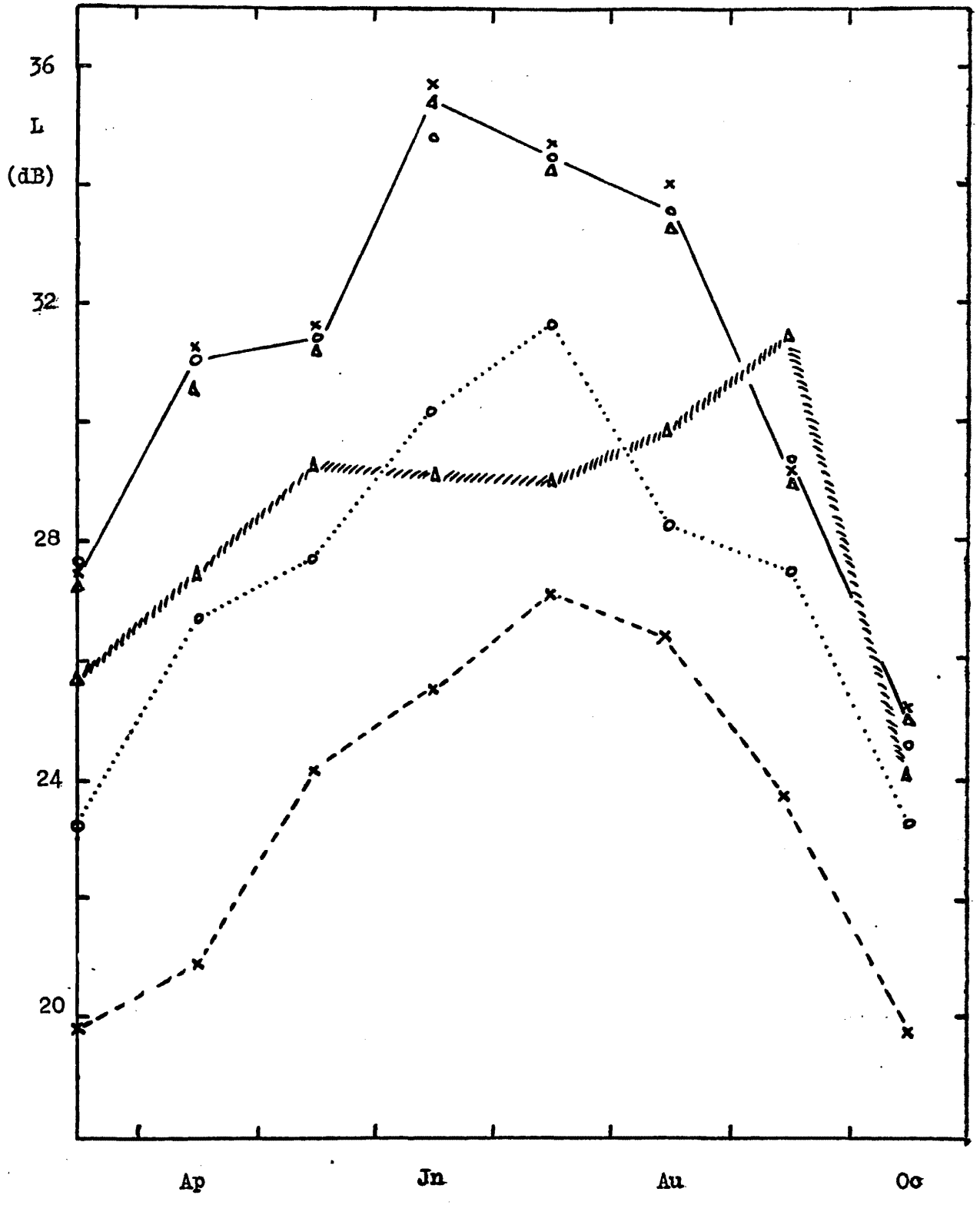

Fig. 7.22

Seasonal Variation in Absorption at R = 0

- - - - - - × de Bilt, 1.95 MHz)
/////////// Δ Slough, 2.00 MHz) Mean experimental data
..... o Freiburg, 2.05 MHz)

——— Δ × o Model values of absorption, corresponding to the above experimental results.

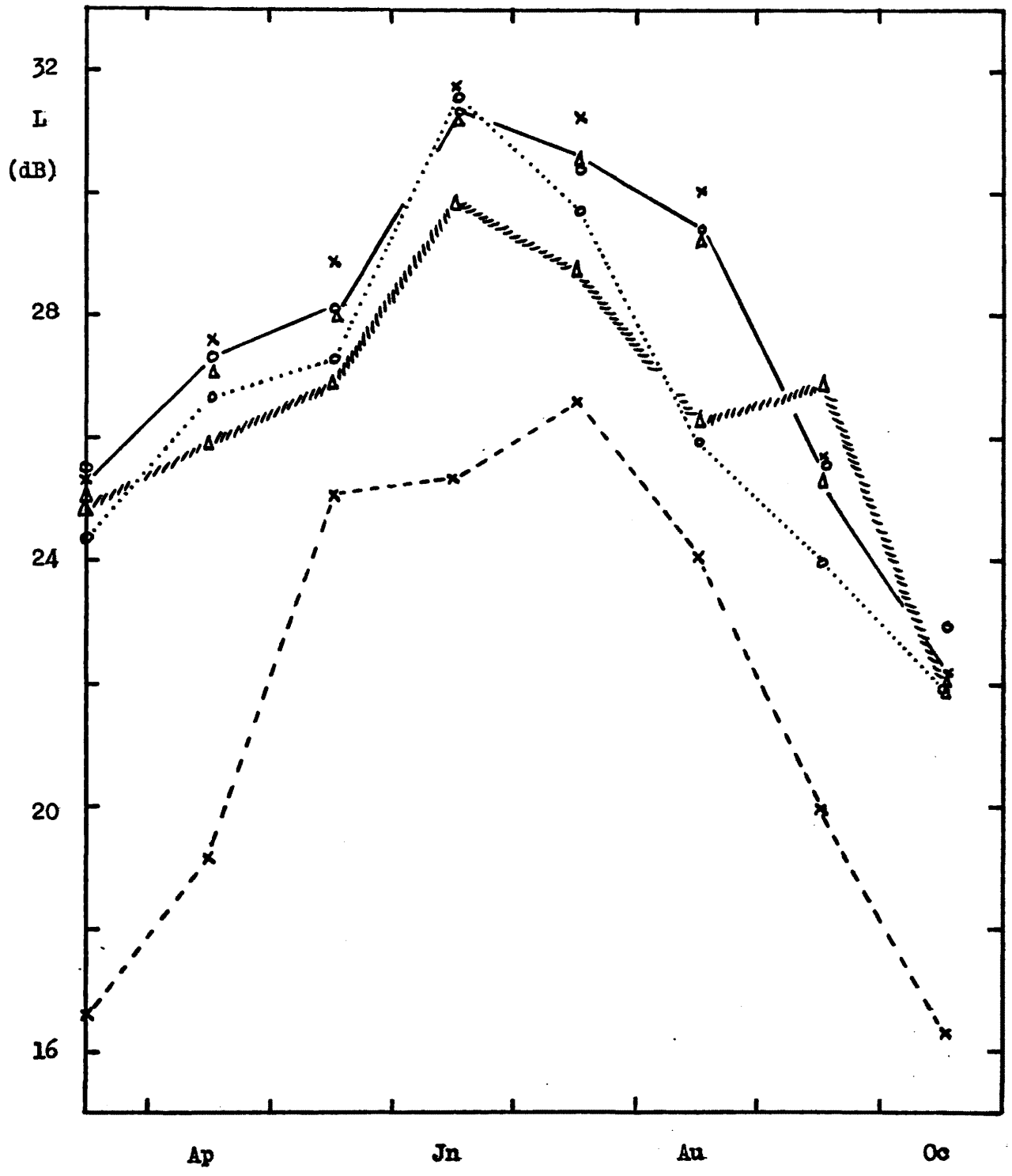

Fig. 7.23

Seasonal Variation in Absorption at R = 0

----x de Bilt, 2.30 MHz)
/////////Δ Slough, 2.40 MHz) Mean experimental data
.....o Freiburg, 2.44 MHz)

———— Δ x o Model values of absorption, corresponding to the above experimental results.

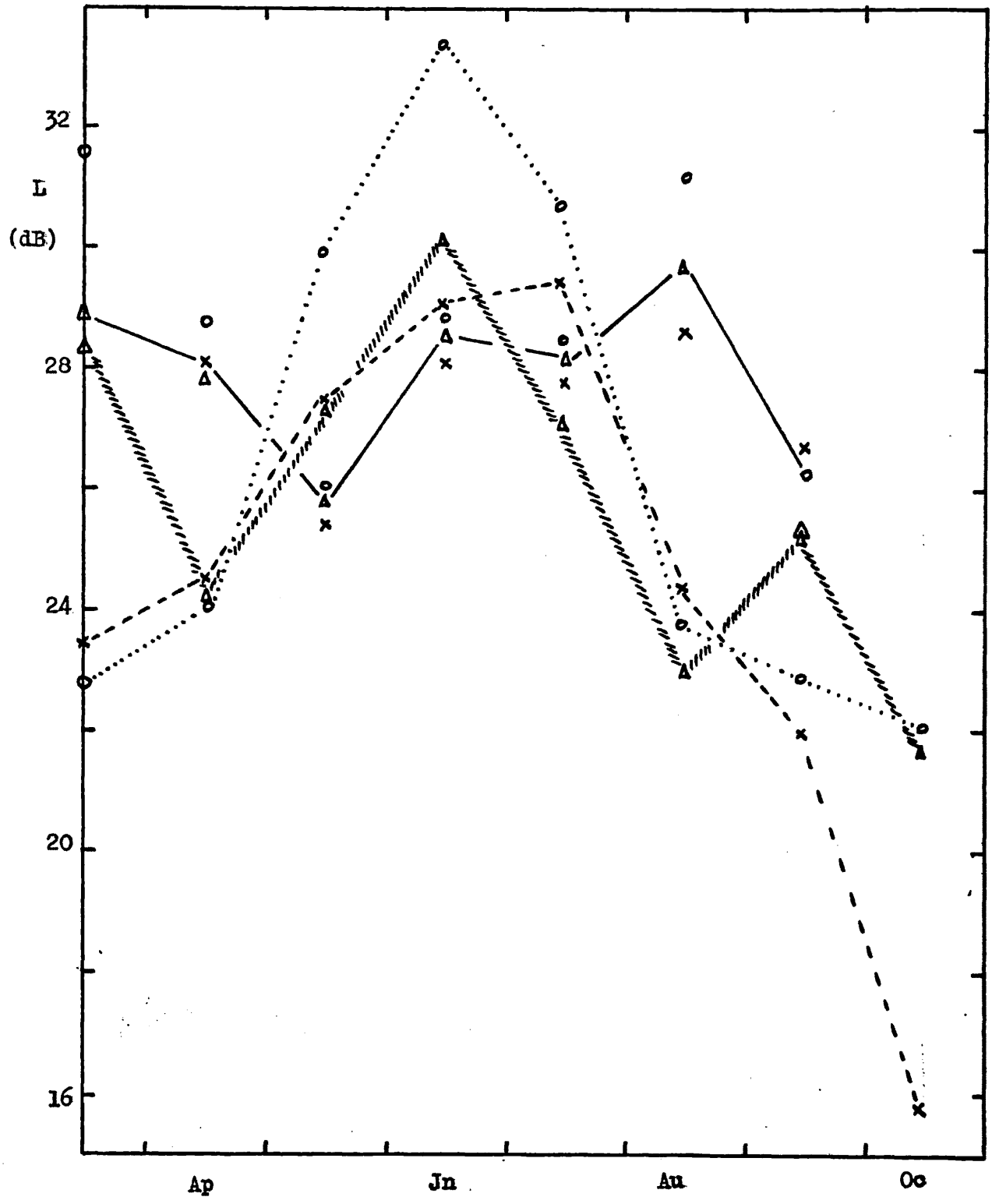

Fig. 7.24

Seasonal Variation in Absorption at R = 0

Δ Slough, 2.80 MHz)
× de Bilt, 2.90 MHz) Mean experimental data
o Freiburg, 2.90 MHz)

Model values of absorption, corresponding to the above experimental values. In those cases where no value is shown, the frequency is in excess of f_oE.

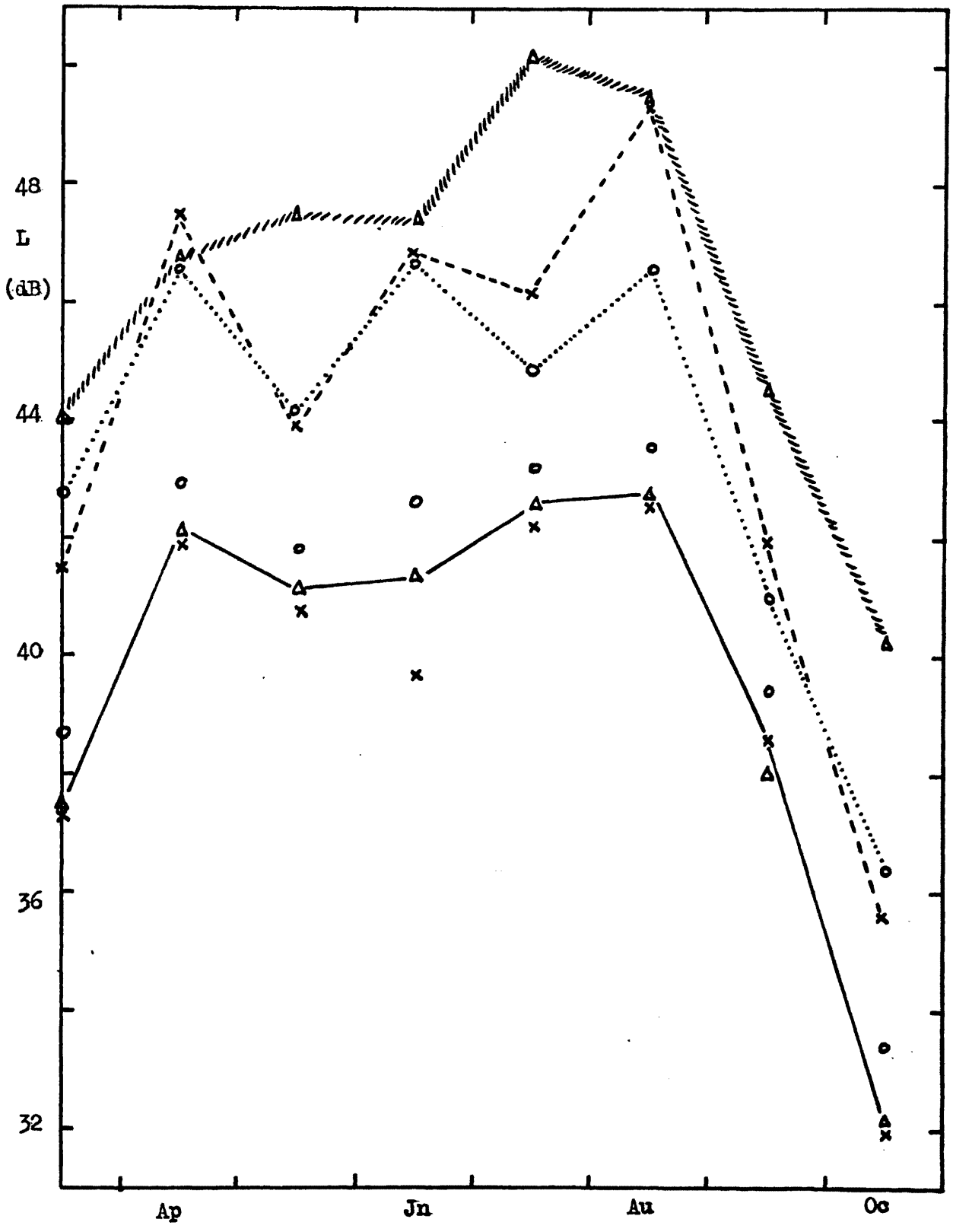

Fig. 7.25

Seasonal Variation in Absorption at R = 175

- - - - -× de Bilt, 1.95 MHz)
////////////Δ Slough, 2.00 MHz) Mean experimental data
.....o Freiburg, 2.05 MHz)

———— o × Δ Model values of absorption, corresponding to the above experimental results.

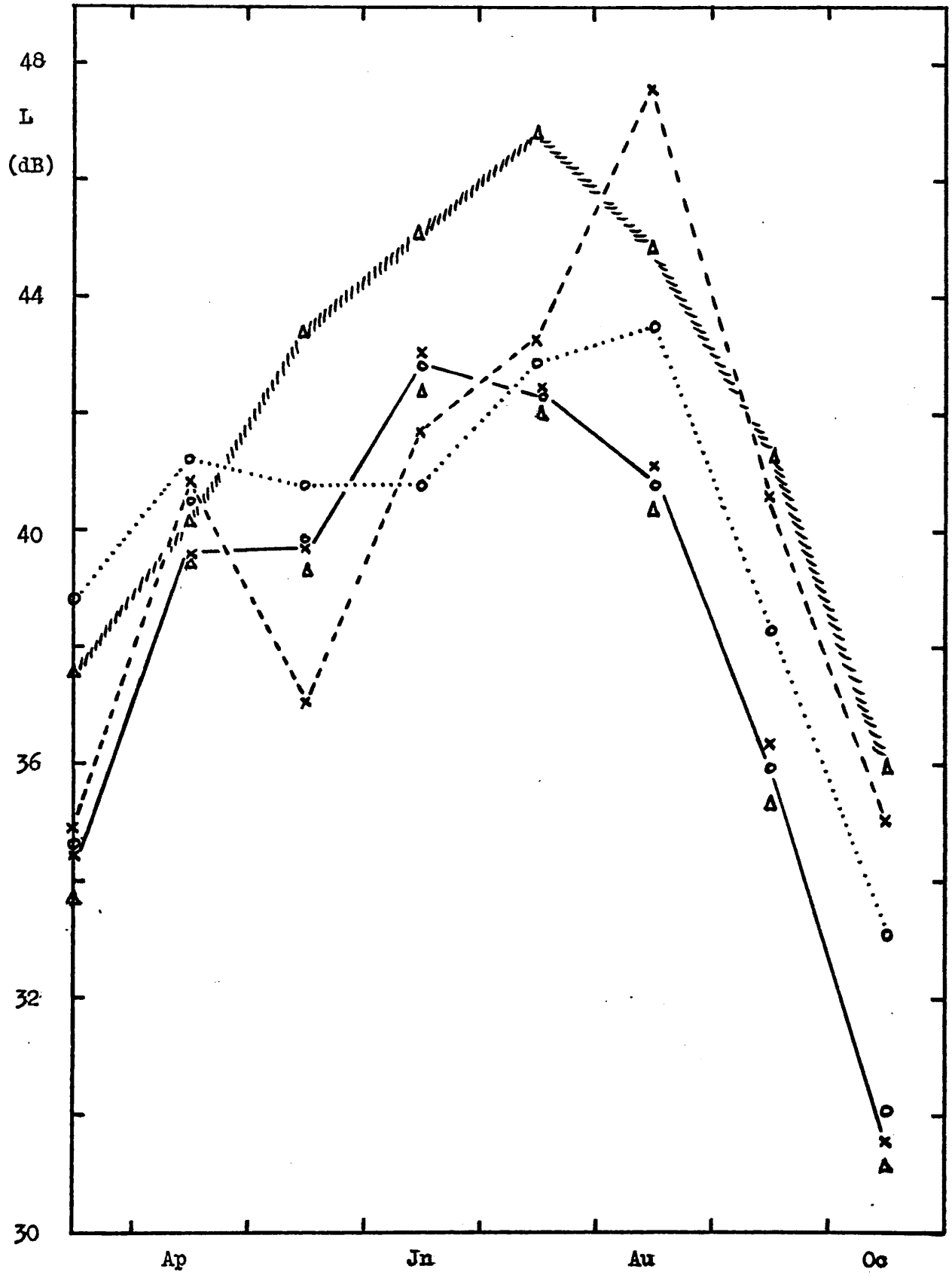

Fig. 7.26 Seasonal Variation in Absorption at R = 175

----x de Bilt, 2.30 MHz)
//////Δ Slough, 2.40 MHz) Mean experimental data
.....o Freiburg, 2.44 MHz)

Δ
———— x Model values of absorption, corresponding to the above experimental results.
o

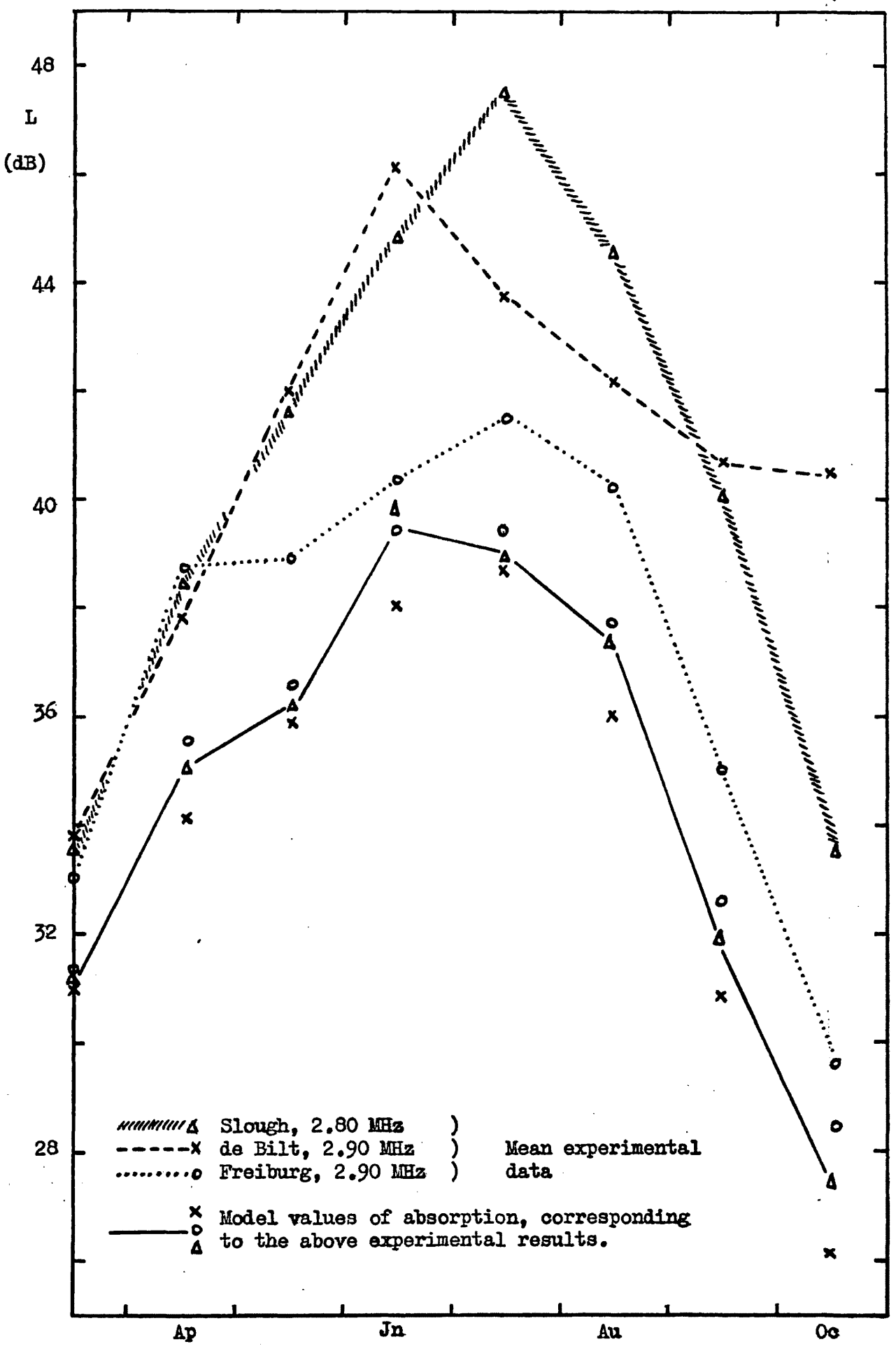

Fig. 7.27 Seasonal Variation in Absorption at R = 175

7.2.2 Agreement of Model with Experimental Values of Absorption and "Delay" at R = 100 .

Because of their different latitudes, the stations Freiburg, Slough, and de Bilt each have different values of Cos χ for their local noon. As this is a term in the calculation of the optical depth, and hence also electron density and absorption, the model yields slightly different values of absorption for each of the three stations. All other parameters have of necessity been assumed to be identical. Fig. 7.16 shows a comparison of theoretical and experimental values of absorption at the three stations at around 2.0 MHz. The enhancement in April in the experimental values has a rather less pronounced counterpart in the model values. In general, the models are in better agreement with the experimental values taken as a whole than one experimental value with another.

The same can be said of Fig. 7.17 , which shows the values of absorption at around 2.4 MHz. Model and experiment both show an April enhancement, but this time to a smaller extent. Fig. 7.18 shows the situation at around 2.9 MHz. The June and July values for the model are rather on the low side (cf. 2.0 MHz).

Fig. 7.19 shows the values of "Delay" calculated for the models at R = 100 . It will be seen that from 1.8 to 3.0 MHz the station of lowest latitude (Freiburg) has the highest delay, but above this frequency the situation is reversed. The experimental values of delay (Figs. 6.6 - 6.8) do not appear, however, to exhibit a similar general trend.

The significance of the delay values for frequencies below 1.8 MHz will be discussed in §7.4.1 .

7.3 Observations from the Model.

7.3.1 The Relative Importance of the Different Ionisation Processes for the Various Solar Activities.

The grouping of the ionisation processes into categories:-

(i) Lyman alpha

(ii) Lyman beta, and 30-120 Å X rays

(iii) Ionisation of $O_2(^1\Delta_g)$

(iv) 2-10 Å X rays

is similar to that adopted by Thomas (1971). Fig. 7.20 shows the June production rates for groups (i), (ii), and (iv) both at R = 0 and R = 175. It will be seen that although the largest relative change has taken place in the 2-10 Å X rays, Lyman alpha and Lyman beta plus soft X rays still maintain overall control. No solar dependence of the nitric oxide concentration has been included in the model but, as Thomas (1971) has pointed out, this is likely to be more significant than the change in Lyman alpha flux.

Fig. 7.21 shows the production rates corresponding to R = 100 for March, June, and August for each of the groups. Cosmic rays have been excluded from the diagram, since their electron production rates only become significant at altitudes where little absorption is taking place.

7.3.2 The Model's Values of Absorption at Low and High Sunspot Numbers, and a Comparison with Experimental Values.

Figs. 7.22 - 7.24 show the comparison of model and and experimental absorption values at R = 0 for frequencies near 2.0, 2.4, and 2.9 MHz respectively. Figs. 7.25 - 7.27 indicate the corresponding situation at R = 175 .

At R = 0 , for 2.0 and 2.3 MHz again the model yields rather too much absorption in June. At a frequency of 2.9 MHz, this is very

near to, or in excess of, f_oE, except in the mid-Summer months. In these circumstances, the model might be expected to yield unreliable results. Where no result at all is indicated , f_oE has been exceeded.

For R = 175 , it is the experimental values of absorption at 2.0 and 2.3 MHz that exhibit a most irregular behaviour. This effect will be discussed in §7.6 . For all frequencies, the theoretical model yields absorption values slightly on the low side.

Direct comparison of the results in the present work with those of George (1971) is not possible for the following reasons:-

(i) All his absorption measurements have been normalised to the overhead sun position (i.e. $\cos\chi = 1$). This has involved the use of a direct $\cos^n\chi$ relationship, which has, in the present work, been shown to be unreliable.

(ii) In order to calculate $\int N\nu dh$, he has used the absorption data at several frequencies, and has assumed that the absorption is proportional to $(f + f_L)^{-2}$. Quite apart from the previous evidence, outlined in §4.4.1 of the present work, Figs. 6.2, 6.3, and 6.4 certainly seem to suggest that the frequency dependence is a function of season.

7.4 The Variations in Delay.

7.4.1 An Extension of the Model to Lower Frequencies.

Appleton and Piggott (1954) have pointed out that the use of an absorption formula at frequencies lower than about 2.0 MHz leads to inaccuracies in the final result. It was decided, nonetheless, to investigate whether the values of delay obtained for the theoretical values of absorption in the range upwards from 0.9 MHz would yield any insight into the overall processes. A graph of delay of theoretical absorption as a function of frequency for Freiburg at R = 100 is shown in Fig. 7.29 .

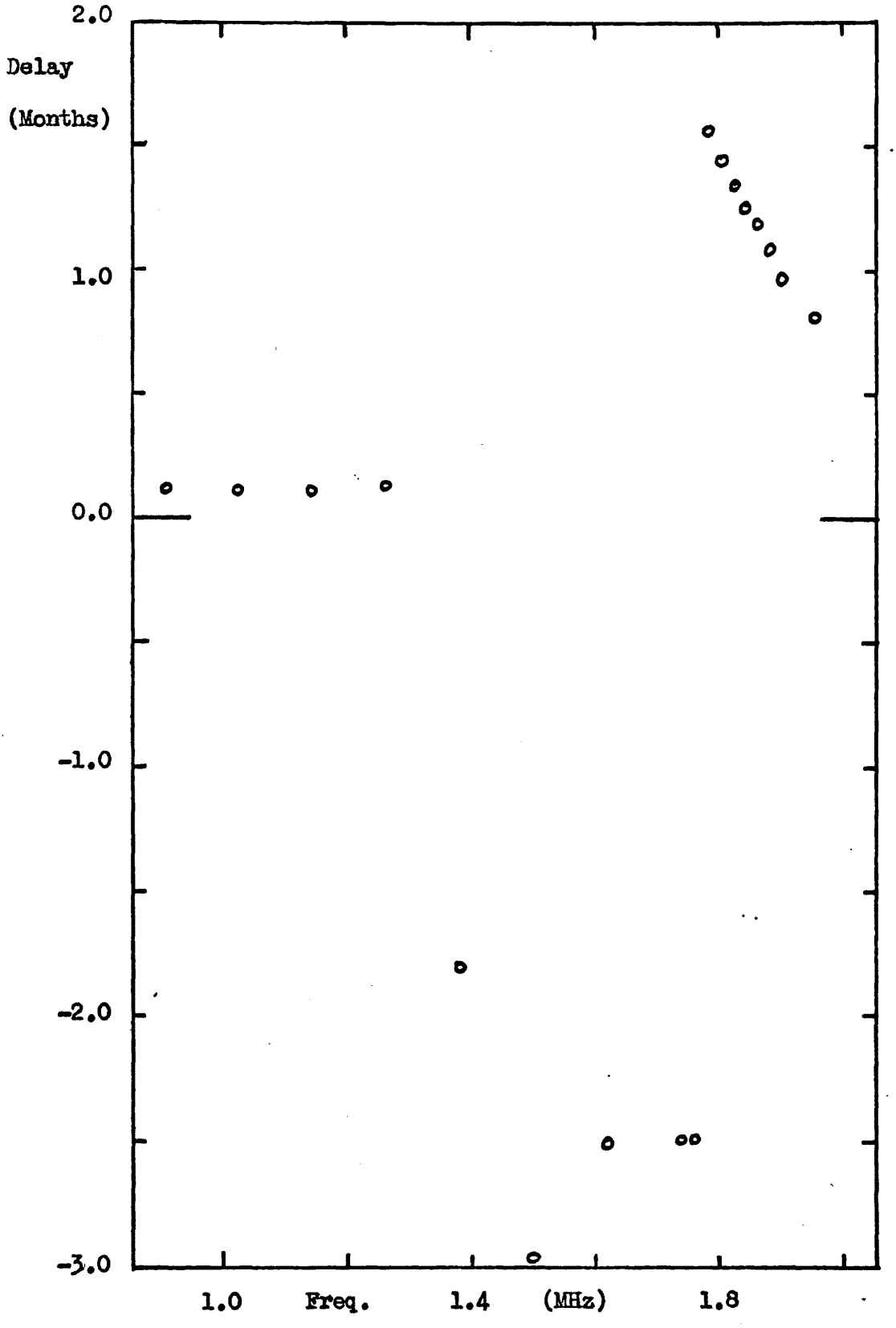

Fig. 7.28

"Delay" Values obtained from the Absorption Model for Lower Frequencies at Freiburg (R = 100)

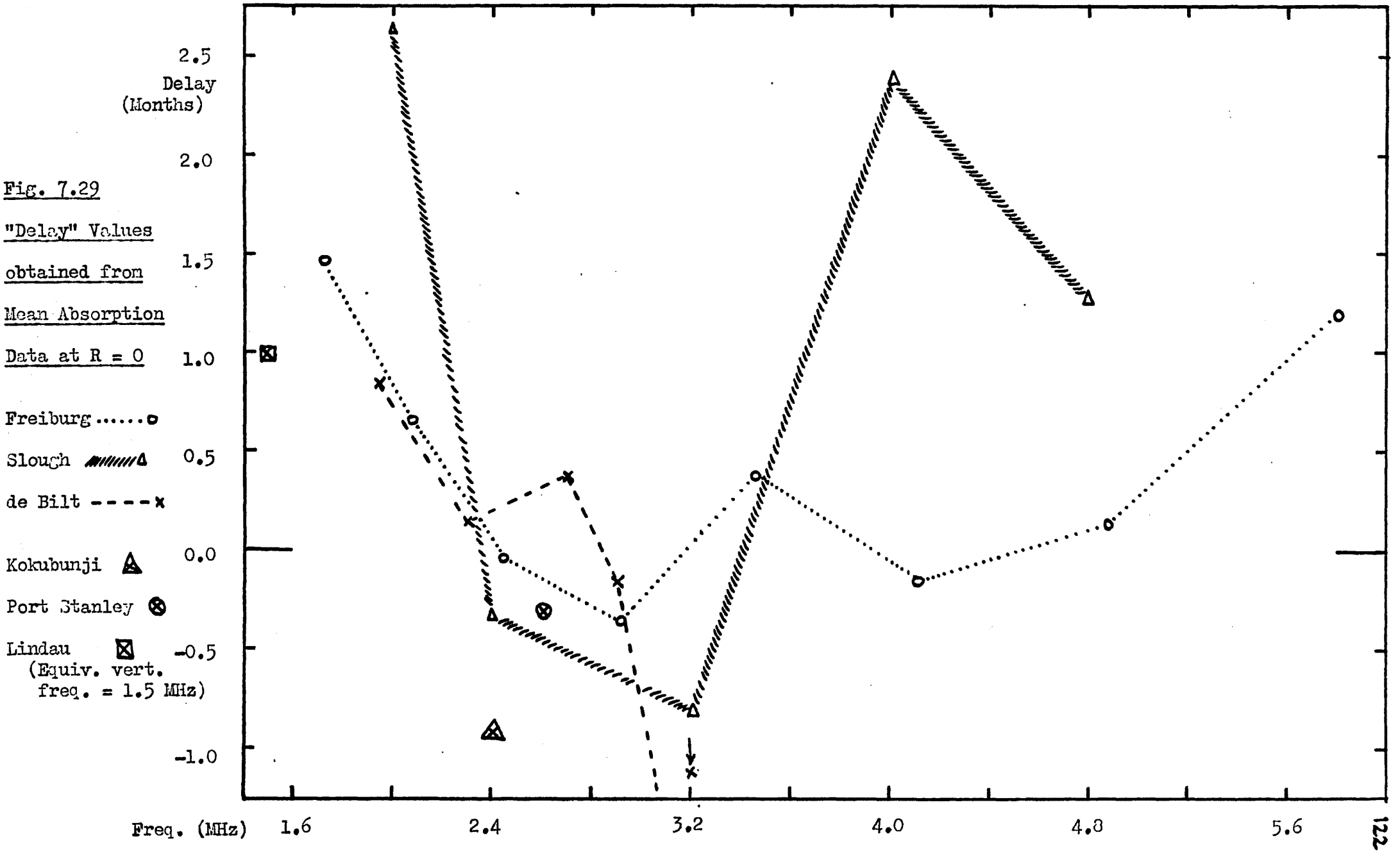

Fig. 7.29

"Delay" Values obtained from Mean Absorption Data at R = 0

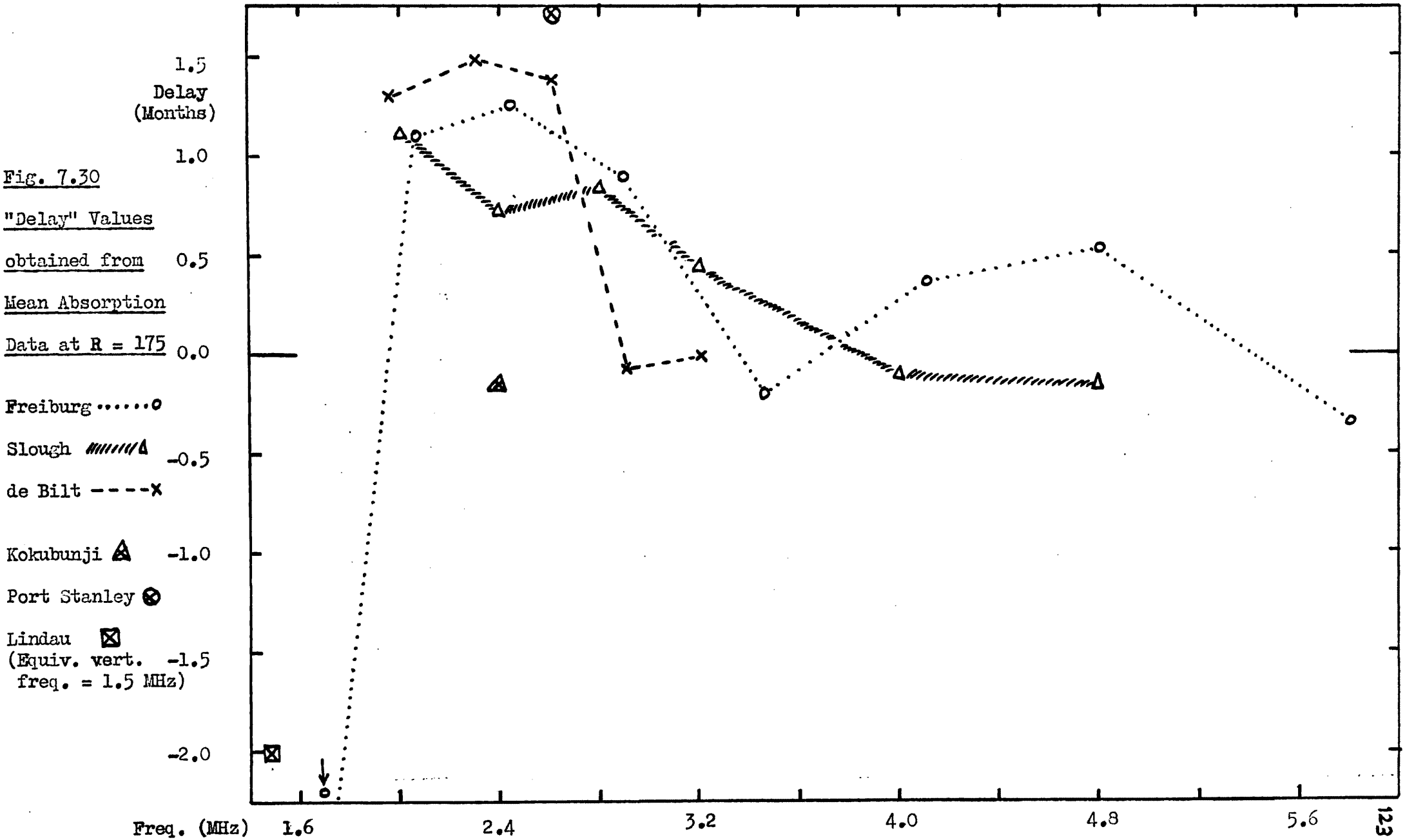

Fig. 7.30

"Delay" Values obtained from Mean Absorption Data at R = 175

"Delay" Values obtained from the Absorption Model

Δ Slough

× de Bilt

o Freiburg

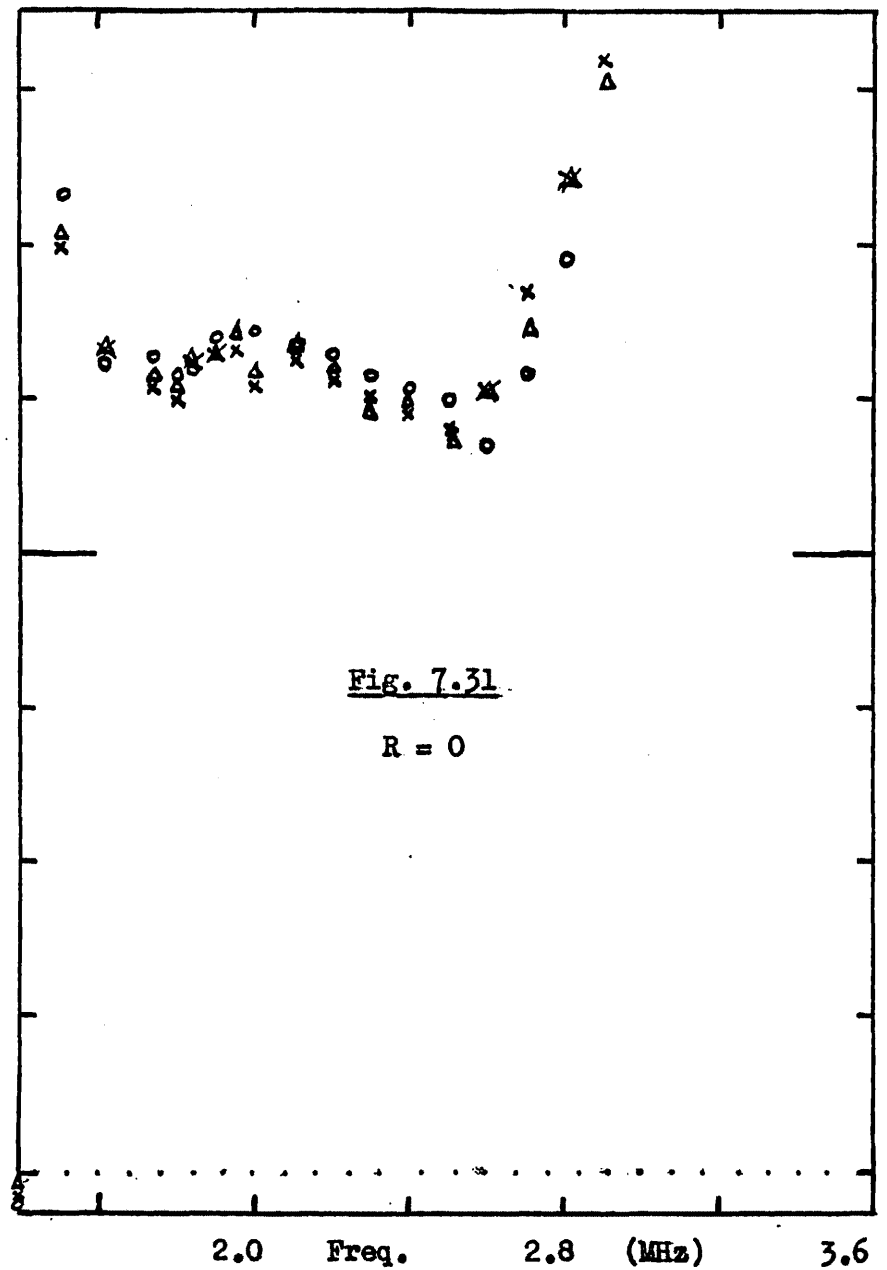

Fig. 7.31

R = 0

Delay (Months)

1.0

0.0

-1.0

-2.0

<-2.0

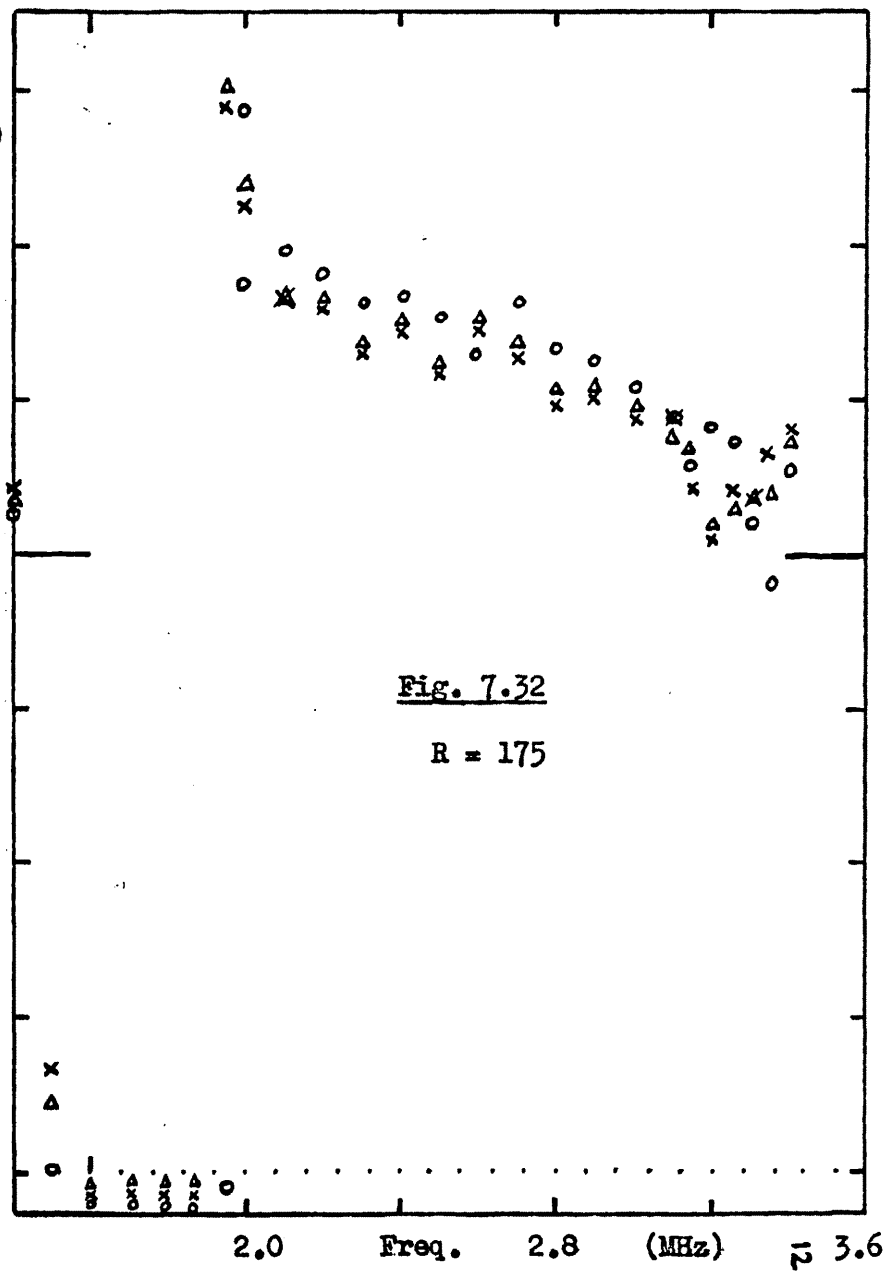

Fig. 7.32

R = 175

Up to 1.26 MHz the delay is static, after which a peak in absorption appears in April, which turns the delay into a lead. At 1.74 MHz there is a clear minimum in the June absorption, and by 1.78 MHz the August peak has become larger than that in April or May, with the result that the delay changes "asymptotically" from $-2\frac{1}{2}$ to $+1\frac{1}{2}$ months. Above this frequency, the delay gradually diminishes. Further information on this can be obtained by considering the effect of varying sunspot number.

7.4.2 The Effects of Varying Solar Activity on Experimental and Theoretical Values of Delay.

Figs. 7.29 and 7.30 show the values of delay for the experimental results as a function of frequency, corresponding to R = 0 and R = 175 respectively, in the same format as that for R = 100 (Fig. 6.8).

Various features emerge from the figures:-

(i) In the range 2.2 MHz to 3.2 MHz, each station exhibits increasing Delay with increasing solar activity. Above this frequency there would seem to be evidence that it is the lower sunspot number that will have the greater delay, and at frequencies above about 4.0 MHz no real conclusions may be drawn, due to a shortage of data.

(ii) In the case of Lindau, it can be argued that this is perhaps at the frequency where there is the "asymptotic" change in delay, mentioned above. Moreover, the relative values for the delay for the three different solar activities, and also the delay value at Freiburg for R = 175 , lead to the conclusion that possibly the position of the "asymptote" might be determined by solar activity; the higher the sunspot number, the higher the frequency at which the asymptote occurs.

Figs. 7.31 and 7.32 show the values of delay for the model at R = 0 and R = 175 (the values at R = 100 having already been given in Fig. 7.19). It will be seen that these show the same overall patterns as the experimental counterparts, notably that at frequencies above about 2.0 MHz, with higher solar activity, there will be greater delay. The reversal of this situation seems to occur in the model at a slightly lower frequency, 2.7 MHz, than in the experimental results. Groves (1970) indicates, however, that above 90 km his temperature and pressure models will be considerably less reliable than those below. These results are, of course, used not only in calculating the electron densities, but also the collision frequencies.

Again the movement of the "asymptote" with changes in solar activity can be detected. These similarities give rise to the following tentative suggestion:-

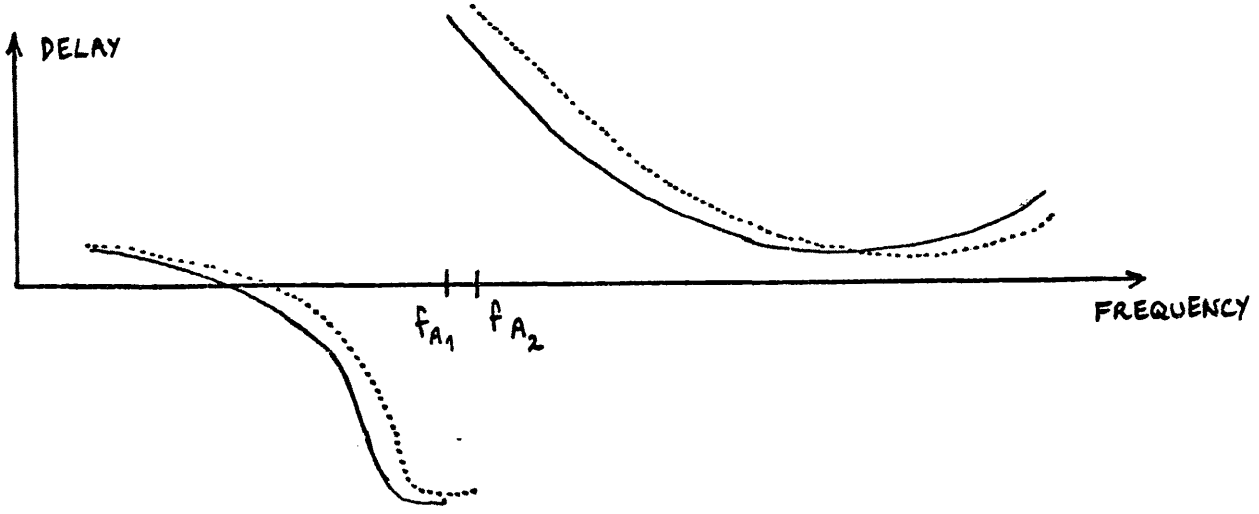

The continuous curve indicates a delay / frequency curve. A small increase in solar activity would have the effect of pushing the whole curve slightly to the right (i.e. to the dotted curve). Although Port Stanley and Kokubunji both exhibit increasing delays with increased solar activity, clearly they cannot be included in the above argument, because of their lack of multi-frequency data.

This effect would be caused by the varying relative importance of the different ionisation processes at a particular altitude for different seasons and solar activities.

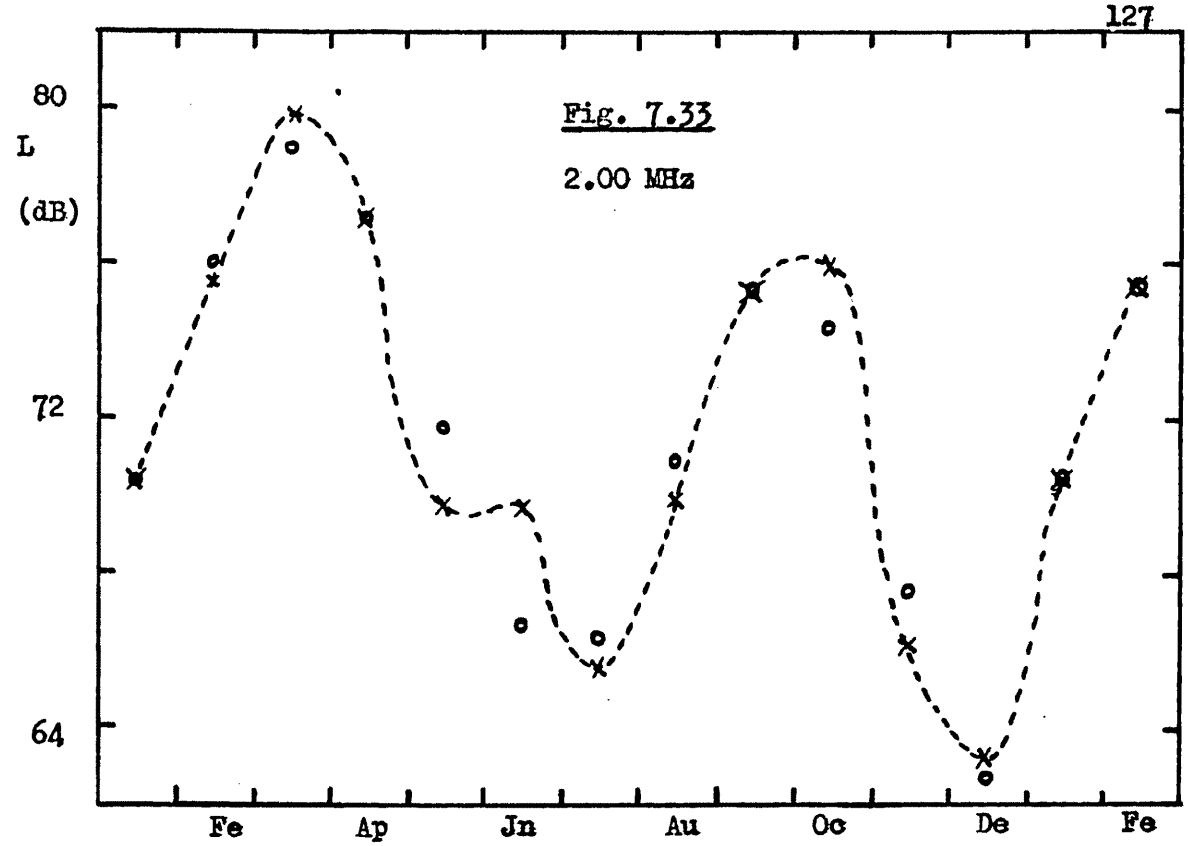

Fig. 7.33

2.00 MHz

SEASONAL VARIATION IN ABSORPTION AT IBADAN

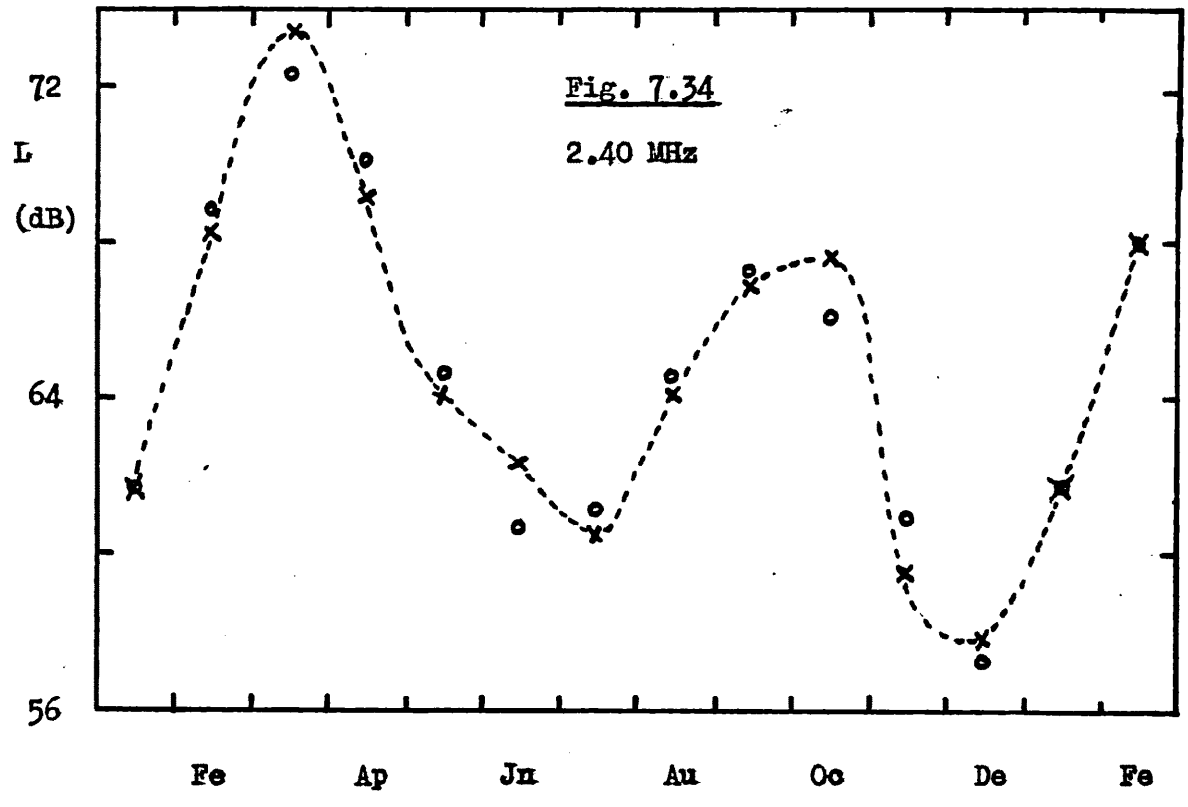

Fig. 7.34

2.40 MHz

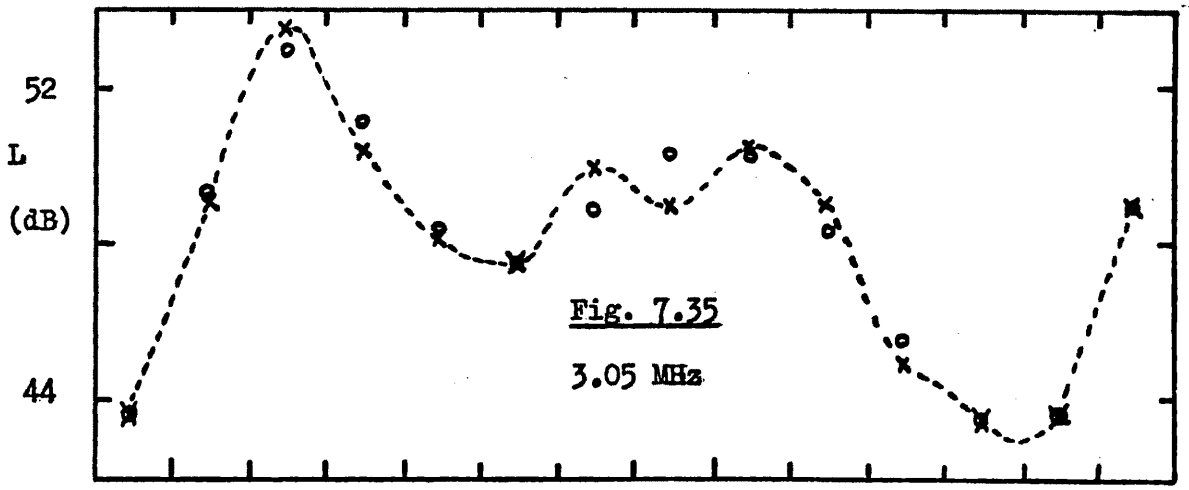

Fig. 7.35

3.05 MHz

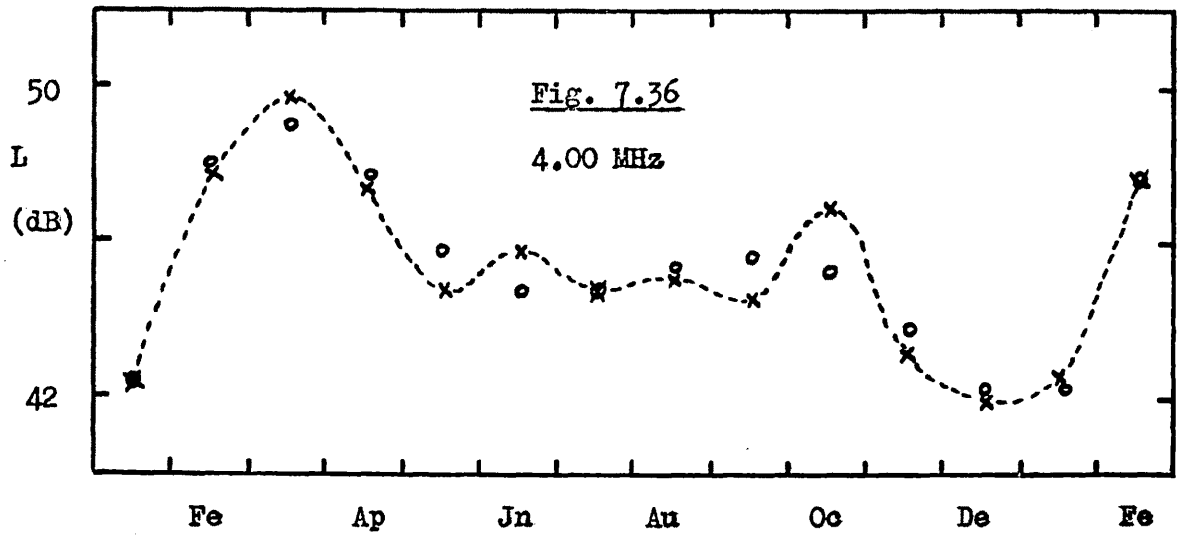

SEASONAL VARIATION IN ABSORPTION AT IBADAN

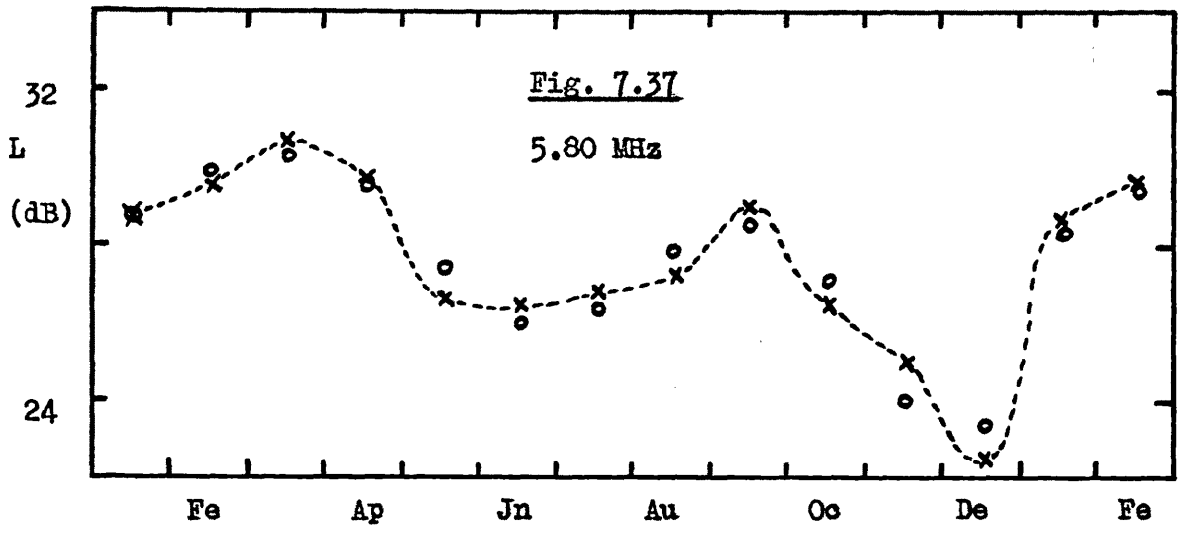

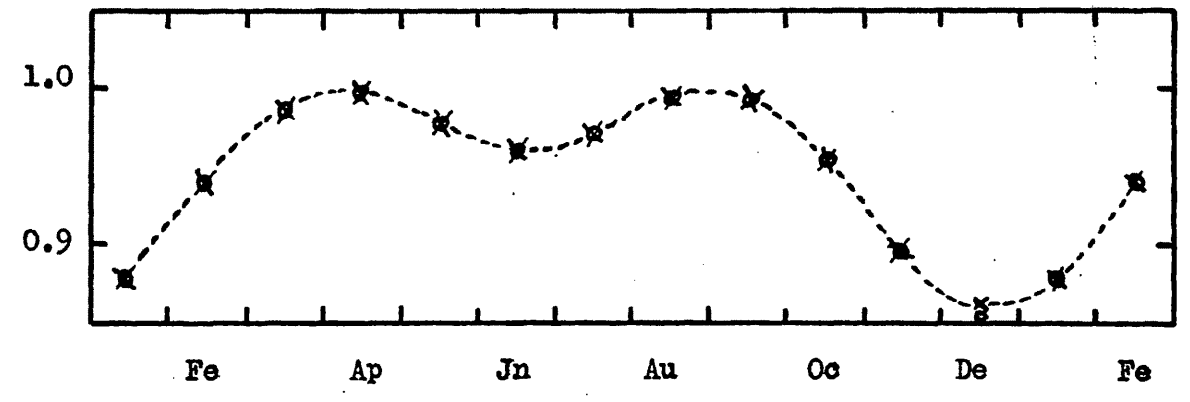

Fig. 7.38

SEASONAL VARIATION IN COS χ AT IBADAN

7.5 Interpretation of Experimental Results at Low Latitudes for R = 100.

An initial investigation of the data for low latitude stations indicated that it would be more difficult to interpret their results than those at mid-latitudes. This is because their two values of peak absorption occurring in March / April, and August / September are relatively close to the value at the June minimum, thus resulting in poorly defined curves.

Figs. 7.33 - 7.37 show the absorption results for Ibadan. The discontinuous line joins the "raw data" points, while the circles indicate the "best fit" polynomial of degree eight (the largest available on the computer subroutine), which in several instances has resulted in the incorrect positioning of the peak or trough. Fig. 7.38 shows the variation in Cos χ. The delay values are given in the table below, and those values which from a visual inspection do not agree with the raw data have been bracketed.

Freq. MHz.	First Max.	Mid-Yr. Min.	Second Max.	End-of-Yr. Min.
2.00	-0.39	(+0.48)	(+0.81)	-0.20
2.40	-0.52	(+0.34)	(+0.68)	-0.12
3.05	-0.52	(-0.30)	(-0.12)	+0.37
4.00	-0.80	(+0.37)	(+0.45)	+0.35
5.80	-0.65	(+0.24)	+0.35	(-0.50)

It will be seen that those turning points before which a large change in absorption has taken place are much better defined than the others. There seems to be a systematic change in the delay values of the first maximum. In general, the rate of change of delay with frequency is in the same sense as that for mid-latitude stations at comparable frequencies. There seems to be no detectable systematic change in the delay values for the December minimum. (Winter anomaly in any case precludes comparison with the mid-latitude data.)

One further point is that despite the complete symmetry of Cos χ about 21st June, the value of absorption at the first peak is always significantly larger than that at the second. This provides a certain amount of confirmation that the absorption is tending to lead Cos χ , because the minimum value of Cos χ following the first maximum is higher than that following the second.

Further evidence of a lead at low latitude may be found in a recent paper by Purkait and Datta (1972). A visual examination of their graphs of the seasonal variation in vertical incidence absorption data at 2.2 MHz at Haringhatta (22.9°N 88.6°E) indicates a clear lead of the order of half a month. Their corresponding curves, however, peaking at the Summer solstice, effectively appear to be forcing the data to fit a theoretical $\text{Cos}^n\chi$ variation.

It has already been shown that Kokubunji (35.7°N) suffers a lead in absorption at 2.4 MHz, as opposed to the delay at comparable frequencies experienced at higher latitudes (Figs. 6.8, 7.29, and 7.30).

Because of the comparative lack of data , and also the complication of the double peak, it was felt that no further relevant conclusions could be drawn from the absorption data of equatorial stations.

7.6 Interpretation of the Absorption Data of Individual Years.

In the analysis of data for individual years, it had been the intention to search for any long term trends in the year by year delays, having applied the sunspot correction, described in § 6.2 , to eliminate as far as possible any effects due to changes in solar activity.

If the absorption is corrected to a mean sunspot number within a particular year, then it cannot be said that the effects of changes of solar activity have been eliminated from year to year.

If, however, the correction were to a common sunspot number for all years (e.g. 100), then the "small" correction at low and high extremes of solar activity could exceed ± 10 dB, i.e. over thirty percent of the uncorrected value in some instances. An extrapolation of this order would have been unacceptable, and correction was made, therefore, to a mean sunspot number in a particular year.

It will furthermore be seen from the table below that the results of individual years in isolation can be very unreliable.

	Ashkabad		Aberystwyth		Rugen		Lindau	
	A1 3.0 MHz		A1 1.95 MHz		A1 3.86 MHz		A3 2.614 MHz	
	1958 $\bar{R}$ = 190		1965 $\bar{R}$ = 10		1964 $\bar{R}$ = 10		1966 $\bar{R}$ = 50	
	(i)	(ii)	(i)	(ii)	(i)	(ii)	(i)	(ii)
Mar.	32	32.07	21.95	21.74	18.6	18.20	29.0	32.21
Apr.	29	28.60	25.40	25.78	20.8	21.05	30.4	30.56
May	58	58.75	30.25	28.98	21.1	21.14	34.8	35.32
Jun.	39	39.88	29.80	29.27	21.2	21.26	33.3	33.58
Jul.	34	33.52	29.45	29.32	21.0	21.59	37.7	37.10
Aug.	21	19.74	29.00	29.11	19.6	19.68	34.8	34.67
Sep.	15	14.23	27.80	27.32	17.1	17.43	40.6	40.58
Oct.	26	26.68	21.15	20.34	15.7	15.92	38.4	37.61

Column (i) gives the experimental value of absorption, column (ii) gives the result corrected to a mean sunspot number, $\bar{R}$.

The first example is of a single peak which is almost certainly anomalous. The second and third are examples of very poorly defined peaks, while the fourth has no less than three apparently sharp peaks.

In view of these fluctuations in the comparatively limited data available, it was considered that physically meaningful delays would not be obtained, thereby precluding the detection of any long term trends that might have been present. This approach was, therefore, not pursued.

The results of the experimental work described in Chapter Five must be considered in a similar manner. It was not possible to prolong the experimental work, but with only two years' data for two stations, it was found difficult to detect genuine seasonal variations amongst the anomalous ones.

In order to check, however, that the overall pattern of Delay values for individual years was not totally at variance with that of the long term analysis, the following procedure was adopted:-

Years were arranged in groups according to whether there was low, medium, or high solar activity. Within each group there were five frequency sectors. In each case the mean and r.m.s. deviation of all the meaningful delays (defined in §6.3.3) within a sector were calculated. Only the results of Freiburg, Slough, and de Bilt were included because of their comparatively close geographical location, and because many years of Al measurements at comparable frequencies were available. In addition, these were the only stations for which individual L / R graphs could be drawn, the gradient being needed for the correction in absorption to a common sunspot number.

The following table shows the results of these calculations. In each case the upper delay written is the one found by degree four polynomial, the lower by degree five. The figure in parentheses is the number of delay values from which the mean was calculated. If two numbers appear, it signifies that a particular delay value had to be excluded from the mean, because it failed to satisfy the necessary criteria.

Station / Freq. MHz	$\bar{\bar{R}} = 25$	$\bar{\bar{R}} = 85$	$\bar{\bar{R}} = 170$
a Fre.	0.3 ± 1.6 (3)	0.8 ± 1.8	-1.8 ± 0.2 (2)
a 1.725	-0.1 ± 1.7 (4)	-0.3 ± 2.3 (6)	-1.2 (1)
b deB./Slo./Fre.	1.1 ± 1.1	0.9 ± 1.5	-0.2 ± 1.2
b 1.95 2.00 2.05	1.0 ± 1.3 (12)	0.6 ± 1.8 (10)	-0.1 ± 1.3 (7)
c deB./Slo./Fre.	0.5 ± 0.3	0.6 ± 1.2 (10)	0.8 ± 0.8
c 2.30 2.40 2.44	0.4 ± 0.7 (12)	0.3 ± 0.8 (9)	0.7 ± 0.7 (6)
d Slo./deB./Fre.	0.1 ± 0.6	0.4 ± 0.9 (10)	0.6 ± 0.3
d 2.80 2.90 2.90	-0.2 ± 0.7 (12)	0.2 ± 0.5 (9)	0.3 ± 0.4 (6)
e Slo./deB./Fre.	-0.1 ± 1.1	0.1 ± 0.8	0.5 ± 0.3
e 3.20 3.20 3.45	-0.4 ± 1.3 (12)	0.0 ± 0.8 (10)	-0.1 ± 0.3 (6)

$\bar{\bar{R}}$ represents the mean sunspot number for the group of years.

It has already been suggested that the frequency at which the "asymptotic" change in delay occurs may well be a function of solar activity, and it is reasonable to suppose that it may well vary slightly from year to year also. Its position in the table above would be recognised by a delay value fairly close to zero but with a large r.m.s. deviation. According to this argument, therefore, and with regard to the mean values of the delay, the "asymptote" lies somewhere in the range 1.7-2.0 MHz for low, 1.7-2.3 MHz for medium, and 2.0-2.3 MHz for high sunspot numbers respectively. This is consistent with both the long term analysis, and the theoretical model.

Beyond the asymptote, the delay in general tends to decrease with increasing frequency, and increase with increasing solar activity. These conclusions also are consistent with both the analysis and the model.

One further trend emerges from the table. Just beyond the asymptote, the r.m.s. deviation decreases, as might be expected. For high sunspot number, this is true in all five frequency sectors; whereas there is a slight increase in deviation in sector e for medium sunspot number, and a large increase for low sunspot number. At high solar activity, the frequencies in sector e are, in the Summer months, still well away from f_oE, whilst at $\bar{R} = 25$, f_oE for de Bilt is 3.3 MHz. It would seem significant that of the two occasions when there is large uncertainty in the date of peak absorption, one is where dN(e)/dh will be becoming increasingly small, while, for the other one, the frequency corresponding to the asymptotic change in delay, there is a sudden reduction in dN(e)/dh near the reflection level.

7.7 A Suggested Explanation of the Delay Phenomenon.

Before the argument is developed, it may be recalled that if, for some reason, dN(e)/dh becomes smaller, then the following changes take place:-

(i) Reflection will take place higher, hence $\int K\,dh$ will be larger than it would be, but:-

(ii) K will become slightly smaller than it would otherwise be, except that:-

(iii) if the frequency is close to the critical frequency for the layer, K will become larger (deviative absorption).

It seems that in general Effect (i) predominates.

If dN(e)/dh becomes smaller around the 90 km level, then for the lower frequencies, it is only in the non-Summer months that the wave will have to go to a higher altitude before reflection. The fact that it happens quite suddenly (i.e. $d^2N(e)/dh^2$ is large and negative), results in an accentuation of the effect, with a corresponding increase in the total absorption.

This would cause the June peak in absorption to be much less well defined, or even to disappear altogether in favour of Spring and late Summer peaks. If this is the case, then it is possible that meteorological factors, such as diffusion or turbulence, may determine which of the two peaks is the greater in any particular year. Slightly higher frequencies (e.g. > 2.0 MHz) will experience this effect to a lesser extent because, although the relative distances between the reflection heights for the various months are still about the same as for the lower frequency, the ionisation at these greater heights is much more subject to solar control. The value of K therefore acquires a more sharply defined peak in June.

If however the frequency approaches f_oE, again it is the waves in the non-Summer months that will have to go higher for reflection, and in this case they will suffer significant deviative absorption. Once again this effect may eliminate any clear peak of absorption in June.

Summarising therefore:-

It has already been shown that experimental values of D and E Region absorption cannot in general be regarded as directly proportional to a $\cos^n\chi$ law. There is some evidence to suggest that the breakdown is centred in two frequency zones:-

(i) Those frequencies that are reflected at or slightly above heights where there has been a sudden reduction in dN(e)/dh;

(ii) Those frequencies that are close to the critical frequency of the E region (at reflection $dN(e)/dh \backsim 0$);

the underlying cause in each case being the way in which dN(e)/dh varies as a function of height and season.

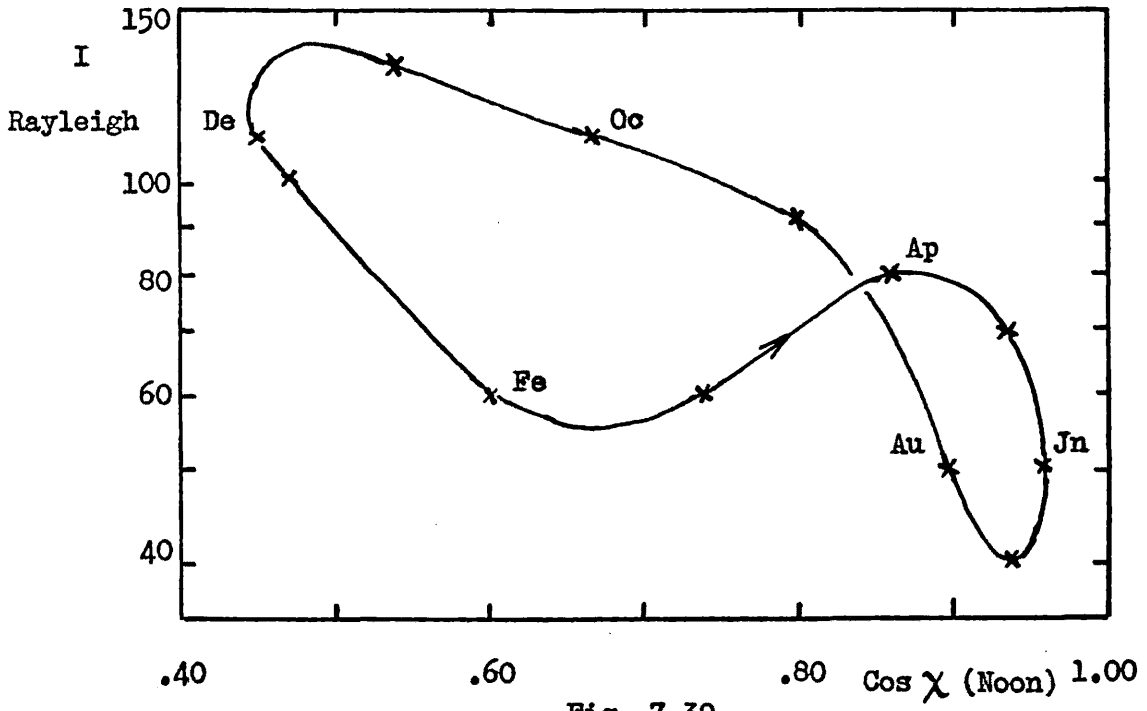

Fig. 7.39

Seasonal Variation of Hydroxyl Night Airglow Intensity (6700 K)

at 44° N (Huruhata, 1965)

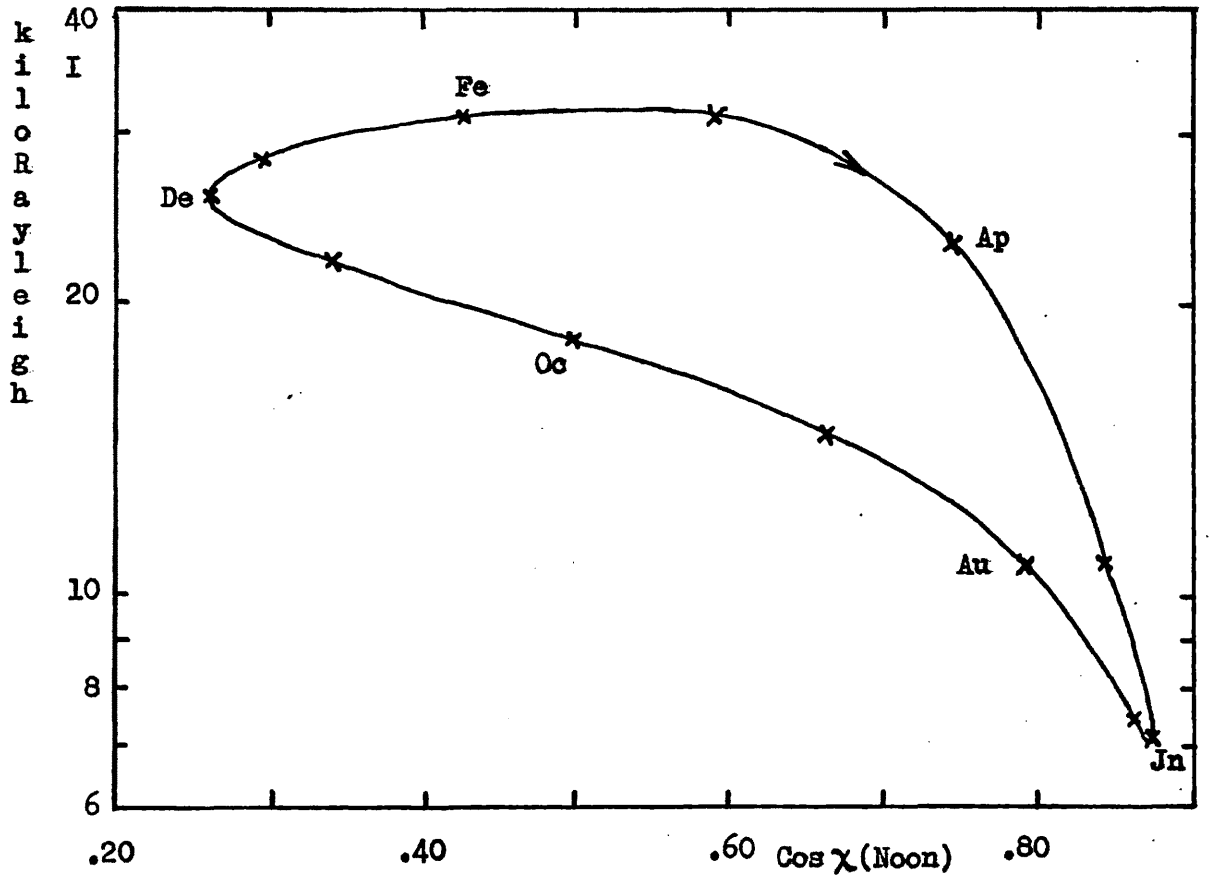

Fig. 7.40

Seasonal Variation of Sodium Twilight Airglow Intensity

at 52° N (Barbier, private communication)

7.8 Other Parameters related to Absorption.

7.8.1 Minor Constituents.

It has already been shown that in order to obtain an accurate theoretical value of the seasonal variation in radio wave absorption, it is necessary to know the variation in the effective electron loss coefficient, which is highly dependent upon the concentration of water cluster ions. A systematic investigation of the seasonal variation of these ions would be relevant, but as yet insufficient rocket flights have been made to permit this.

Sechrist (1972) has recently suggested that the reaction:-

$$O_2^+.(O_2) + H_2O \rightarrow O_2^+.(H_2O) + O_2$$

(No. (iv) in § 2.3.7), in the formation of water cluster ions, is interrupted by the reaction:-

$$O_2^+.(O_2) + O \rightarrow O_2^+ + O_3$$

It would seem, therefore, that the steep reduction in the cluster ion concentration near 85 km may well be attributed to the abrupt increase in the atomic oxygen concentration, that occurs at about this height. A seasonal change in n(O) might thus be accompanied by a change in the cluster concentration, causing a change in α overall and also in the height of the ledge in the α profile, with the corresponding changes in N(e). It will be seen therefore that measurements of seasonal variations in $n(O)/n(O_2)$ are needed for all heights, since this has in addition a bearing not only on the electron production rates but also on the collision frequencies.

The seasonal variation of the concentrations of two other minor constituents, the hydroxyl radical and sodium can be estimated from the measurement of airglow intensities. Figs. 7.39 and 7.40 show respectively the variations in the night airglow intensity at 6700 K (Huruhata, 1965), and the twilight sodium emission (Barbier, private communication).

A clear seasonal asymmetry will be seen to exist in both cases.

Gibson and Sandford (1971) have measured the seasonal variation of the height distribution of the night-time sodium layer at 51° N by means of the resonance scattering of a tuned laser beam. They conclude that the Winter maximum of abundance is a result of the appearance of sodium on the lower side of the layer, and that the Summer minimum is caused by a loss from the topside. The altitude of the peak of the layer seems to undergo a strongly asymmetric semi-annual variation, with minima of 87.5 km in Winter and 91 km near the end of June, and maxima of 94 km in April and 93 km in late August.

Since the hydroxyl radical takes part in reactions for the formation of water cluster ions (§2.3.7), its seasonal variation may in some way influence, or be related to, the value of the profile of the effective electron loss coefficient. Certain reactions have been proposed for sodium and the hydroxyl, including:-

$$H + O_3 \rightarrow OH^* + O_2$$

$$O_2^* + H \rightarrow OH^* + O$$

$$OH^* \rightarrow OH + h\nu$$

$$OH + O \rightarrow H + O_2$$

$$NaO + O \rightarrow Na(^2P) + O_2$$

$$NaH + O \rightarrow Na(^2P) + OH$$

$$NaH + H \rightarrow Na(^2P) + H_2$$

$$Na + O_2 \rightarrow Na(^2P) + O_2$$

(vibrationally excited)

(Whitten and Poppoff, 1971)

but their validity and relative importance have yet to be established.

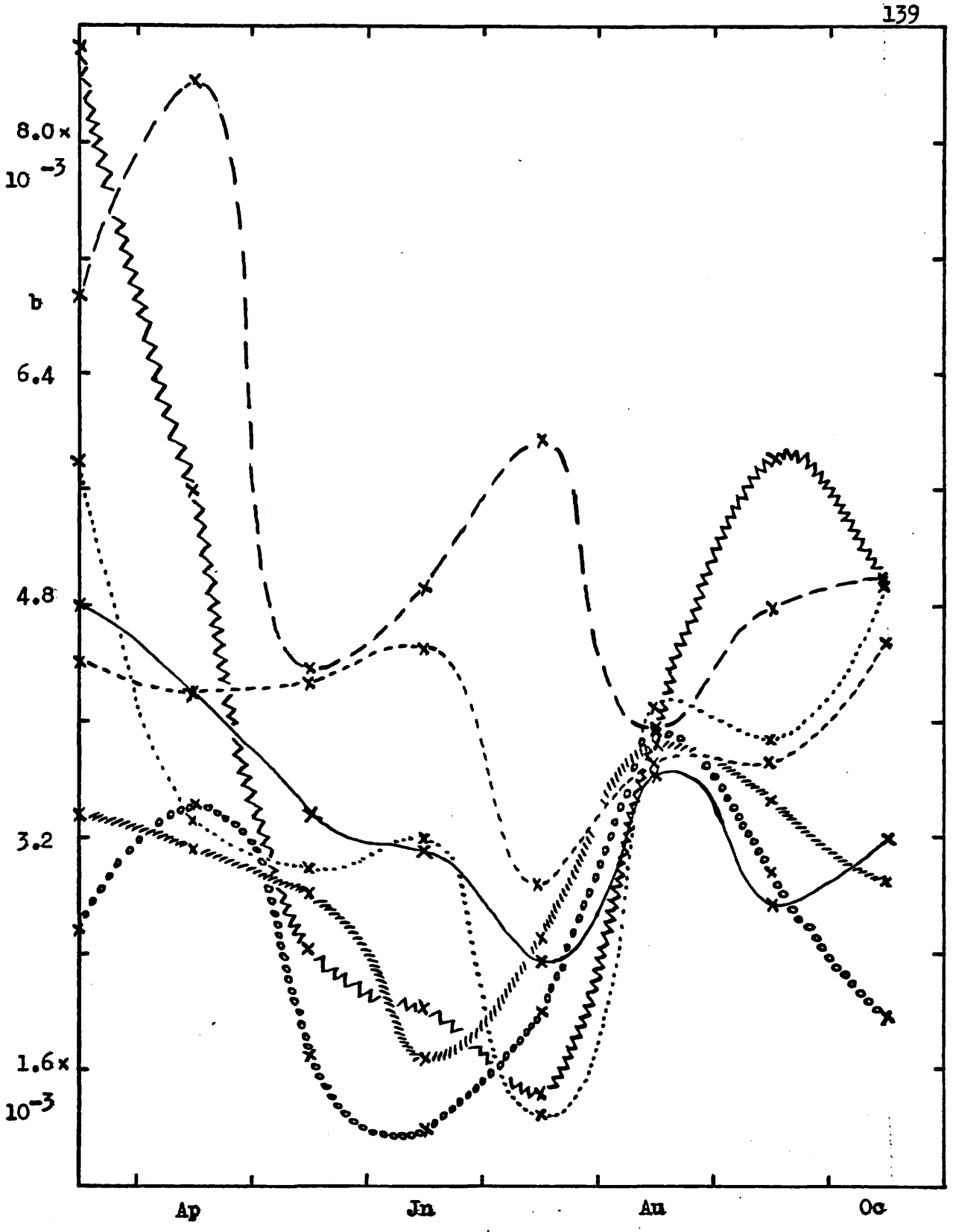

Fig. 7.41

Seasonal Variation in the Value of b : Freiburg

1.725 MHz
2.05 MHz
2.44 MHz
2.90 MHz
3.45 MHz
4.10 MHz
4.88 MHz

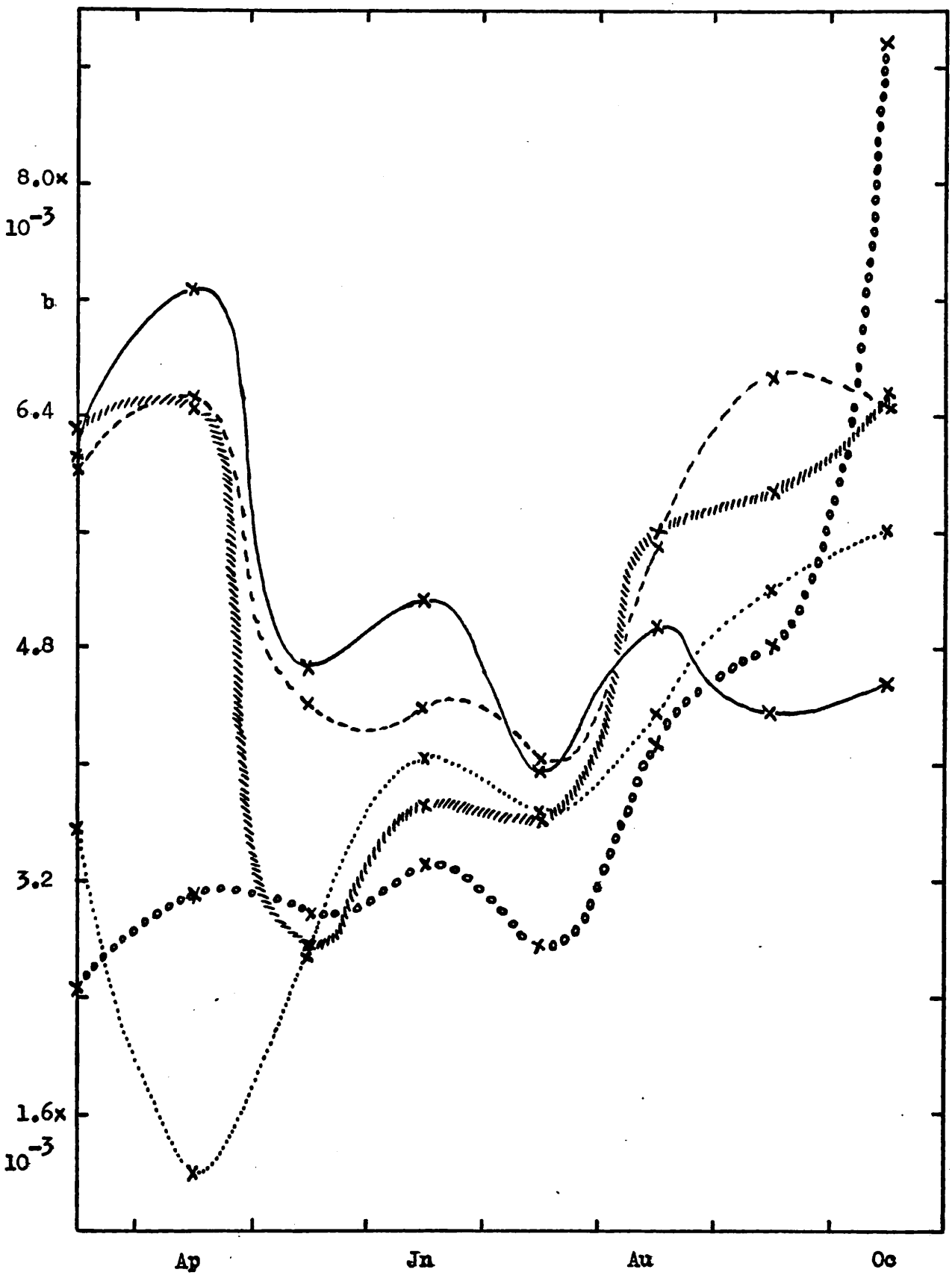

Fig. 7.42

Seasonal Variation in the Value of b : de Bilt

1.95 MHz
2.30 MHz
2.60 MHz
2.90 MHz
3.20 MHz

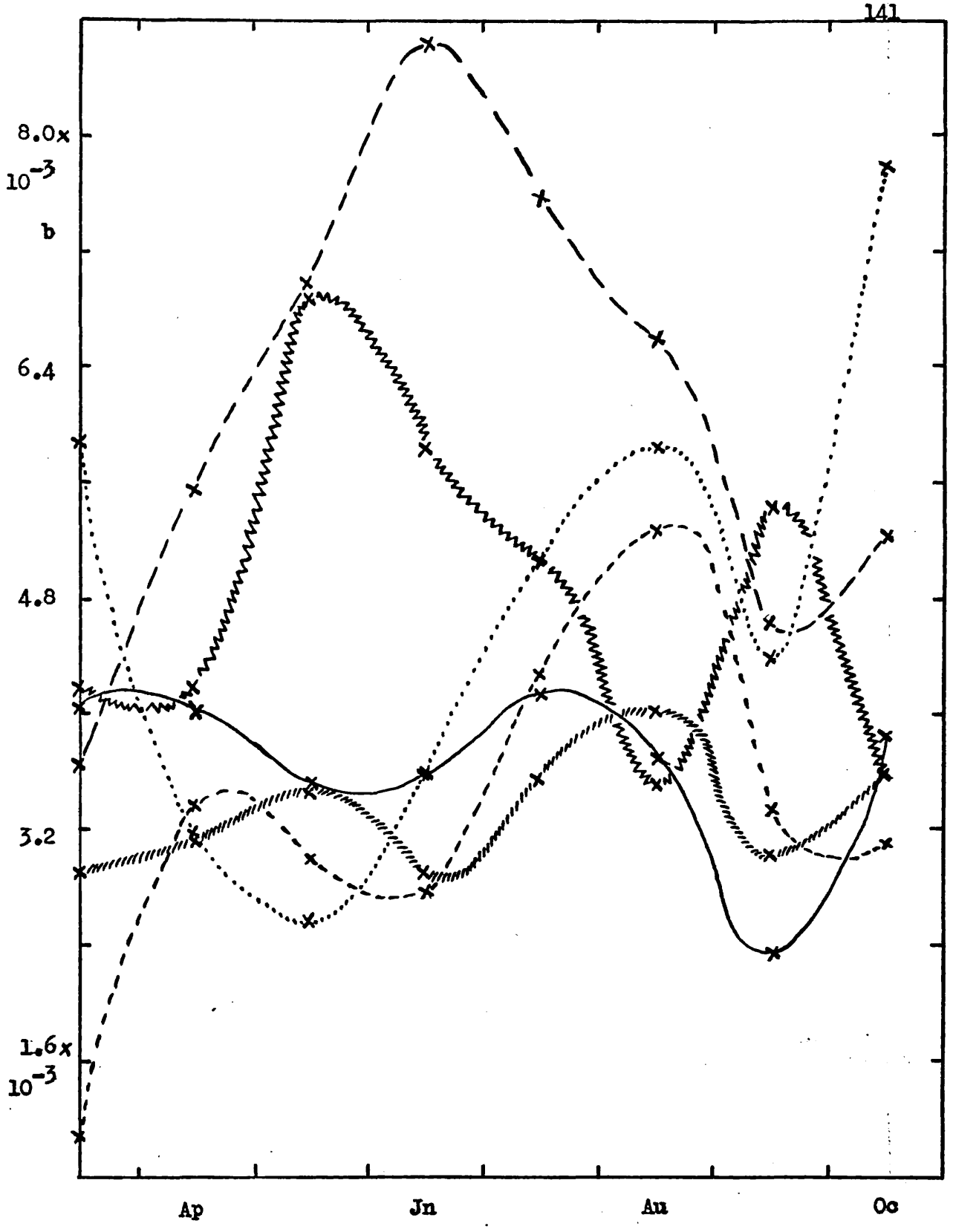

Fig. 7.43

Seasonal Variation in the Value of b : Slough

2.00 MHz
2.40 MHz
2.80 MHz
3.20 MHz
4.00 MHz
4.80 MHz

Fig. 7.44

Seasonal Variation in the Value of b

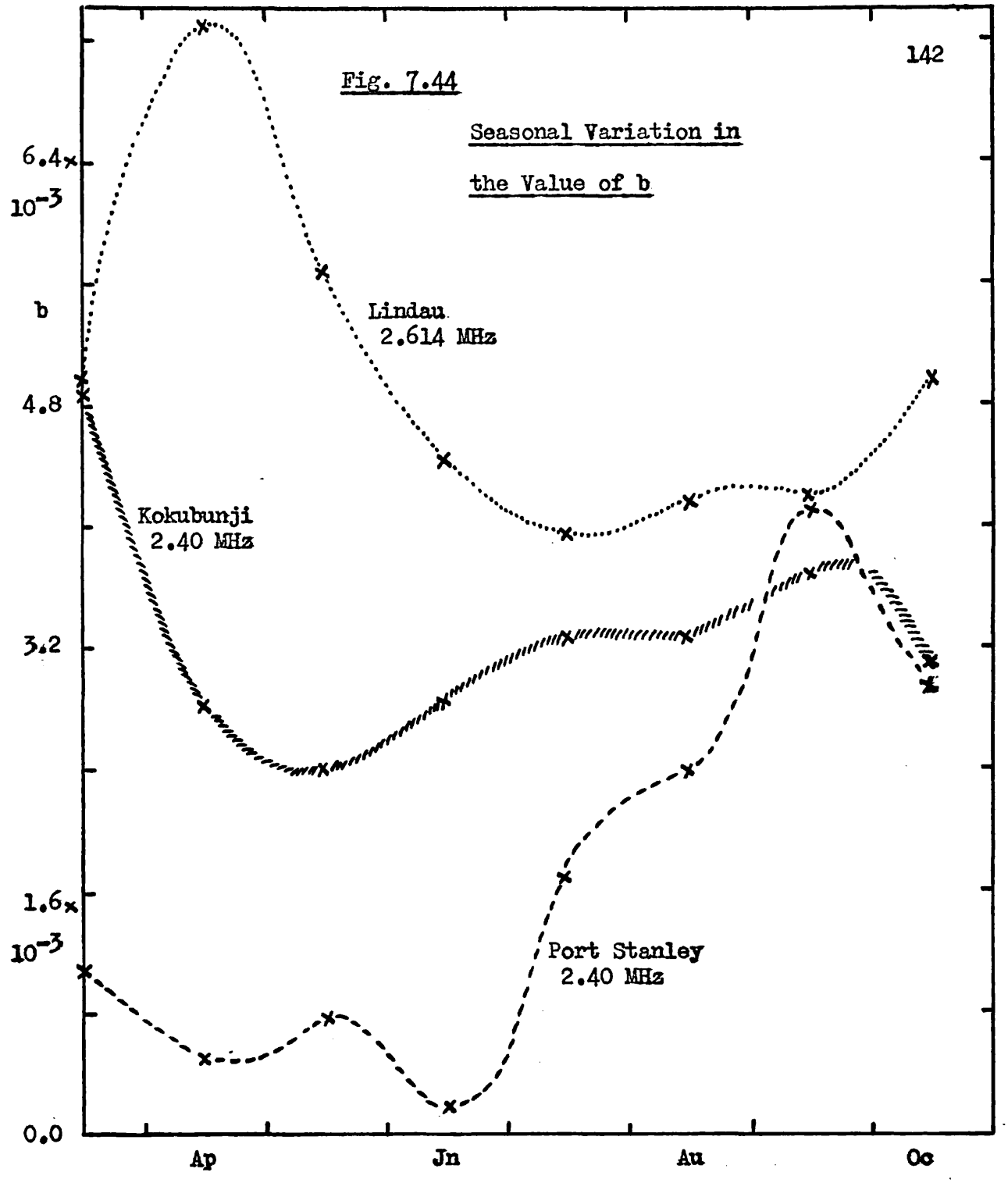

Fig. 7.45 Seasonal Variation in the Value of b'

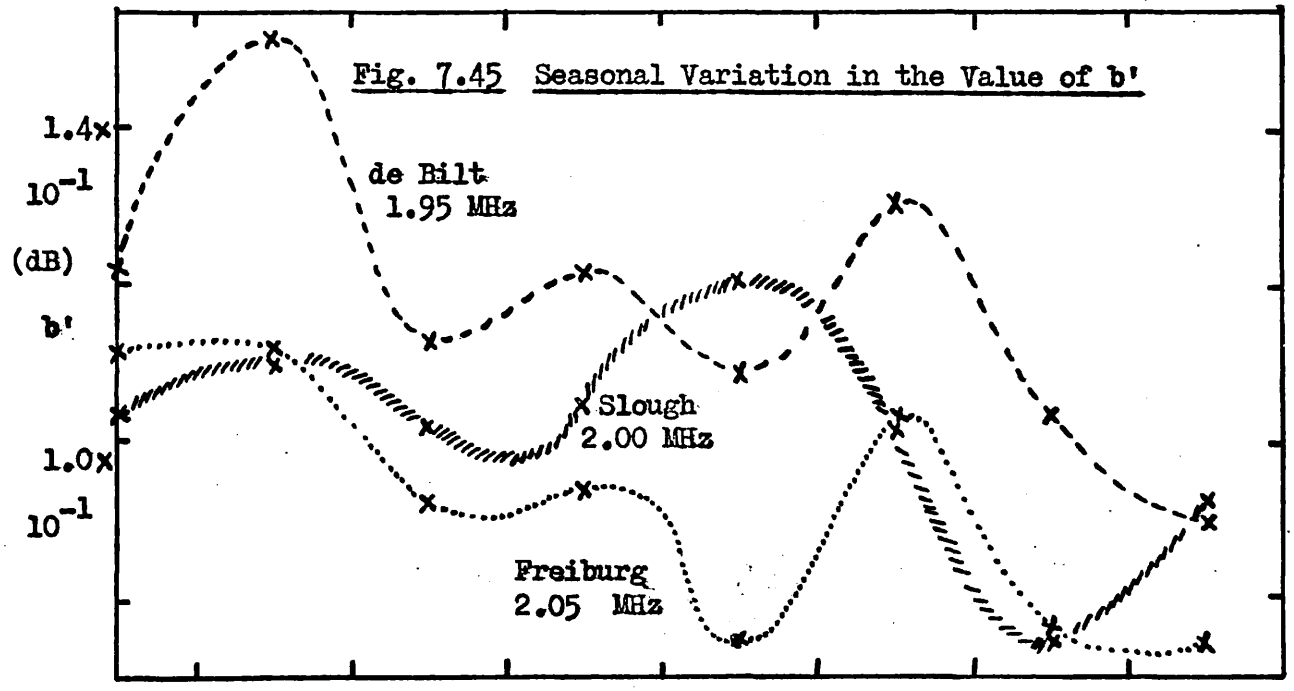

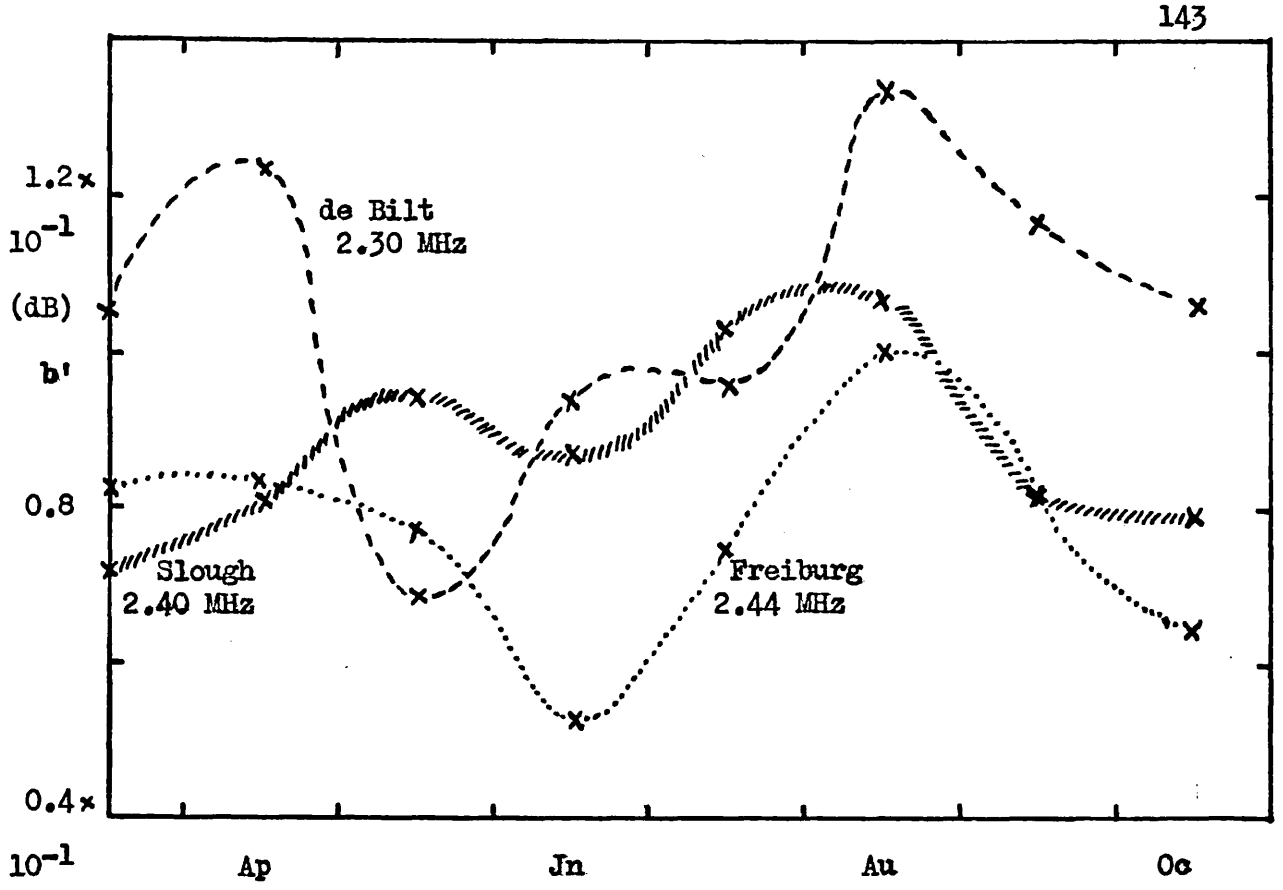

Fig. 7.46

Seasonal Variation in the Value of b'

Fig. 7.47

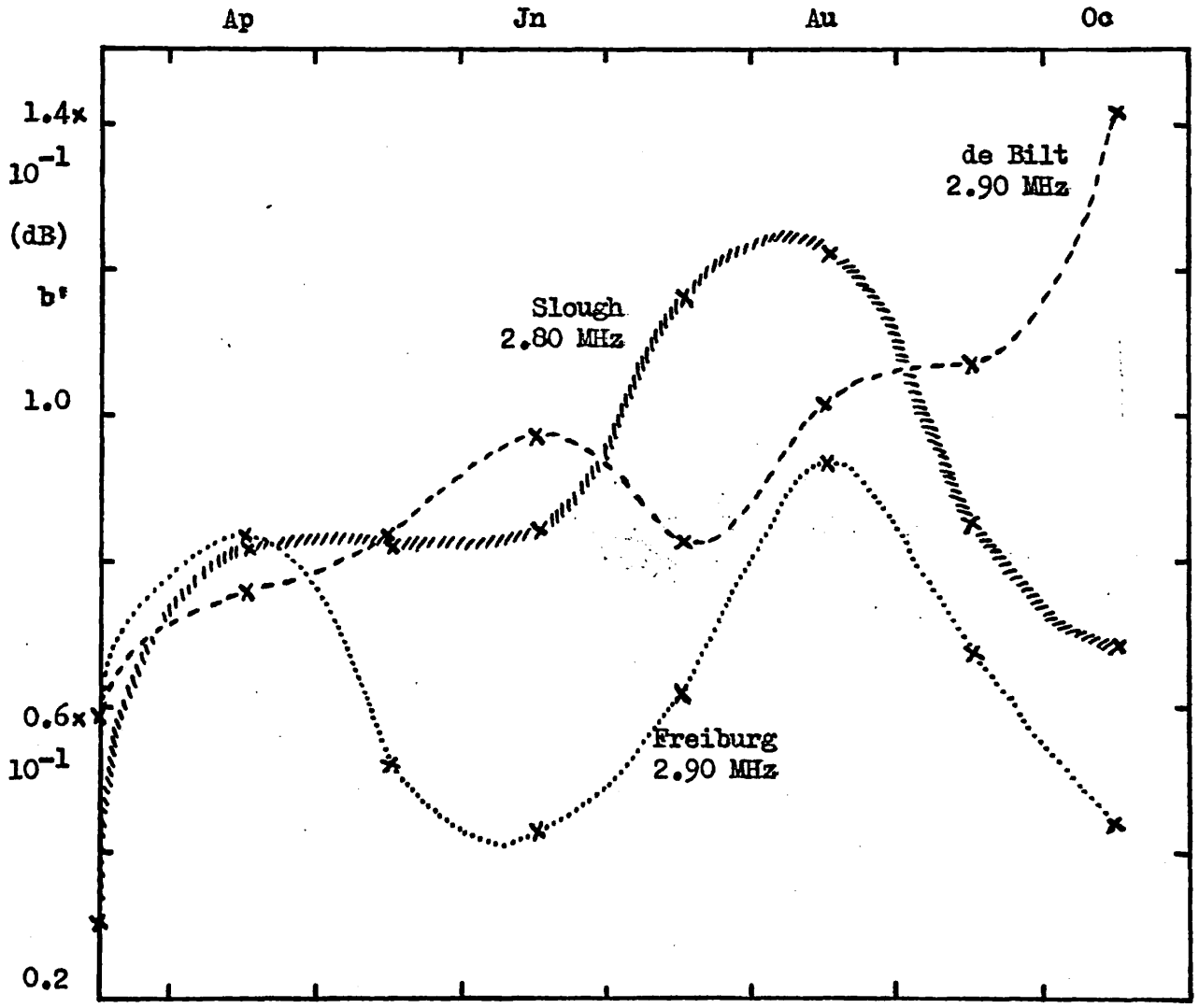

Whilst the twilight glow of sodium, and the nightglow of the hydroxyl may be taken as indicators of their concentrations at their respective times, it is difficult to assess what effect, if any, the seasonal variations of these two excited constituents might have on the seasonal variation of noon radio wave absorption. Instead, the seasonal asymmetry of these emissions may perhaps merely be an indicator of the asymmetric variation of certain other more relevant parameters.

Wu and Newell (1972) suggest tentatively that the hydroxyl emission may be a rough measure of water cluster concentration. Reference to equations (vii) and (ix) in § 2.3.7 suggests that this may well be correct. If, however, the hydroxyl radical is produced instead mainly by some other mechanism, then an increase in OH might possibly push the above reactions backwards, in which case, the argument of Wu and Newell would not necessarily be correct. It is probably significant that the Na and OH emissions both exhibit a lag behind the Summer solstice.

In a study of data collected during the I.Q.S.Y. at mid-latitudes, Willmann (1966) has shown that the time of the greatest probability of the occurrence of noctilucent clouds is in July. These clouds in general occur in the range 80 - 90 km, and may be formed from ice. As water vapour in the atmosphere may be responsible for the formation of not only these clouds but also cluster ions, a seasonal asymmetry in the occurrence of noctilucent clouds may therefore be linked tentatively with a possible similar asymmetry in the profile of the electron loss coefficient.

7.8.2 The Variations of b and b'.

The seasonal variation of b in the formula:-

$$L = a(1 + bR)$$

is shown in Figs. 7.41, 7.42, and 7.43 for Freiburg, de Bilt, and Slough respectively. (The curve for 5.8 MHz at Freiburg has been omitted owing to

lack of data.) Although no systematic trend has been detected, it is particularly noticeable how in the case of Freiburg and de Bilt there is in early August a convergence to essentially a single value of b for all frequencies.

The values obtained for Slough at 4.0 MHz (1947 - 1955) may be compared with those given in § 4.2 (Cambridge and Slough, 1935 - 1952). Although the present values exhibit the same general trends as before (apart from August), they are overall 30 - 50 percent lower, despite the overlap of data. This would perhaps suggest the presence of some additional factor in absorption which is not necessarily related to a solar cycle variation. It may be for this reason that, in the case of Slough, there is no apparent convergence of b in early August, as in the case of Freiburg and de Bilt.

For comparison, the values of b for Lindau, Kokubunji, and Port Stanley (during local Summer) are shown in Fig. 7.44. Once again, a convergence to a value comparable to that of Freiburg or de Bilt can be detected, although it seems to occur later. Overall, the values at Port Stanley are lower than those elsewhere. This may be connected with the fact that it is in the Southern hemisphere. If this is so, then any adjustment to bring its values into line with the Northern hemisphere stations, would result in the date of convergence being moved forward and closer to that of Freiburg and de Bilt. These results are difficult to interpret in the light of our present knowledge.

Schwentek (1971) has obtained values of b ($\cos\chi = 0.1$) at Lindau for the years 1961 -1970, and reports a steady increase in its value from 0 in March to 13×10^{-3} in January. As has already been pointed out, however, noon measurements cannot be directly compared with those at constant χ .

Figs. 7.45, 7.46, and 7.47 show the seasonal variations in b' for the three stations at frequencies near 2.0 MHz, 2.4 MHz, and 2.9 MHz respectively.

The "small" sunspot correction term in the results of individual years can have a variation of as great as $\pm$ 0.5 dB for the different values of b' at the various individual stations. This amount is, of course, very significant in the determination of the position of a peak value. In Fig. 7.45, the trends of Freiburg and de Bilt are similar, whereas in Figs. 7.46 and 7.47 no station is really consistent with either of the other two stations.

Overall, however, the graphs show some evidence of maxima in April and August. These are months during which the D region absorption is lower than that in June. On the other hand, the E region absorption is larger because the waves are being reflected at greater altitudes. It may be argued, therefore, that there is greater sunspot control on absorption in the E region than that in the D region. This is in agreement with the findings of Skinner and Wright (1964), which were discussed in § 4.2

It might in principle be possible to obtain from these graphs more detailed information as to the relative responses of the constituents to changes in ionisation by (a) Lyman alpha (NO), (b) Lyman beta (O_2), and (c) soft X rays (O_2, O, and NO), caused by changes in solar activity. Development of this concept might yield information on the relative changes in the concentrations of the constituents. Such a change in ionisation brings about a change not only in the profile of the absorption coefficient, but also in the reflection height, detailed calculations being required to determine, for a given frequency, the size, and even the direction of the change in the total absorption. Any sunspot variation in the profile of the loss coefficient would introduce further unknowns into the already complicated equations.

Considerable care, however, should be taken in interpreting these results in view of their lack of consistency, and it is for this reason that no further conclusion has been drawn from them.

7.8.3 Winds and Turbulence.

Blamont (1963) has suggested that neutral atmosphere parameters in the range 80 - 120 km may be summarised by the following:-

(i) An absence of turbulence below 85 km altitude;

(ii) A turbulent mixing regime in the layer 85 - 104 km;

(iii) A diffusive equilibrium regime above 104 km;

(iv) A sharp boundary between (ii) and (iii) at a height estimated to lie between 96 km and 112 km, averaged at 104 km.

More recently Hines (1972) has suggested that this height is likely to vary seasonally, especially at high latitudes, having possible values of 115 km in Winter and 85 km in Summer, and that even at mid latitudes the height variation may be significantly large.

Turbulence, and also to a lesser extent diffusion, will apply to ions as well as neutral molecules, and can result in a redistribution of the profiles of constituents. Turbulence gives rise to irregularities in the D region from which radio waves are scattered. In addition, Ellyet and Watts (1959) have provided evidence of stratification in the D region, thereby implying abrupt changes in the refractive index over a very small change in height. In these circumstances, ray theory will be inadequate, since it assumes that the refractive index does not change significantly over one wavelength. Small zones of additional absorption will occur, these not having been taken into account in the present calculations.

Lauter and Sprenger (1967) have pointed to correlations between the semi-annual variations in phase height at 160 kHz (at constant χ), and the prevailing zonal wind component in the 80 - 100 km range. The minima in the D region ionisation in Spring and Autumn were found almost to coincide with the reversals of the zonal circulation in the lower ionosphere, and at about the times of reversal of the polar vortex in the stratosphere. This correlation is thought to be connected with the vertical Lorentz force acting upon electrons moving in the direction of the prevailing

zonal wind, in the presence of the geomagnetic field. Depending on its direction, a vertical shear of zonal winds can cause either compression or rarefaction of an electron density profile. This will affect the absorption in the ways described in § 7.7 .

Whitehead (1967) has used a similar theory as a possible explanation of the sporadic E phenomenon, which previously had been shown (Whitehead, 1961) to exhibit an asymmetric variation about the Summer solstice in the probability of its occurrence.

Sprenger and Schminder (1967) have drawn attention to seasonal variations in the phase of ionospheric drift measurements.

From all these results, Lauter and Sprenger (1967) conclude that there is a definite lag in the values of several parameters of the upper atmosphere after the Summer solstice.

In a recent analysis of I.Q.S.Y. data, Wu and Newell (1972) have found that HF radio absorption correlates negatively with 10 mb ($\sim$ 25 km) zonal wind (positive towards East), but positively with 10 mb temperature. In addition, in Winter months, the meridional wind (positive towards North) correlates positively with absorption. They argue that the poleward transport of high atomic oxygen concentrations results in warming both by adiabatic compression on descent, and by recombination to form O_2. It is suggested that O rather than NO is the critical trace substance causing anomalously high Winter absorption, through the reduction of the electron loss rate by the method described previously. The authors point out, however, that a definite conclusion cannot at this stage be drawn from the limited data available.

Through its study of the seasonal variation in radio wave absorption, the present work has provided evidence that this variation is asymmetric about the Summer solstice, and is a function of wave frequency. An asymmetric variation of nitric oxide has been hypothesised to account for this effect, and the theoretical absorption, computed from the proposed model, exhibits the principal features observed in the experimental results. It has been demonstrated that a seasonal variation in other parameters, such as atomic oxygen, may also be partly responsible for the observed variation in absorption.

A number of neutral atmosphere parameters in the height range 80 - 110 km have been shown to exhibit an asymmetry in their seasonal variation, often taking the form of a lag after the Summer solstice. These are thought to be related to the lag in radio wave absorption, but the precise mechanism for this relationship has yet to be elucidated.

7.9 The Implications of the Present Work.

The present work has a possible application in the field of long distance radio communications, where the choice of transmitting frequency is governed by two principal factors:-

(i) The frequency of the signal must be sufficiently high (the Lowest Usable Frequency, L.U.F.) to prevent an unacceptable amount of absorption in the D region, rendering it indistinguishable from background noise.

(ii) The frequency must be sufficiently low (the Maximum Usable Frequency, M.U.F.) to permit reflection of the wave by the ionosphere at a sufficiently small angle of incidence for transmission to the receiver. To allow for day to day changes in the critical frequency, the Optimum Working Frequency, F.O.T. (= 0.85 x the monthly median of the M.U.F.) is commonly used as a measure of an upper limit on working frequencies.

The L.U.F. is thus dependent upon the characteristics of the receiving system as well as the ionosphere, whereas the M.U.F. depends only upon ionospheric parameters.

The present work has dealt with the absorption of vertically incident waves of frequency around 3 MHz, which, according to the work of Martyn (1935), would be equivalent to higher frequencies at oblique incidence. It would seem, therefore, that the departure of absorption values from a direct $\cos^n \chi$ relationship could have significant implications in the choice of L.U.F., insofar as it has been shown in the present work that the time of maximum absorption is a function of frequency. This effect does not appear to have been incorporated in previous L.U.F. predictions, and most recently George (1971) has published a map showing the global distribution of $\int N\nu\, dh$, in which the frequency-dependent lag is eliminated by the analysis.

It is suggested, therefore, that for the lower frequencies used in oblique incidence transmissions, where the L.U.F. is of considerable importance, the normal predictions may well be inaccurate, in that the absorption, both at mid and low latitudes, is not in phase with $\cos \chi$, and moreover the departure from such a seasonal variation is a function of frequency, location, and sunspot number.

APPENDIX A

SUGGESTIONS FOR FURTHER WORK

It is suggested that further information on the asymmetric variation in ionospheric absorption might be obtained from a study of the following:-

(a) In the present work, only a preliminary study has been made of the seasonal variation in absorption at equatorial stations. This might well be extended to include further stations. In addition, the data for more years will now be available. The construction of a theoretical absorption model might yield, by analogy with the conclusions of the present work, a certain insight into the seasonal variation in nitric oxide at low latitudes.

(b) Although in the present work it has been thought sufficient to use the Sen and Wyller generalisation of the Appleton-Hartree equation in the evaluation of absorption in view of the comparatively large uncertainties in the values of the parameters, it is possible that the errors involved in calculating the absorption near the reflection level are larger than anticipated. Equally important, these errors may not be of a consistent size. A full wave calculation would remove this uncertainty by taking into account the complex component of the refractive index.

(c) It has already been shown how winds can theoretically be related to absorption, and with more wind data becoming available, further experimental correlation may be found.

(d) The construction of theoretical models will be of limited use, until the seasonal variation in nitric oxide is known. This will require, however, a new method of its determination at mesospheric heights. Probably equally important is a knowledge of the atomic oxygen concentration. Again, a new method of measurement is needed at mesospheric heights.

(e) A rather more detailed knowledge of the effects of vertical transport on the distribution of minor constituents would be of assistance in the construction of model ionisation profiles.

APPENDIX B

COMPUTER PROGRAM OF THE THEORETICAL ABSORPTION MODEL

```
JOB(UAAP013,J6,CM21000,T18,LC1500)REES
ATTACH(EXCERN,CERNUP)
REWIND(EXCERN)
UPDATE(Q,P=EXCERN)
RETURN(EXCERN)
COPYCF(INPUT,DISC)
COPYCF(COMPILE,DISC)
REWIND(DISC)
SMOOTH(DISC,FORTR)
REWIND(FORTR)
FUN(S,I=FORTR,B=NCY130)
COMMON(NCY130)


*COMPILE,E208,F100,V301,V300


      DIMENSION C(56,8), R(56,8), SCRIP(56,8), F(56,8), T(56,8), AD(5),
     1 FL(25),ODEL(56,8),REC(56),ZP(56,8),X(56,8),YP(8),XP(8),AM(6)
      COMMON M, N1, A(150), NH, Y(15), S(35), INFLUX, E(56,8), V(56,8),
     1 LAMBDA, NOPRINT, EP(56,8)  $ REAL INFLUX, LAMBDA, NIT(56,8)
      PRINT 100 $ READ 150,(A(J),J=71,79),NOP,NP1,NP2,NP3,NP4
     1  ,NP5,(FL(I),I=10,17) $ PRINT 150,(A(J),J=71,79),NOP,NP1,
     1  NP2,NP3,NP4,NP5,(FL(I),I=10,17)
100   FORMAT (1H1)
150   FORMAT (9F5.2,6I3,/,8E10.3)
132   FORMAT (3I3,3E9.2,F6.3,F10.7,/,8F7.3,I3,E9.3,/,9F7.3,2I3,
     1 E8.1,2(/,5E9.2),7(/,8E10.2),7(/,8E10.3),/,8F7.3)
93    FORMAT (1H1,! TEMPERATURE!)
90    FORMAT (! PRESSURE!)
66    FORMAT( F10.1,6E10.2)
      READ  132,NH,N1,I5,BOLTZ,EVCONV,GYRO,FACNIT,PI,(Y(K),K=1,8),
     1  MTEST,FREQ,(S(I),I=21,29),M,MF,STRMIN,(NIT(I,1),I=1,5),
     1  (R(I,1),I=1,NH),DUM1,D5,D6,D7,D8,(REC(J),J=6,NH),DUM2,D1,D2,D3,
     1 D4,  (A(J),J=81,88)     $  NOPRINT=NP1
      PRINT 132,NH,N1,I5,BOLTZ,EVCONV,GYRO,FACNIT,PI,(Y(K),K=1,8),
     1  MTEST,FREQ,(S(I),I=21,29),M,MF,STRMIN,(NIT(I,1),I=1,5),
     1  (R(I,1),I=1,NH),DUM1,D5,D6,D7,D8,(REC(J),J=6,NH),DUM2,D1,D2,D3,
     1 D4,  (A(J),J=81,88)  $ DO 51 J=29,NH
51    REC(J)=REC(J)*A(79) $ PRINT 100 $ TPISQ=4.0*PI*PI $ DO 65 J=1,NH
      READ 66,A(J),X(J,1),ODEL(J,1),EP(J,1),C(J,1),D8 $ D1=R(J,1)*3.0
      D2=EP(J,1)*FL(10) $ DO 65 K=1,8 $ R(J,K)=D1*A(K+70) $ EP(J,K)=D2
65    ODEL(J,K)=ODEL(J,1) $ DO 10 I=1,5 $ REC(I)=0.0 $ DO 10 K=2,8
      NIT(I,K)=NIT(I,1) $ X(I,K)=X(I,1)
10    C(I,K)=C(I,1) $ IF (NOPRINT.NE.0) GO TO 94 $ DO 12 J=1,NH
12    PRINT 66,A(J),X(J,1),ODEL(J,1),EP(J,1),C(J,1),REC(J) $ PRINT 93
94    CALL EXDAT(T) $ PRINT 90 $ CALL EXDAT(F) $ DO 39 J=6,NH
      FACNIT=FACNIT+0.9E-03$ FACOX=1.0-FACNIT$ IF(J-31) 140,140,141
140   A(J+90)=0.7*X(J,1)/C(J,1)
141   DO 39 K=1,8 $ E(J,K)=0.0 $ D1=F(J,K)/(T(J,K)*BOLTZ)
      IF(J-31) 155,155,156
155   D2=A(J+90)*A(K+80) $ C(J,K)=D1*FACOX/(1.0+D2)
      X(J,K)=D2*C(J,K) $ GO TO 39
156   C(J,K)=D1*FACOX $ X(J,K)=X(J,1)
39    NIT(J,K)=FACNIT*D1 $ D1=D2=D3=0.0 $ DO 157 K=1,8
      D1=D1+X(6,K) $ D2=D2+C(6,K)
157   D3=D3+NIT(6,K) $ DO 158 K=1,8  $ XP(K)=K+1.5
      D4=8.0*X(6,K)/D1 $ D5=8.0*C(6,K)/D2
      D6=8.0*NIT(6,K)/D3 $ DO 158 J=4,5
      X(J,K)=X(J,K)*D4 $ C(J,K)=C(J,K)*D5
158   NIT(J,K)=NIT(J,K)*D6
      DO 13 K=1,8   $   S(K) = (S(29)/S(K+20))**2    $   DO 13 J=1,NH
13    SCRIP(J,K) = C(J,K) + 0.5*X(J,K)
      IF (NOPRINT.EQ.1) GO TO 143  $  PRINT 91  $  CALL APRINT(R,1,NH)
91    FORMAT (     ! NITRIC OXIDE CONCENTRATION!)
82    FORMAT (     ! NITROGEN MOLECULE CONCENTRATION!)
      PRINT 82   $    CALL APRINT (NIT, 1, NH)
92    FORMAT (  ! OXYGEN MOLECULE CONCENTRATION!)
      PRINT 92   $   CALL APRINT (C, 1, NH)
      PRINT 11 $ CALL APRINT (X,1,NH)  $ NOPRINT=NOP
11    FORMAT (! ATOMIC OXYGEN CONCENTRATION !)
71    FORMAT (     ! LYMAN BETA!)
143   READ 130, LAMBDA, INFLUX, SIGOX, SIGN2, ZERO
      INFLUX=INFLUX*FL(11)
      SIONOX=0.64*SIGOX $ IF (NOPRINT.EQ.0) PRINT 71
      CALL OPDEP (C, NIT, C, C, SIGOX, SIGN2, ZERO, ZERO,
     1 SIONOX,C,ZERO,C) $ READ 73,(FL(LX),LX=1,9),IT $ LAMBDA=2.5E-9
73    FORMAT (9F8.2,I5)
72    FORMAT (! X RAYS OF WAVELENGTH INTERVAL +/- 5.0E-10 ABOUT LAMBDA!)
      DO 62 LX=1,9 $ IF (NOPRINT.EQ.0) PRINT 72 $ LAMBDA=LAMBDA+1.0E-9
      INFLUX=FL(LX)*(10.0**IT)*FL(12)
      CONSIG = EXP(2.5*ALOG(LAMBDA*1.0E+10))
      SIGOX=2.27E-27*CONSIG $ SIGN2=1.33E-27*CONSIG $TEM1=3.54E-8/LAMBDA
      SIONOX=SIGOX*TEM1 $ TEM2=SIGN2*TEM1
      CALL OPDEP (SCRIP, NIT, C, C, SIGOX, SIGN2, ZERO, ZERO,
     1SIONOX, SCRIP, TEM2, NIT)
62    CONTINUE
134   FORMAT (/,! TOTAL ELECTRON PRODUCTION RATES FOR PROCESSES!,I3,! TO
     1!,I3,! INCLUSIVE!,/)
133   NOPRINT=NP2
      IF (NOPRINT.NE.0) GO TO 7 $ PRINT 134,MF,M $ CALL APRINT (E,6,NH)
```

```
7     DO 135 K=1,8 $ DO 135 J=6,NH
135   E(J,K)=0.0  $  MF=M+1  $  MTEST=MTEST+1 $ NOPRINT=NOP
      GO TO (136,137,138) MTEST
136   DO 67 LX=1,9 $ READ 68,INFLUX,DELION,SIGOX,LAMBDA,AN,BN
68    FORMAT (6F8.2)
      INFLUX=INFLUX*1.0E+12*FL(11) $ DELION=DELION*1.0E-23
      SIGOX=SIGOX*1.0E-23 $ IF (LAMBDA-0.5) 69,198,198
198   LAMBDA=LAMBDA*1.0E-10 $ IF (NOPRINT.EQ.0) PRINT 120 $ GO TO 121
120   FORMAT (! WAVELENGTH                    IONISATION OF O(2)DELTA!)
69    AN=AN*1.0E-10 $ BN=BN*1.0E-10 $ IF (NOPRINT.EQ.0) PRINT 123,AN,BN
123   FORMAT (2E14.5,! CONTINUUM WAVELENGTHS IONISATION OF O(2)DELTA!)
121   CALL OPDEP (C, ODEL, C, C, SIGOX, DELION, ZERO, ZERO,
     1DELION, ODEL, ZERO, C)
67    CONTINUE   $   GO TO 133
137   LAMBDA=0.0 $ DO 125 LX=1,5 $ READ 124,INFLUX, SIGOX, SIGN2
124   FORMAT (E6.1,2F5.0)
      SIGOX = SIGOX*2.0*2.66E-27   $   SIGN2 = SIGN2*2.0*2.33E-27
C        CONVERSION TO MOLECULAR CROSS SECTION
      LAMBDA=LAMBDA + 2.0E-10 $ TEM1=3.54E-8/(LAMBDA)
      SIGNOX=SIGOX*TEM1 $ TEM2=SIGN2*TEM1
      INFLUX=INFLUX*FL(LX+12) $ IF (NOPRINT.EQ.0) PRINT 6
6     FORMAT (! HARD X RAYS OF WAVELENGTH +/- 1.0E-10 ABOUT LAMBDA!)
      CALL OPDEP (SCRIP, NIT, C, C, SIGOX, SIGN2, ZERO, ZERO,
     1SIGNOX, SCRIP, TEM2, NIT)
125   CONTINUE   $   GO TO 133
138   READ 130, LAMBDA,INFLUX,SIGNO,SIGOX,SIGN2 $ NOPRINT=NP2
70    FORMAT (! LYMAN ALPHA!)
130   FORMAT (5E10.2,F5.1)
      IF (NOPRINT.EQ.0) PRINT 70 $ P=1.0E-18 $ INFLUX=INFLUX*FL(11)
      CALL OPDEP (C,NIT,R,C,SIGOX,SIGN2,SIGNO,ZERO,SIGNO,R,ZERO,R)
      NOPRINT=NP5 $ DO 14 K=1,8 $ DO 14 J=6,NH
14    E(J,K)=SQRT(EP(J,K)/REC(J))' $ PRINT 95 $ CALL APRINT (E,6,NH)
      NOPRINT=NP3 $ DO 43 J=6,NH $ DO 43 K=1,8 $ Q=SQRT(T(J,K))
43    V(J,K)=(NIT(J,K)*Q*9.605 +C(J,K)*(121.0+2.61*Q) +187.2*X(J,K))*Q*P
      IF (NOPRINT.EQ.1) GO TO 159 $ PRINT 89 $ CALL APRINT (V,6,NH)
      PRINT 5 $ CALL APRINT (EP,6,NH)
95    FORMAT (! MONTHLY ELECTRON DENSITY PROFILES PER CUBIC METRE!)
89    FORMAT (! COLLISION FREQUENCY!)
5     FORMAT (    ! SUM OF ALL ELECTRON PRODUCTION RATES!)
159   CONFAC=1250.0*(EVCONV**2)/(8.854E-12*3.0E+8*9.18E-31)
      AREAFAC=8/(15*SQRT(PI))
      DO 197 MD=1,5 $ GO TO (206,201,202,203,202), MD
206   STEP=.12E+06 $ GO TO 205
201   STEP=.20E+05 $ GO TO 205
202   STEP=.50E+05 $ GO TO 205
203   STEP=.10E+06
205   DO 55 L=1,8 $ FREQ=FREQ+STEP
      C(51,L)=FREQ $ FREQ2=FREQ*FREQ $ ELDEN=FREQ2/80.5 $ NOPRINT=NOP
      D1=GYRO+FREQ $ GYPFR=D1*D1*TPISQ $ DO 17 K=1,8 $ KR=10+K
      C(K,L)=EP(K,L)=0.0 $ FRAC=1.0 $ NMARK=0 $ DO 17 I=1,15
      J=NH-I+1 $ N=J+1 $ IF (NMARK) 45,45,50
45    XVAR2 = GYPFR/(V(J,K)*V(J,K))   $   AREA = EPS = OLDFEPS = 0.0
      DELEPS = 0.003   $   DO 2 JS = 1, 1000   $   EPS = EPS + DELEPS
      FEPS= EXP(2.5*ALOG(EPS) - EPS)/(EPS*EPS + XVAR2)
      STRIP = 0.5*(OLDFEPS + FEPS)*DELEPS   $   AREA = AREA + STRIP
      SOVA = STRIP/AREA   $   IF (STRMIN-SOVA) 1,1,131
1     OLDFEPS = FEPS
2     DELEPS = DELEPS*1.17
131   SCRIP(J,K) = AREA*AREAFAC   $   IF (ELDEN-E(J,K)) 52, 8, 8
8     RIJ = SQRT(1.0 - E(J,K)/ELDEN)   $   GO TO 53
52    NMARK = 1   $   FRAC = (ELDEN -E(N,K))/(E(J,K) - E(N,K))
      RIJ = 0.0   $  C(K,L) = A(N) + FRAC*(A(J) - A(N))
53    IF (J-NH) 60, 17, 60
60    AVKAP = (E(J,K) + E(N,K))*(SCRIP(J,K) + SCRIP(N,K))/
     1(V(J,K) + V(N,K))   $   AVRI = 2/(RIJ + RIN)
      ZP(J,K)  = CONFAC*AVKAP*FRAC*(A(J) - A(N))*AVRI
      EP(K,L)=EP(K,L)+ZP(J,K)  $ C(KR,L)=8.7*EP(K,L)  $  GO TO 17
50    SCRIP(J,K)=ZP(J,K)=0.0
17    RIN=RIJ $ IF (NP4) 196,196,55
196   PRINT 103,FREQ,ELDEN $ CALL APRINT (SCRIP,6,NH)
103   FORMAT(    ! FREQUENCY =!,1PE10.2,! HZ   ELECTRON DENSITY FOR REFL
     1ECTION =!,E9.2,!    SCRIPT INTEGRALS!)
3     FORMAT (! REFLECTION HEIGHT(KM)!,/,0F11.1,/,! TOTAL ABSORPTION(NEP
     1ER)!,/,0E11.3,/,! TOTAL ABSORPTION(DECIBEL)!,
     1/,0F11.1,!    MODEL!)
      PRINT3,(C(K,L),K=1,8),(EP(K,L),K=1,8),DUM2,(C(K,L),K=11,18)
      PRINT 96 $ NOPRINT=NP4  $  CALL APRINT (ZP,6,N1)
96    FORMAT (! ABSORPTION IN INTERVAL TO HEIGHT INDICATED(NEPER)!)
55    CONTINUE $ PRINT 87,DUM2 $ ID=1 $ DO 187 K=1,8 $ KR=K+10
87    FORMAT (!       MAR         APR         MAY         JUN         JUL
     1      AUG         SEP         OCT   MODEL!,F4.0,/,! DEGREE4(1ST.APPROX
     1.FOR PEAK ABSORPTION/ITERATIONS TO FIND PEAK/POSITION OF PEAK)!,
     1 /,! /DITTO FOR DEGREE5/FREQUENCY(HZ)/REFLECTION HEIGHT/RAW DATA/
     1SMOOTHED4/SMOOTHED5!)
      X(K,1)=C(K,1) $ X(KR,1)=C(KR,1) $ C(KR,1)=Y(K)
187   C(K,1)=0.0 $ X(51,1)=C(51,1) $ C(51,1)=0.0 $ L=1
186   DO 163 K=1,8 $ KR=10+K
163   YP(K)=C(KR,L) $ J=5 $ CALL LSQ(8,XP,YP,J,AD) $ DO 162 I=1,5
162   AM(I)=AD(I) $ GO TO 164
165   J=6 $ CALL LSQ(8,XP,YP,J,AM)
164   DO 169 I=1,15
169   FL(I)=2.0+0.5*I $ IB=0
181   IB=IB+1 $ S(IB)=0.0 $ D4=1.0
```

```
      DO 168 KR=1,J $ S(IB)= S(IB)+D4*AM(KR)
168   D4=D4*FL(IB) $ IF (IB-15) 181,167,174
167   DO 171 K=1,8 $ KR=K+10*J-30 $ I=2*K-1
171   C(KR,L)=S(I) $ DO 172 I=2,15 $ IF (S(I)-S(1)) 172,172,173
173   S(1)=S(I) $ FL(1)=FL(I)
172   CONTINUE $ KC=15+5*J
      C(KC+1,L)=FL(1) $ C(KC+2,L)=S(1) $ IC=0
176   D5=1.0 $ D6=D7=0.0 $ DO 175 KR=3,J $ K1=KR-1 $ K2=KR-2
      D6=D6+K2*AM(K1)*D5 $ D7=D7+K1*K2*AM(KR)*D5
175   D5=D5*FL(1) $ D6=D6+K1*AM(KR)*D5
      D3=D6/D7 $ D8=D3*D3 $ FL(16)=FL(1)-D3
      IC=IC+1 $ FL(1)=FL(16) $ IF (IC-20) 177,177,178
178   PRINT 179,D3,FL(16) $ GO TO 181
179   FORMAT (F8.4,!=DIFFERENCE ......HOPELESS SITUATION AT!,F6.3)
177   IF (D8-0.00001) 181,176,176
174   C(KC+3,L)=IC $ C(KC+4,L) = FL(16)
      C(KC+5,L)=S(16) $ IF (J-6) 165,166,166
166   PRINT 183, (C(K,L),K=41,51) $ DO 160 KR=1,31,10 $ K2=KR+7
183   FORMAT (/,2(2F7.3,F4.0,2F12.3,3X),1PE8.2)
161   FORMAT (8F11.3)
160   PRINT 161,(C(K,L),K=KR,K2) $ IF (ID) 188,188,189
188   C(52,L)=C(44,L)-X(44,2) $ C(53,L)=C(49,L)-X(49,2)
      L=L+1 $ IF (L-8) 186,186,190
189   X(44,2)=C(44,1) $ X(49,2)=C(49,1) $ ID=0 $ C(51,1)=X(51,1)
      DO 193 K=1,8 $ KR=K+10 $ C(K,1)=X(K,1)
193   C(KR,1)=X(KR,1) $ GO TO 186
194   FORMAT (2X)
192   FORMAT (2X,8F12.3)
190   PRINT 194 $ DO 191 K=51,53
191   PRINT 192, (C(K,L),L=1,8)
197   PRINT 100 $ STOP $ END


      SUBROUTINE OPDEP (CA, CB, CC, CD, SIGA, SIGB, SIGC, SIGD,
     1SIGNE, CE, SIGNF, CF)    $   REAL INFLUX, LAMBDA
      DIMENSION CA(56,8), CB(56,8), CC(56,8), CD(56,8),
     1 O(56,8), CE(56,8), CF(56,8)
      COMMON M, N1, A(150), NH, Y(15), S(35), INFLUX, E(56,8), V(56,8),
     1 LAMBDA, NOPRINT, EP(56,8) $ M=M+1 $ DO 7 K=1,8
      O(1,K)=0.0    $   DO 10 I=1,N1    $   J=I+1
      O(J,K) = O(I,K) + 500*((CA(I,K)+CA(J,K))*SIGA
     1  + (CB(I,K) + CB(J,K))*SIGB + (CC(I,K) + CC(J,K))*SIGC
     2  + (CD(I,K) + CD(J,K))*SIGD)*(A(I)-A(J))/Y(K) $  IF (J-6) 10,6,6
6     IF (O(J,K)-40.0) 9,4,4
9     V(J,K) = S(K)*EXP(-O(J,K))*INFLUX*(SIGNE*CE(J,K) + SIGNF*CF(J,K))
      E(J,K) = E(J,K) + V(J,K)    $   EP(J,K) = EP(J,K) + V(J,K)
10    CONTINUE    $   GO TO 7
4     DO 5 L=J,NH
5     V(L,K) = O(L,K) = 0.0
7     CONTINUE    $   IF (NOPRINT.EQ.1) GO TO 3
      PRINT 8, LAMBDA, M, SIGA, SIGB, SIGC, SIGD, SIGNE, SIGNF, INFLUX
8     FORMAT (E20.5,/,!  M     SIGA       SIGB        SIGC        SIGD
     1 SIGNE       SIGNF    INFLUX[PHOTON RATE/SQU.METRE]!,/,I3,7E11.3,
     14X,! OPTICAL DEPTH!)
      CALL APRINT (O, 2, NH)   $ PRINT 96 $ CALL APRINT (V,6,NH)
96    FORMAT (! ELECTRON PRODUCTION RATE!)
3     RETURN    $   END


      SUBROUTINE APRINT (PRIN, J1, J2)        $   DIMENSION PRIN(56,8)
      COMMON M, N1, A(150), NH, Y(15), S(35), INFLUX, E(56,8), V(56,8),
     1 LAMBDA, NOPRINT, EP(56,8)
87    FORMAT (!        MAR         APR         MAY         JUN         JUL
     1      AUG         SEP         OCT    HEIGHT[KM]!)
      IF (NOPRINT.EQ.1) GO TO 3    $   PRINT 87    $   DO 2 J = J1, J2
2     PRINT 16, (PRIN(J,K), K = 1, 8), A(J)    $ PRINT 100
100   FORMAT (1H1)
16    FORMAT (8E11.3,F10.1)
3     RETURN    $   END


      SUBROUTINE EXDAT (F) .  $   DIMENSION F(56,8), Z(15,8)
      COMMON M, N1, A(150), NH, Y(15), S(35), INFLUX, E(56,8), V(56,8),
     1 LAMBDA, NOPRINT, EP(56,8)
      DO 23 J = 1, 15    $   READ 18, (Z(J,K), K = 1, 8), I
18    FORMAT (8F4.0,I5)
      DO 23 K = 1, 8
23    Z(J,K) = Z(J,K)*(10.0**I)    $   DO 20 K = 1, 8    $   N = 0
      DO 31 J=6,51,5 $ N=N+1
31    F(J,K)=Z(N,K) $ DO 32 J=6,46,5 $ DO 32 N=1,4
32    F(J+N,K)=0.2*((5-N)*F(J,K)+N*F(J+5,K)) $ DO 28 J=52,56
28    F(J,K)=Z(J-41,K) $ CALL APRINT(F,6,NH)
C   A=HEIGHT[KM]: C=(02): X=(0): Y=COS(CHI): O=OP.DEPTH[NO UNIT]: R=(NO):
C   S=SUN-EARTH DIST.[AST.UNIT]: F=PRESSURE: T=TEMP[K]: S.I.UNITS USED EXCEPT
C   WHERE OTHERWISE INDICATED.  THE ABSORPTION (DEV.+NON-DEV.) IS FOR THE
C'  ORDINARY RAY.  CONFAC INCLUDES FACTORS FOR OBTAINING ABSORPTION BEFORE AND
C   AFTER REFLECTION, AND CONVERTING HEIGHTS INTO METRES.
      RETURN    $   END
```

REFERENCES

Aikin A.C., Kane J.A., and Troim J. 1963 Goddard Space Flight Center, Sci. Report X-615-63-159

Appleton E.V. 1927 U.R.S.I. Proc., Washington

Appleton E.V. 1937 Proc. Roy. Soc. A 162, 451

Appleton E.V. 1953 J.A.T.P. 3, 282

Appleton E.V. and Barnett M.A.F. 1925 Nature 115, 333

Appleton E.V. and Barnett M.A.F. 1925 Proc. Roy. Soc. A 109, 621

Appleton E.V. and Piggott W.R. 1954 J.A.T.P. 5, 141

Bailey V.A. and Martyn D.F. 1934 Phil. Mag. 18, 369

Balfour Stewart 1902 Ency. Brit. (Ninth Edition) 16, 181

Banks P.M. 1966 Planet. Space Sci. 14, 1085

Bardsley J.N. and Biondi M.A. 1970 Adv. At. Mol. Phys. 6, 1

Barrington R.E. and Thrane E.V. 1962 J.A.T.P. 24, 31

Barth C.A. 1966 Planet. Space Sci. 14, 623

Bates D.R. and Massey H.S.W. 1947 Proc. Roy. Soc. A 192, 1

Belrose J.S. 1965 Physics of the Upper Atmosphere: Prentice Hall

Belrose J.S. 1967 Nature 214, 660

Belrose J.S. and Burke M.J. 1964 J.G.R. 69, 2799

Best J.E. and Ratcliffe J.A. 1938 Proc. Phys. Soc. A 150, 267

Beynon W.J.G. and Brown G.M. 1959 J.A.T.P. 14, 138

Beynon W.J.G. and Davies K. 1954 The Physics of the Ionosphere: Report of Physical Society Conference, p. 40

Beynon W.J.G. and Jones E.S.O. 1965a Proc. Roy. Soc. A 288, 558

Beynon W.J.G. and Jones E.S.O. 1965b Nature 206, 1243

Bibl K., Paul A., and Rawer K. 1962 J.A.T.P. 23, 244

Bibl K., Paul A., and Rawer K. 1965 J.A.T.P. 27, 145

Bibl K., and Rawer K. 1951 J.A.T.P. 2, 51

Blamont J.E. 1963 COSPAR Information Bulletin 13, 34

Bossolasco M. and Elena A. 1963a Planet. Space Sci. 15, 1777

Bossolasco M. and Elena A. 1963b C.R. Acad. Sci. 256, 4491

Bowman M.R., Thomas L., and Geisler J.E. 1970 J.A.T.P. 32, 1661

Breit G. and Tuve M.A. 1925 Nature 116, 357

Breit G. and Tuve M.A. 1926 Phys. Rev. 28, 554

Budden K.G. 1966 Radio Waves in the Ionosphere: Cambridge University Press

Chapman S. 1931 Proc. Phys. Soc. 43, 26

Clark I.D. and Wayne R.P. 1970 Mol. Phys. 18, 523

Colegrove F.D., Hanson W.B., and Johnson F.S. 1965 J.G.R. 70, 4931

Davies K. 1965 Ionospheric Radio Propagation: National Bureau of Standards Monograph 80: Washington

Dieminger W., Rose G., Schwentek H., and Widdel H.U. 1968 Space Res. VII (ed. R.L. Smith-Rose), 228

Ditchburn R.W., Bradley J.E.S., Cannon C.G., and Munday G. 1954 Rocket Exploration of the Upper Atmosphere, 327 : Pergamon Press

Donahue T.M. 1972 Radio Sci. 7, 73

Eccles W.H. 1912 Proc. Roy. Soc. A 87, 79

Ellyet C. and Watts J.M. 1959 J. Res. NBS 63D (Radio Prop.), 117

Evans J.V. 1967 Chapter II, Solar-Terrestrial Physics (ed. J.W. King and W.S. Newman): Academic Press

Evans W.F.J., Hunten D.M., Llewellyn E.J., and Vallance Jones A. 1968 J.G.R. 73, 2885

Faucher G.A., Morrissey J.F., and Stark C.N. 1967 J.G.R. 72, 299

Faucher G.A., Procunier R.W., and Sherman F.S. 1963 J.G.R. 68, 3437

Fedele D. 1966 Winds and Turbulence in Stratosphere, Mesosphere, and Ionosphere: Proceedings of the Nato Advanced Study Institute, Lindau: publ. 1968 North Holland, 34

Fedynsky A.V. 1966 Noctilucent Clouds: International Symposium, Tallin: publ. 1967, Moscow, 131

Fehsenfeld F.C. and Ferguson E.E. 1969 J.G.R. 74, 2217

Fehsenfeld F.C., Ferguson E.E., and Bohme D.K. 1969 Planet. Space Sci. 17, 1759

Fehsenfeld F.C., Schmeltekopf A.L., Schiff H.I., and Ferguson E.E. 1967 Planet. Space Sci. 15, 373

Ferguson E.E. 1971 Rev. Geophys. Space Phys. 9, 997

Folkestad K. 1970 N.D.R.E. Report No. 59: Norwegian Defence Research Establishment, Kjeller, Norway

Folkestad K., Thrane E.V., and Thomas J.O. 1972a J.A.T.P. 34, 955

Folkestad K., Thrane E.V., and Landmark B. 1972b J.A.T.P. 34, 963

Gardner F.F. and Pawsey J.L. 1953 J.A.T.P. 3, 321

Gattinger R.L. and Vallance Jones A. 1966 Planet. Space Sci. 14, 1

George P.L. 1971 J.A.T.P. 33, 1893

Gibson A.J. and Sandford M.C.W. 1971 J.A.T.P. 33, 1675

Goldberg R.A. and Blumle L.J. 1970 J.G.R. 75, 133

Gordon W.E. 1958 Proc. I.R.E. 46, 1824

Green A.E.S. 1966 The Middle Ultraviolet, Its Science & Technology: John Wiley and Sons

Gregory J.B. 1965 J. Atmosph. Sci. 22, 18

Groves G.V. 1969 Seasonal and Latitudinal Models of Atmospheric Structure Between 30 and 120 km Altitude: Paper h.1 Open Meeting COSPAR W.G. IV , Prague

Groves G.V. 1970 Seasonal and Latitudinal Models of Atmospheric Temperature, Pressure, and Density, 25 to 110 km: Survey in Geophysics No. 218: United States Air Force Office of Aerospace Research

Hall L.A. and Hinteregger H.E. 1970 J.G.R. 75, 34

Hartree D.R. 1931 Proc. Cambridge Phil. Soc. 27, 143

Heaviside O. 1902 Ency. Brit. (Ninth Edition) 33, 215

Henry R.J.W. 1967 Planet. Space Sci. 15, 1747

Hesstvedt E. 1968 Geophys. Publr. 27, 1

Hesstvedt E. 1969 A Photochemical Atmosphere Model containing Oxygen Hydrogen and Nitrogen: Inst. Geophys. University of Oslo (unpublished).

Higashimura K., Sinno K., and Hirukawa Y. 1969 J. Radio Res. Labs. 16, 131

Hines C.O. 1972 Phil. Trans. R. Soc. Lond. A 271, 457

Hinteregger H.E. and Watanabe K. 1962 J.G.R. 67, 3373

Huffman R.E., Paulsen D.E., Larabee J.C., and Cairns R.B. 1971 J.G.R. 76, 1028

Hulbert E.O. 1928 Phys. Rev. 31, 1018

Hunt B.G. 1966 J.G.R. 71, 1385

Hunten D.M. and McElroy M.B. 1968 J.G.R. 73, 2421

Hunten D.M. and Wallace L. 1967 J.G.R. 72, 2803

Huruhata M. 1965 J.G.R. 70, 4927

Huxley L.G.H. 1959 J.A.T.P. 16, 46

Jaeger J.C. 1947 Proc. Phys. Soc. 59, 87

Jain A.R. and Setty C.S.G.K. 1968 J.A.T.P. 30, 1353

Johannessen A., Krankowsky D., Arnold F. Riedler W., Friedrich M., Folkestad K., Skovli G., Thrane E.V., and Troim J. 1972 Nature 235, 217

Kane J.A. 1962 J.A.T.P. 23, 338

Kennelly A.E. 1902 Elec. World and Eng. 39, 473

Kistiakowsky G.B. and Volpi G.G. 1957 J. Chem. Phys. 27, 1114

Kotadia K.M. and Patel B.M. 1969 J.A.T.P. 31, 621

Larmor J. 1924 Phil. Mag. 48, 1025

Larson L.E. and Houston R.E. Jr. 1969 J.G.R. 74, 2402

Lauter E.A. 1966 Ann. Geophys. 22, 289

Lauter E.A. and Mitzsche 1967 J.A.T.P. 29, 533

Lauter E.A. and Sprenger K. 1967 A.M.S. Symposium, Miami

Lee P. 1955 J. opt. Soc. Am. 45, 703

Little C.G. and Leinbach H. 1958 Proc. I.R.E. 46, 334

Marr. G.V. 1967 Photoionization Processes in Gases: Academic Press

Martyn D.F. 1935 Proc. Phys. Soc. 47, 323

Mawdsley J. 1961 J.G.R. 66, 1298

Mawdsley J. 1971 J.G.R. 76, 1017

Meira L.G. 1971 J.G.R. 76, 202

Mitra A.P. 1966 J.A.T.P. 28, 945

Mitra A.P. 1968 J.A.T.P. 30, 1065

Narcisi R.S. and Bailey A.D. 1965 J.G.R. 70, 3687

Narcisi R.S., Bailey A.D., Della Lucca L.E., and Sherman C.
1969 Trans. Am. Geophys. Un. 50, 654

Narcisi R.S., Philbrick C.R., Ulwick J.C., and Gardner M.E.
1972 J.G.R. 77, 1332

Nicolet M. 1945 Mem. Inst. Meteorol., Belgium 19, 83

Nicolet M. and Mange P. 1954 J.G.R. 59, 15

Nicolet M. and Swider W. 1963 Planet. Space Sci. 11, 1459

Mitzsche P. 1967 Introduction to I.Q.S.Y. absorption data at Neustrelitz:
National Committee on Geodesy and Geophysics, Berlin

Norton R.B. and Barth C.A. 1970 J.G.R. 75, 3903

Pack J.L. and Phelps A.V. 1966 J. Chem. Phys. 45, 4316

Parthasarathy R., Lerfald G.M., and Little C.G. 1963 J.G.R. 68, 3581

Pearce J.B. 1969 J.G.R. 74, 853

Phelps A.V. and Pack J.L. 1959 Phys. Rev. Letters 3, 340

Piggott W.R. 1953 Proc. Inst. Elect. Eng. Part III 100, 61

Piggott W.R. 1964 Research in Geophysics (ed. H. Odishaw):
M.I.T. Press Cambridge Mass.

Piggott W.R., Beynon W.J.G., Brown G.M., and Little C.G. 1957
Annals of I.G.Y. III Part II: Pergamon Press

Pokhunkov A.A. 1966 Ann. Geophys. 22, 92

Purkait N.N. and Datta S.K. 1972 J.G.R. 77, 2397

Rangaswamy S. 1969 Ph.D. Thesis: University of Wales

Rao A.S.M. and Rao B.R. 1968 J.A.T.P. 30, 1239

Rao M.K., Mazumdar S.C., and Mitra S.N. 1962 J.A.T.P. 24, 245

Ratcliffe J.A. 1959 The Magneto-Ionic Theory and its Applications to
the Ionosphere: Cambridge University Press

Reed E.I. 1968 J.G.R. 73, 2951

Reid G.C. 1970 J.G.R. 75, 2551

Rishbeth H. and Garriott O.K. 1969 Introduction to Ionospheric Physics:
Academic Press

Samson J.A.R. and Cairns R.B. 1964 J.G.R. 69, 4583

Schwentek H. 1965 Special Committee for the International Years of the
Quiet Sun IQSY 20 (65): IQSY Secretariat, London

Schwentek H. 1971 J.A.T.P. 33, 1839

Sechrist C.F. 1967 J.A.T.P. 29, 113

Sechrist C.F. 1972 J.A.T.P. 34, 1565

Seddon J.C. 1953 J.G.R. 58, 323

Seddon J.C. 1958 J.G.R. 63, 209

Sen H.K. and Wyller A.A. J.G.R. 1960 65, 3931

Shapley A.H. and Beynon W.J.G. 1965 Nature 206, 1242

Shimazaki T., and Laird A.R. 1972 Radio Sci. 7, 23

Skinner N.J. 1956 Ph.D. Thesis: University of London

Skinner N.J. and Wright R.W. 1956 J.A.T.P. 9, 103

Skinner N.J. and Wright R.W. 1964 J.A.T.P. 26, 1221

Smith L.G. 1962 Geophys. Corp. Amer. Tech. Report 62-1-N

Smith L.G. 1966b J.A.T.P. 28, 1195

Smith R.A. 1966a DRTE / AFCRL Conference on the Lower Ionosphere

Smith E.K. and Matsushita A. 1962 Ionospheric Sporadic E:
Macmillan

Smith-Rose R.L. and Barfield R.H. 1926 Proc. Roy. Soc. A 110, 580

Smith-Rose R.L. and Barfield R.H. 1927 Proc. Roy. Soc. A 116, 682

Sprenger K. and Schminder R. 1966 Kleinheubacher Berichte 11, 79

Strobel D.F. 1971 J.G.R. 76, 2441

Strobel D.F. 1972 J.G.R. 77, 1337

Strobel D.F., Hunten D.M., and McElroy M.B. 1970 J.G.R. 75, 4307

Stroud W.G., Nordberg W., Bandeen W.R., Bartman F.L., and Titus P.
1960 J.G.R. 65, 2307

Swider W. 1969 Rev. Geophys. 7, 573

Swider W. 1972 J.G.R. 77, 2001

Taylor E.W. 1948 J. Res. Bur. of Stand. 41, 575

Taylor G.N. 1969 R.R.E. Newsletter and Research Review No. 8 p.23

Thomas L. 1962 The Winter Anomaly in Ionospheric Absorption, Radio Wave
Absorption in the Ionosphere: AGARDograph No. 53 (ed. N.C. Gerson):
Pergamon Press

Thomas L. 1971 J.A.T.P. 33, 157

Thrane E.V. 1972 Radio Sci. 7, 143

Thrane E.V. and Piggott W.R. 1966 J.A.T.P. 28, 721

VanZandt T.E. and Knecht R.W. 1964 Space Physics: John Wiley and Sons

Wagner C.U. 1966 J.A.T.P. 28, 607

Wakai N., Ouchi C., Nemoto C., Kogaku T., and Echizenya Y. 1960
J. Radio Res. Labs. 7, 551

Warren E.S. 1963 Nature 197, 636

Watanabe K., Matsunaga F.M., and Sakai H. 1967 Appl. Opt. 6, 391

Webber W. 1962 J.G.R. 67, 5091

Weeks L.H. and Smith L.G. 1968 Planet. Space Sci. 16, 1189

Whitehead J.D. 1957 J.A.T.P. 10, 12

Whitehead J.D. 1961 J.A.T.P. 20, 49

Whitehead J.D. 1967 Planet. Space Sci. 15, 1055

Whitten R.C. and Poppoff I.G. 1971 Fundamentals of Aeronomy:
John Wiley and Sons

Wilkes M.V. 1954 Proc. Phys. Soc. 67B, 304

Willmann C. 1966 Noctilucent Clouds: International Symposium, Tallin:
publ. 1967, Moscow, 19

Wu Mao-Fu and Newell R.E. 1972 J.A.T.P. 34, 1999

Yasuda J. 1963 J. Radio Res. Labs. 10, 213

Yonezawa T. 1962 Proc. N.A.T.O. Advanced Studies Institute, Skiehampen,
Norway 1961: publ. Pergamon Press (ed. B. Maehlum), 80